IDENTIFYING NOVEL INTERACTIONS BETWEEN HUMAN UBIQUITIN-SPECIFIC PROTEASE 7 (USP7) AND HISTONE METHYLATING/DEMETHYLATING PROTEINS

ANNA BOJAGORA

A THESIS SUBMITTED TO THE FACULTY OF GRADUATE STUDIES IN

PARTIAL FULFILLMENT OF THE REQUIREMENTS FOR THE DEGREE OF

MASTER OF SCIENCE

GRADUATE PROGRAM IN BIOLOGY

YORK UNIVERSITY

TORONTO, ONTARIO

June 2020

ABSTRACT

The deubiquitinase, Ubiquitin-Specific Protease 7 (USP7) is an indispensable protein responsible for regulating appropriate turnover of proteins involved in numerous signaling pathways and biological processes including immune response, DNA damage response, DNA replication, epigenetics and cell division. USP7 plays an important role in regulating the stability of several tumour suppressors and oncogenic drivers, demonstrated by the extensive implication of USP7 in several human cancers. Furthermore, USP7 is frequently targeted by numerous viral proteins to manipulate cellular processes to promote viral persistence and propagation.

USP7's role in epigenetics is emerging and studies have demonstrated that USP7 modulates several epigenetic modifiers. This thesis further explores USP7's role in epigenetics, investigating USP7's novel regulation of two histone modifying enzymes highly implicated in oncogenesis, Enhancer of Zeste Homolog 2 (EZH2) and Retinoblastoma Binding Protein 2 (RBP2). Based on previous findings, our group identified probable interaction sites in these proteins and pursued to characterize the interactions.

Chapter 2 focuses on the functional relationship between USP7 and EZH2. EZH2, a H3K27 methyltransferase, is the catalytic component of the PRC2 complex, a transcriptional repressor of genes involved in differentiation and development. Our group has previously co-crystallized USP7 and EZH2, and I further explore the intricacies of this interaction and the regulation of EZH2 downstream function. My work supports that EZH2 interacts with the ^{761}MDGD^{764} interaction site located in Ubl2 of USP7 via the ^{489}PRKKKRK^{495} sequence. Moreover, USP7 deubiquitinates EZH2 and affects the downstream function of EZH2.

In Chapter 3, I explore the regulatory axis of USP7 and RBP2, a H3K4 demethylating enzyme that regulates the expression of loci associated with development, differentiation, circadian rhythm, mitochondrial function, and oncogenesis. My work characterizes the novel interaction between RBP2 and USP7 and suggests a regulatory relationship between USP7 and RBP2. The data suggests RBP2 interacts with both the ^{164}DWGF^{167} and ^{761}MDGD^{764} motifs of USP7. Additionally, USP7 appears to regulate RBP2 stability and affect RBP2's downstream function.

ACKNOWLEDGEMENTS

First and foremost, I would like to express my sincere gratitude to my supervisor, Dr. Vivian Saridakis, for providing me with the opportunity to be a part of your lab, as well as guidance and continued support throughout my time as a graduate student. I could not have asked for a more supportive, engaging and positive supervisor. Not only did you help me develop my technical skills, you taught me how to approach scientific questions creatively and encouraged scientific curiosity.

Thank you, to my advisor, Dr. Mark Bayfield, for guiding me and fostering the advancement and success of my projects. Your questions and advice challenged me and allowed me to develop a clear path for my projects.

Thank you, Niha for teaching me the vital skills I needed to succeed during my master's. I would like to thank Danica, Nadine, Helen, Krstina, Sukhdeep and Aneesah for being wonderful labmates and never failing to put a smile on my face.

I am indebted to my cohort and to many members of the Biology department for providing me with their appreciated support, guidance and knowledge. Furthermore, I am extremely grateful for the friendships I have been able to cultivate with many of you.

To my family and Gabriel, I am touched by the unwavering support and encouragement you have provided me. It has guided my resilience and triumph throughout many challenges.

I will forever cherish the memories I have made during my time at York University and will sentimentally look back at these times.

TABLE OF CONTENTS

ABSTRACT ii

ACKNOWLEDGEMENTS iii

TABLE OF CONTENTS iv

LIST OF TABLES ix

LIST OF FIGURES x

LIST OF ABBREVIATIONS xii

CHAPTER 1 : INTRODUCTION 1

1.1 Ubiquitination 1

1.2 Deubiquitination 4

1.3 USP7 7

1.3.1 USP7 Domain Organization, Structure, and Characteristics 8

1.4 USP7's multifaceted role in the cell 12

1.4.1 USP7's role in DNA Damage Response 14

1.4.2 USP7's role in DNA Replication and Cell Division 17

1.4.3 USP7 in Oncogenesis 18

1.4.4 USP7's role in Immune Response and Viral Infection 21

1.5 USP7 in Epigenetic Regulation 22

1.6 Thesis Rationale 25

CHAPTER 2 : EZH2 and USP7 27

2.1 INTRODUCTION 27

2.1.1 EZH2 and the PRC2 Complex 27

2.1.2 PRC2-mediated H3K27 methylation 30

2.1.3 EZH2 dysregulation in Cancer 33

2.1.4 Rationale 34

2.2 MATERIALS AND METHODS 35

2.2.1 Plasmids 35

2.2.2 Bacterial Transformation 36

2.2.3 Bacterial Expression of Recombinant Protein 36

2.2.4 Nickel Affinity Chromatography 36

2.2.5 GST Purification and Pull-down 37

2.2.6 Mammalian Cell Culture and Transfections 38

2.2.7 Antibodies and Immunoblotting 38

2.2.8 MG132 Proteasomal Inhibition 39

2.2.9 Endogenous Co-immunoprecipitation 39

2.2.10 FLAG-EZH2 and USP7 Co-immunoprecipitations 40

2.2.11 *In Vivo* Deubiquitination Assay 41

2.3 RESULTS 42

2.3.1 Predicting the EZH2 interaction site 42

2.3.2 EZH2 stability is UPS dependent 43

2.3.3 Endogenous EZH2 and USP7 interact 44

2.3.4 Direct interaction between USP7 and EZH2 44

2.3.5 EZH2 interacts with USP7 using a KxxxK motif 46

2.3.6 USP7 deubiquitinates EZH2 47

2.3.7 USP7 mediates EZH2 function 48

2.4 DISCUSSION 49

2.4.1 EZH2 stability is UPS dependent 49

2.4.2 USP7 and EZH2 interact in Human Osteosarcoma cells 50

2.4.3 USP7 interacts with EZH2 via ^{761}MDGD^{764} 50

2.4.4 USP7 deubiquitinates EZH2 52

2.4.5 USP7 affects EZH2 downstream function 53

2.4.6 USP7-EZH2 mechanisms and clinical relevance 53

CHAPTER 3 : RBP2 and USP7 55

3.1 INTRODUCTION 55

3.1.1 The KDM5 demethylase subfamily 56

3.1.2 RBP2 role in a cell 58

3.1.3 RBP2 domain organization 59

3.1.4 RBP2 in human disease 59

3.1.5 Project Rational 60

3.2 MATERIALS AND METHODS 62

3.2.1 Plasmids 62

3.2.2 Bacterial Transformation 62

3.2.3 Bacterial Expression of GST-Ubl1-5 62

3.2.4 GST Purification of GST-Ubl1-5 63

3.2.5 GST-Ubl1-5 and FLAG-RBP2 pulldown 63

3.2.6 Mammalian Cell Culture, Transfection and Sample Preparation 64

3.2.7 Antibodies and Immunoblotting 64

3.2.8 Proteasomal Inhibition Using MG132 65

3.2.9 RBP2 and USP7 Co-immunoprecipitation 65

3.2.10 RBP2 and USP7 Interaction Site Mutant Co-immunoprecipitations 67

3.2.11 USP7 Reconstitution in USP7$^{-/-}$ Cells 68

3.2.12 USP7 siRNA Knockdown Assay 69

3.3 RESULTS 71

3.3.1 RBP2 sequence analysis 71

3.3.2 RBP2 stability is USP7 dependent 71

3.3.3 USP7 and RBP2 interact 75

3.3.4 The USP7-RBP2 interaction mediates H3K4me3 demethylation by RBP2 80

3.4 DISCUSSION 81

3.4.1 USP7 regulates RBP2 stability 81

3.4.2 USP7 interacts with RBP2 82

3.4.3 USP7 affects RBP2-mediated H3K4 demethylation 83

CHAPTER 4 : CONCLUSIONS 86

4.1 EZH2 and USP7 86

4.2 RBP2 and USP7 87

4.3 USP7 in Epigenetics 87

REFERENCES 88

APPENDIX A: Usp7 Manipulation by Viral Proteins Review 105

APPENDIX B: RBP2 Isoform 2 Secondary Structure Prediction 106

..... 106

LIST OF TABLES

Table 2-1. Plasmid Constructs used for bacterial transformation and expression. 35

Table 3-1. Double stranded siRNA Sequences. 69

Table 3-2. RBP2 candidate sequences. 71

Table 3-3. H3K4 modifying enzymes 84

LIST OF FIGURES

Figure 1-1. The structure of ubiquitin displaying seven Lysine residues and Methionine1..... 2

Figure 1-2. The ubiquitination pathway..... 4

Figure 1-3. Roles of DUBs in the cell..... 5

Figure 1-4. Organization of DUB subfamilies..... 7

Figure 1-5. USP7 domain organization and structural characteristics..... 11

Figure 1-6. USP7 interactors have diverse cellular roles..... 13

Figure 1-7. Translesional DNA synthesis pathways regulated by USP7..... 17

Figure 2-1. Histone Lysine methyltransferase mechanism..... 27

Figure 2-2. Domain architecture of EZH2..... 28

Figure 2-3. Human PRC2 complex constituents..... 30

Figure 2-4. PcG components and H3K27me3 promote transcriptional repression. 32

Figure 2-5. Sequence alignment of the EZH2 ^{489}PRKKKRK^{495}. 42

Figure 2-6. EZH2 stability is Ubiquitination Dependent..... 43

Figure 2-7. Endogenous EZH2 and USP7 interact. 44

Figure 2-8. EZH2 interacts with USP7-CTD via MDGD *In Vitro*. 45

Figure 2-9. USP7-EZH2 interaction dependent on KKKRK..... 46

Figure 2-10. USP7 Deubiquitinates EZH2. 47

Figure 2-11. USP7 Mediates EZH2 Function..... 48

Figure 3-1. Catalytic mechanisms of Histone demethylases. 56

Figure 3-2. Domain organization of KDM5 family proteins. 57

Figure 3-3. RBP2 Domain Organization. 59

Figure 3-4. RBP2 Stability is DUB dependent. 72

Figure 3-5. USP7 regulates RBP2 stability..... 74

Figure 3-6. USP7 and RBP2 interact. 76

Figure 3-7. RBP2 interacts with USP7-CTD. 77

Figure 3-8. RBP2-USP7 interaction is dependent on DWGF and MDGD..... 79

Figure 3-9. USP7 regulates RBP2 and H3K4me3. 80

LIST OF ABBREVIATIONS

AA	Amino acid		
		A	Ala	Alanine
		C	Cys	Cysteine
		D	Asp	Aspartic acid/Aspartate
		E	Glu	Glutamic acid/Glutamate
		F	Phe	Phenylalanine
		G	Gly	Glycine
		H	His	Histidine
		I	Ile	Isoleucine
		K	Lys	Lysine
		L	Leu	Leucine
		M	Met	Methionine
		N	Asn	Asparagine
		P	Pro	Proline
		Q	Gln	Glutamine
		R	Arg	Arginine
		S	Ser	Serine
		T	Thr	Threonine

V	Val	Valine
W	Trp	Tryptophan
Y	Tyr	Tyrosine

ABRO1	Abraxas Brother 1
ADV	Adenovirus
AEBP2	Adipocyte Enhancer-Binding Protein 2
ALT	Alternative Lengthening of Telomeres
APC	Adenomatous Polyposis Coli
ARID	AT-Rich Interacting Domain
ATF3	Activating Transcription Factor 3
ATM	Ataxia-Telangiectasia Mutated
ATP	Adenosine Triphosphate
ATR	Ataxia Telangiectasia and Rad3-Related Protein
BER	Base Excision Repair
bp	Base Pair
BRCA1	Breast Cancer Type 1 Susceptibility Protein
BRE	Brain and Reproductive Organ Expressed
CAT	Catalytic Core Domain
CDC25A	Cell Division Cycle 25A
CDK1	Cyclin Dependent Kinase
CHFR	Checkpoint with Forkhead and Ring Finger Domains

Chk1	Checkpoint Kinase 1
Chk2	Checkpoint Kinase 2
co-IP	Co-Immunoprecipitation
Cry1	Cryptochrome 1
Cry2	Cryptochrome 2
CTD	Carboxy-Terminal Domain
DAXX	Death Domain-Associated Protein
DNA	Deoxyribonucleic Acid
DNMT1	DNA Methyl Transferase 1
DOT1-like	Disruptor of Telomeric Silencing 1-Like
DUB	Deubiquitinating Enzyme
E1	Ubiquitin Activating Enzyme
E2	Ubiquitin Conjugating Enzyme
E3	Ubiquitin Ligase
EBNA1	Epstein-Barr Virus Nuclear Antigen 1
EBOV	Ebola Virus
EED	Embryonic Ectoterm Development
EPOP	Elongin Bc & Polycomb Repressive Complex 2 Associated Protein
ERCC6	Excision Repair Cross-Complementation Group 6
EV	Empty Vector

EZH2	Enhancer of Zeste Homolog 2
FAD	Flavin Adenine Dinucleotide
FBXL3	F-Box and Leucine Rich Repeat Protein 3
FBXO38	F-Box Only Protein 38
FOXO1	Forkhead Box O1
FOXO4	Forkhead Box O4
GMPS	Guanine Monophosphate Synthetase
H2A	Histone Protein H2A
H2B	Histone Protein H2B
H3	Histone Protein H3
H4	Histone Protein H4
HAUSP	Herpesvirus-Associated Ubiquitin-Specific Protease
HCT116	Colorectal Carcinoma Cell Line
HCT116 USP7 -/-	Colorectal Carcinoma Cell Line Usp7 Knock-Out
HDAC	Histone Deacetylase
HECT	Homologous to the E6Ap Carboxyl Terminus
HeLa	Human Cervical Adenocarcinoma Cell Line
HIV	Human Immunodeficiency Virus
HLTF	Helicase like Transcription Factor
HMT	Histone Methyltransferases

HPV	Human Papillomavirus
HSV	Herpes Simplex Virus
ICP0	Infected Cell Protein 0
IKK	IκB Kinase complex
IKK-γ	Inhibitor of Nuclear Factor Kappa-B Kinase Subunit Gamma
ING2	Inhibitor of Growth Family Member 2
IPTG	Isopropyl B-D-1 Thiogalactopyranoside
JAMM	Jamm Motif Proteases
JARID1A	Jumonji/Arid Domain-Containing Protein 1A
JARID2	Jumonji and AT-Rich Interaction Domain Containing 2
JmjC	Jumonji C Domain
JmjN	Jumonji N Domain
KDM	Lysine Demethylase
KDM5A	Lysine Demethylase 5A
KIF20B	Kinesin Family Member 20B
KSHV	Kaposi'S Sarcoma Herpesvirus
LSCC	Laryngeal Squamous Cell Carcinoma
LSD	Lysine-Specific Demethylase
LSD1	Lysine-Specific Demethylase 1
MARCH7	Membrane Associated Ring-Ch-Type Finger 7

MATH	Meprin and Traf Homology
MCM-BP	Minichromosome Maintenance Binding Protein
MCV	Merkel Cell Polyomavirus
MINDY	Motif Interacting with Ub Containing Novel DUB Family
MJD	Machado-Joseph Domain Protease
MLL2	Lysine Methyltransferase 2C
MLL3	Lysine Methyltransferase 2C
MLL5	Mixed Lineage Leukemia 5
NER	Nuclear Excision Repair
NF-ϰB	Nuclear Factor Kappa-Light-Chain-Enhancer of Activated B Cells
NTD	Amino-Terminal Domain
NUP98	Nucleoporin-98
OGT	O-GlcNac Tranferase
ORC2	Origin of Complex 2
OUT	Ovarian Tumour Related Proteases
PcG	Polycomb Group Proteins
PCGF	Pcg Ring Finger Proteins
PCL1	Polycomb-Like 1
PCL2	Polycomb-Like 2
PCL3	Polycomb-Like 3

PCNA	Proliferating Cell Nuclear Antigen
PHD	Plant Homeodomain
PHF8	Plant Homeodomain Finger-Containing Protein 8
PML	Promyelocytic Leukemia Protein
PML-NB	PML Nuclear Bodies
Polh	DNA Polymerase Eta
POT1	Protection of Telomeres 1
PPM1G	Protein Phosphatase, Mg2+/Mn2+ Dependent 1G
PRC	Polycomb Repressive Complex
PRC1	Polycomb Repressive Complex 1
PRC2	Polycomb Repressive Complex 2
PRMT1	Protein Arginine N-Methyltransferase 1
PTM	Post-Translational Modification
RASSF1A	Ras Association Domain Family Member 1
Rb	Retinoblastoma-Associated Protein
RBBP4	Rb Binding Protein 4
RBBP7	Rb Binding Protein 7
RBP2	Retinoblastoma Binding Protein 2
RBR	Ring-Between-Ring
RING	Really Interesting New Gene

RING1A	Ring Finger Protein 1A
RING1B	Ring Finger Protein 1B
RNF168	Ring Finger Protein 168
RNF169	Ring Finger Protein 169
RNF220	Ring Finger Protein 220
SAM	S-Adenosylmethionine
SETD2	Set Domain Containing 2 Histone Lysine Methyltransferase
SIRT1	Silent Information Regulator 1
SRM	Stimulation Response Motif
SUMO	Small Ubiquitin-Like Modifier
SUV39H1	Suppressor of Variegation 3-9 Homolog 1
SUZ12	Suppressor of Zeste 12
SWI/SNF	Switch/Sucrose Non-Fermentable Chromatin Remodeling Complex
Tip60	Tat Interactive Protein 60
TLS	Translesion DNA Synthesis
TRAF	Tumor Necrosis Factor Receptor
TRAF3	TNF Receptor Associated Factor 3
TRAF6	TNF Receptor Associated Factor 6
TRIM27	Tripartite Motif Containing 27
TRIM32	Tripartite Motif Containing 32

TRRAP	Transformation/Transcription Domain Associated Protein
TSPYL5	Testis-Specific Y-Encoded-Like Protein 5
U2OS	Human Osteosarcoma Cell Line
Ub	Ubiquitin
UBA52	Ubiquitin A-52 Residue Ribosomal Protein Fusion Gene
UBA80	Ubiquitin Carboxyl Extension Protein 80 Gene
UBB	Ubiquitin B Gene
UBC	Ubiquitin C Gene
UbE2E1	Ubiquitin-Conjugating Enzyme E2 E1
Ubl	Ubiquitin-Like
UCH	Ubiquitin C-Terminal Hydrolases
UHRF1	Ubiquitin-Like with Phd and Ring Finger Domains 1
UPS	Ubiquitin Proteasome System
USP	Ubiquitin Specific Protease
USP7	Ubiquitin-Specific Protease 7
USP7-CTD	Usp7 C-Terminal Domain
USP7-NTD	Usp7 N-Terminal Domain
USP7S	Ser-18 Phosphorylated Isoform of Usp7
UTX	Histone Demethylase UTX
UVSSA	UV-Stimulated Scaffold Protein A

vIRF	Viral Interferon Regulatory Factor
WDB	WD-40 Binding Domain
XPC	Xeroderma Pigmentosum Complementation Group C
ZF	Zinc-Finger Domain

CHAPTER 1 : INTRODUCTION

1.1 Ubiquitination

Ubiquitination is a cellular process that involves the conjugation of a 76-amino acid polypeptide, ubiquitin, to a target protein [1]. Living up to its name, ubiquitination is truly ubiquitous, evident by its high degree of evolutionary conservation and universal expression in eukaryotic cells. This multifaceted regulatory mechanism is involved in numerous biological processes, most notably in regulating protein degradation, but has been shown to affect protein activity, protein-protein interactions, and alter protein localization [2]. The versatile effects of ubiquitination dictate its involvement in a variety of cellular processes, such as endocytic trafficking, gene expression, DNA repair, immune response and viral infection. Hence, it is not surprising that dysregulation of ubiquitination system components is associated with numerous diseases such as cancer, neurodegenerative and developmental disorders [3]. The importance of ubiquitin-mediated protein degradation was recognized in 2004 when the Nobel Prize in Chemistry was awarded to Aaron Ciechanover, Avram Hershko and Irwin Rose for their contributions to this field [4].

The structure of ubiquitin was published in 1987 by Kumar et al., demonstrating ubiquitin is a highly stable protein consisting of a compact β-grasp fold [5] (**Figure 1-1)**. In animals, ubiquitin is produced as a monomer fused to a ribosomal protein encoded by UBA52 and UBA80 [6,7]; or as a polyubiquitin chain encoded by the polyubiquitin cassettes UBB and UBC [8]. Under basal conditions, ubiquitin is typically expressed as a monomeric ribosomal fusion protein or a polyubiquitin chain [9]. In the response to cellular stress, the expression of ubiquitin from polyubiquitin cassettes is upregulated, allowing for rapid increase in ubiquitination levels [10].

The fate of the ubiquitinated protein depends on both the type of modification (monoubiquitination, multi-monoubiquitination, or polyubiquitination) as well as the type of linkage [11]. Ubiquitin is typically conjugated to substrate lysine (K) residues; however, it has also been shown to undergo conjugation to cysteine (C), serine (S) and threonine (T) residues [12].

In polyubiquitination, ubiquitin is able to form eight different types of chains on itself through its seven lysine (K) residues (K6, K11, K27, K29, K33, K48, K63) or the methionine residue (M1)

[13,14] (**Figure 1-1**). Furthermore, polyubiquitin chains can be homotypic or heterotypic, composed of uniform or mixed linkages respectively. The most commonly observed polyubiquitin chains appear to be K48 and K63 linked.

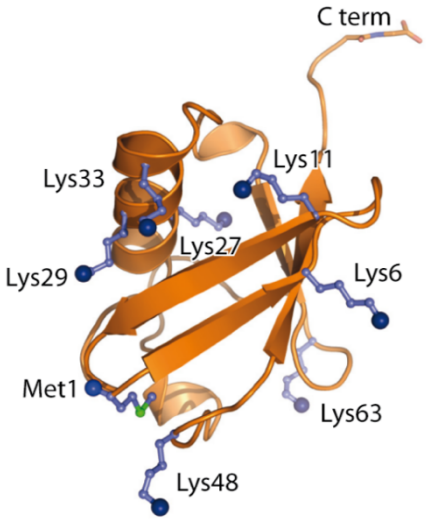

Figure 1-1. The structure of ubiquitin displaying seven Lysine residues and Methionine1. Through one of seven lysine residues (K6, K11, K27, K29, K33, K48, K63) or M1, ubiquitin is able to participate in the formation of polyubiquitin chains. Adapted from [15].

The addition of K48 polyubiquitin chains to a substrate targets it for degradation by the 26S proteasome, a large 2.5 MDa ATP dependent protease complex [16]. Although K48-linked polyubiquitin chains are a well-recognized signal for proteasomal degradation, several other forms of ubiquitination have also been associated with protein turnover [17]. For instance, K11-linked polyubiquitin chains as well as heterotypic K11/K48 polyubiquitin chains have been shown to target proteins for proteasomal degradation [18,19].

Instead of facilitating protein turnover, K63 polyubiquitination appears to have several non-proteolytic roles in endosomal trafficking and DNA damage repair [20,21]. Additionally, K63 and M1 polyubiquitination is associated with the regulation of inflammatory signaling, specifically activation of the NF-κB pathway [22,23]. Less common polyubiquitin chains have also been observed to play important roles in the cell. For instance, K27 polyubiquitination of H2A and H2A.X is critical in DNA damage response, responsible for recruiting DNA damage response factors to DNA damage foci [24]. K6 polyubiquitination has been linked with mitophagy, critical for preventing the buildup of reactive oxygen species in the cell by facilitating the removal of

dysfunctional mitochondria [25]. Additionally, K6 polyubiquitination appears to play a role in mediating response to intracellular pathogens by promoting xenophagy [26].

Ubiquitin is covalently attached to lysine (K) residues on the target protein in an ATP-dependent manner via an enzymatic cascade involving activating (E1), conjugating (E2), and ligating (E3) enzymes. The process of attaching ubiquitin to a target first involves the E1 ubiquitin activating enzyme (**Figure 1-2**) [27]. In an ATP-dependent manner, E1 activates and conjugates ubiquitin to an active-site cysteine in E1, forming a thioester bond. Afterwards, ubiquitin is transferred to a cysteine residue in the active site of a E2 ubiquitin-conjugating enzyme. Finally, a E3 ubiquitin protein ligase enzyme is required to conjugate ubiquitin to lysine residues in the substrate. E3s appear to be the most abundant enzymes in the ubiquitin conjugating cascade, encoding approximately ~600 enzymes [3]. The abundance of E3s is thought to confer substrate specificity and allow for a discrete control of protein turnover in the cell. Three families of E3 enzymes exist and they are defined by the domains they possess which include HECT (Homologous to the E6AP Carboxyl (C) Terminus), RING (Really Interesting New Gene), or RBR (RING-between-RING) domains.

RING-E3s function as scaffolds, facilitating the transfer of ubiquitin directly from E2 to the substrate. RING-E3s contain the RING motif, a zinc-binding domain which facilitates interaction with E2s [28]. A notable example of a RING-E3 is BRCA1 (Breast cancer type 1 susceptibility protein), a tumour suppressor whose mutation is highly associated with an increased predisposition to breast and ovarian cancer [29,30]. Other prominent examples include HDM2/HDMX, PML (promyelocytic leukemia protein), and the HSV-1 protein, ICP0 (Infected cell protein 0) [31–33].

In contrast, the HECT- and RBR-type E3 ligases transfer the ubiquitin to the substrate in a two-step process. The first step involves the transfer of ubiquitin from E2 to the HECT- or RBR-E3s. This is followed by transfer from the HECT or RBR-E3 to the substrate. The HECT domain was initially discovered in the E6-AP cellular ubiquitin ligase that was found to bind the E6 HPV (human papillomavirus) oncoprotein [34]. The recruitment of E6-AP by E6 results in the ubiquitination and subsequent degradation of the human tumour suppressor p53. The downregulation of p53 by HPV promotes cell proliferation and thus development of cervical

cancer. In contrast, RBR E3 ligases are composed of a RING1, in-between RING and a RING2 domain [35]. Parkin is an extensively studied RBR E3 ligase that regulates mitochondrial recycling and implicated with familial Parkinson's disease [36].

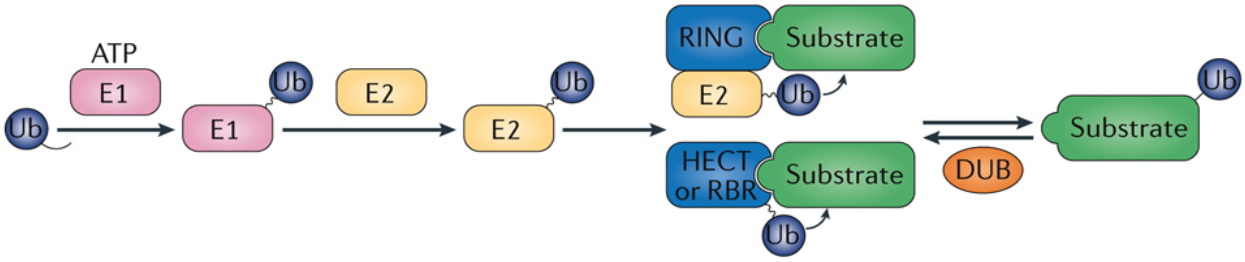

Figure 1-2. The ubiquitination pathway. Three types of enzymes are required to ubiquitinate a substrate: ubiquitin-activating (E1), ubiquitin-conjugating (E2) and ubiquitin-protein ligase (E3) enzymes. The conjugation of ubiquitin to a substrate begins with an E1-mediated ATP-dependent reaction. This reaction involves the formation of a thioester bond between an active site cysteine in the E1 enzyme and the C terminus of the ubiquitin. Afterwards, the ubiquitin moiety is transferred from E1 to an E2 cysteine residue. Finally, the E3 enzyme facilitates the last step of ubiquitination by catalyzing the conjugation of ubiquitin to the target substrate. The abundance of E3s encoded in the human genome confers substrate specificity. Three families of E3s exist: RING, HECT, and RBR. RING E3s carry out the conjugation of ubiquitin directly to the target substrate from E2. In comparison, HECT or RBR E3s function in a two-step process; transferring the ubiquitin from the E2 to the E3, and finally to the substrate. Ubiquitin can be removed from a substrate by deubiquitinases (DUBs). Adapted from [3].

1.2 Deubiquitination

The ubiquitination of proteins is reversed by a class of proteases called deubiquitinases (DUBs). DUBs reverse the process of ubiquitination by hydrolyzing the bonds between the ubiquitin moieties or between ubiquitin and the substrate. DUBs possess several biological roles required for the regeneration of the free ubiquitin pool in the cell (**Figure 1-3**). As previously mentioned, ubiquitin is expressed as a polyubiquitin chain (encoded by UBC, UBB) or a fusion to a ribosomal subunit (encoded by UBA52, UBA80). DUBs are responsible for generating mature ubiquitin by processing ubiquitin precursors into free ubiquitin molecules. Additional avenues by which DUBs regenerate the free ubiquitin pool in the cell involve the deubiquitination of ubiquitinated proteins.

Perhaps the most well-known role of DUBs is their ability to stabilize proteins by removing a ubiquitin tag to salvage the protein from proteolysis by the 26S proteasome. Additionally, certain DUBs associate with the 26S proteasome and deubiquitinate proteins destined for degradation, thereby aiding in ubiquitin recycling. DUBs are also involved in removing non-proteolytic ubiquitin signals from proteins. When a ubiquitin chain is removed from a protein *en bloc*, DUBs are necessary for cleaving the chains to generate free ubiquitin molecules. Aside from this, some DUBs can modify existing ubiquitin tags; In doing so, DUBs can effectively cause the shift from one ubiquitin signal to another.

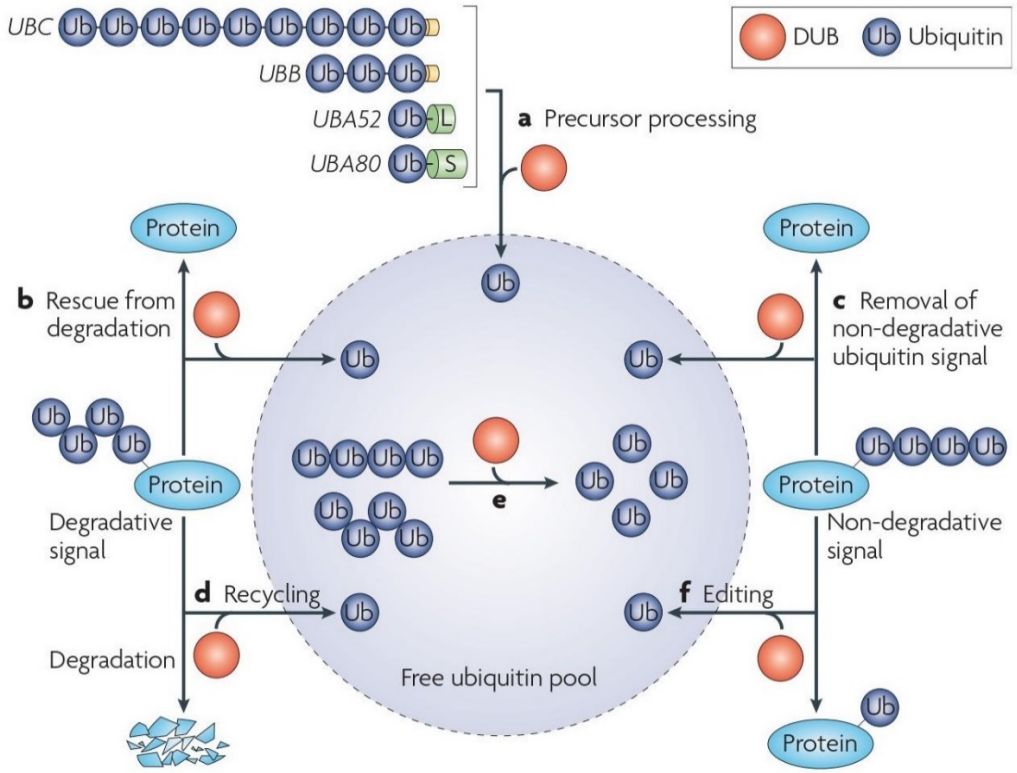

Figure 1-3. Roles of DUBs in the cell. (a) DUBs are required for generating free ubiquitin from precursor molecules. As mentioned previously, ubiquitin is expressed as a ribosomal fusion (UBA52, UBA80) or a polyubiquitin chain (UBC, UBB). (b) DUBs stabilize proteins by removing a ubiquitin signal that would otherwise target the protein for degradation. (c) Non-proteolytic ubiquitin signals can be reversed by DUBs as well. (d) Certain DUBs associate with the 26S proteasome to facilitate the removal of ubiquitin from proteins targeted for degradation. (e) If the ubiquitin chain is removed from a substrate as a whole, DUBs are required to deconstruct the polyubiquitin chains to regenerate the free ubiquitin pool. (f) It is thought that some DUBs can edit ubiquitin chains, resulting in a different ubiquitin signal. Collectively, the various roles of DUBs in the cell generate free ubiquitin molecules that can be ligated to target proteins via the E1-E2-E3 ubiquitination cascade. Adapted from [37].

Collectively, the numerous functions DUBs demonstrate the importance of DUBs in a cell. In combination with the plethora of variable ubiquitin signals, one can appreciate the complexity of ubiquitination system in the cell.

The human genome encodes approximately 100 DUBs that are divided into six families: ubiquitin specific proteases (USP), ubiquitin C-terminal hydrolases (UCH), Machado-Joseph domain protease (MJD), ovarian tumour related proteases (OTU), JAMM motif proteases (JAMM), and motif interacting with Ub containing novel DUB family (MINDY) (**Figure 1-4**) [38]. Comparative analysis of the DUB subclasses revealed variance in the secondary structure between the subclasses. The majority of DUBs are cysteine proteases, with the exception of JAMM domain containing metalloproteases. Cysteine proteases are defined by a catalytic cysteine located in the active site, which cooperates with adjacent histidine and aspartate residues to form a catalytic triad [37].

The largest DUB family is the USP class, with over 50 known members [38]. This class of cysteine proteases exhibits a high degree of sequence variation in the non-catalytic domains which is thought to confer substrate specificity. Interestingly, three catalytic residues in the catalytic domain have been found to be conserved amongst members of this class, including: Cys (C), His (H), and Asp(D)/Asn(N) [39]. In 2002, the structure of a USP catalytic domain belonging to USP7/HAUSP was determined, providing a definition for the USP fold [40]. The USP fold is characterized by a thumb, palm and finger architecture, with the catalytic residues located in the thumb and the palm.

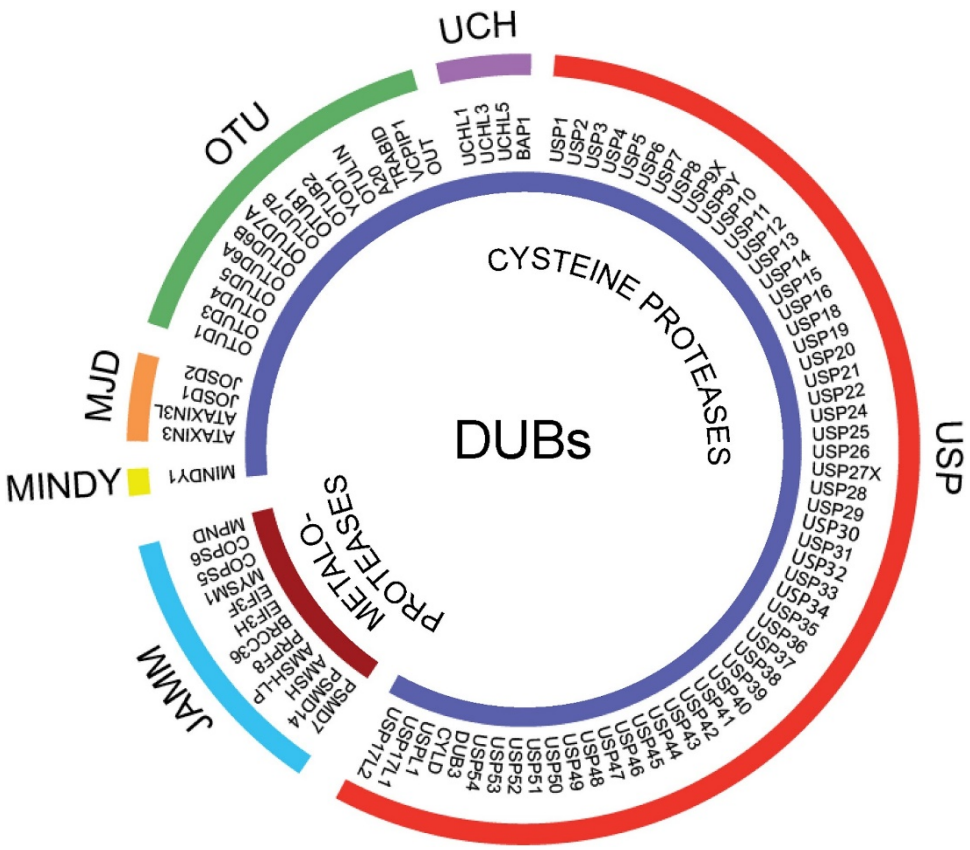

Figure 1-4. Organization of DUB subfamilies. There are two major types of DUBs, cysteine proteases and metalloproteases, which are further grouped into subfamilies. The metalloproteases consist of only one group, the JAMM motif proteases (JAMM). The Cysteine proteases include the largest group ubiquitin specific proteases (USP), as well as ubiquitin C-terminal hydrolases (UCH), ovarian tumour related proteases (OTU), Machado-Joseph domain protease (MJD), and motif interacting with Ub containing novel DUB family (MINDY). Adapted from [41].

1.3 USP7

Human ubiquitin-specific protease 7 (USP7; also known as Herpesvirus-associated ubiquitin-specific protease (HAUSP)) consists of 1102 amino acids (135 kDa) and belongs to the USP class [42]. USP7 was discovered in 1997 by Everett *et al*. and initially found to interact with a herpes simplex virus type 1 (HSV-1) viral protein, ICP0 [43]. USP7 exhibits a high degree of evolutionary conservation as well as sequence homology (~98.6%) with mouse and rat orthologues [44]. USP7 is expressed in all tissue types and is critical for maintaining normal cell function, as perturbations to its expression levels have been associated with numerous

pathological conditions [45]. The functional importance of USP7 has been experimentally demonstrated in USP7 knock-out mice [46]. During development, the knock-out mice embryos exhibited embryonic lethality thought to be due to USP7's involvement in the p53-HDM2 pathway, resulting in the stabilization of p53 and subsequent growth arrest. The generation of p53 and USP7 null mice extended embryonic development but was unsuccessful in fully rescuing the embryonic lethality of the knock-out mice, suggesting novel roles outside the p53-HDM2 context. In more recent years, individuals carrying haploinsufficiencies in the USP7 gene were identified, manifesting clinical features of a neurodevelopmental disorder [47]. The individuals affected exhibited both neurological and behavioral symptoms such as; intellectual disability, autism spectrum disorder, seizures, hypotonia, and speech delays.

Numerous reports have solidified USP7 as an essential protein playing crucial cellular roles with extensive implications in oncogenesis and viral infections [45]. Aberrant expression of USP7 has been associated with various forms of cancer such as, prostate [48], breast [49], colon [50], lung squamous cell carcinoma [51], chronic lymphocytic leukemia [52]. Furthermore, USP7 appears to be frequently deregulated upon viral infection to benefit survival and propagation of the viral niche (Bojagora and Saridakis, 2020). On the basis of these findings, USP7 has been suggested as a promising drug target for cancer therapy and antiviral interventions [53,54]. USP7 inhibitors are an active field of investigation and existing research has delivered encouraging results.

Nevertheless, certain challenges remain, as the majority of USP7 inhibitors demonstrate low selectivity and potency [53]. This is in part due to the high degree of homology between the catalytic domains of USPs. Thus, it has been suggested that identifying novel allosteric binding sites is critical for developing selective and potent USP7 inhibitors.

1.3.1 USP7 Domain Organization, Structure, and Characteristics

USP7 possesses 3 notable domains, the first being an amino-terminal (NTD) tumor necrosis factor receptor–associated factor (TRAF)-like domain (also referred to as MATH), followed by a central catalytic core domain (CAT), and a carboxy-terminal domain (CTD) containing five ubiquitin-like (Ubl 1-5) folds [40,55,56]. Encompassing residues 53-205, the TRAF-like domain is characterized by an eight-stranded, anti-parallel β-sandwich fold [55]. The TRAF-like domain

contains one of two interaction sites USP7 utilizes to interact with its target proteins. The CAT domain is responsible for the catalytic function of USP7, binding ubiquitin and cleaving the isopeptide bond. Spanning residues 208-560, the CAT domain contains the catalytic triad: C223, H464, and D481 [40]. Structurally, the CAT domain resembles a right hand, possessing regions termed the Palm, Thumb, and Fingers. The ubiquitin molecule interacts with the Fingers of the CAT domain while the C-terminus is positioned amid the Palm and Thumb which contain the catalytic cleft. In the hydrophobic catalytic cleft, the histidine residue deprotonates the thiol of the catalytic cysteine, enabling the cysteine to carry out a nucleophilic attack on the isopeptide bond. The aspartate residue functions by stabilizing the positive charge of the histidine residue and polarizing the histidine residue and resulting in cysteine deprotonation. However, apo USP7 is found in an inactive conformation, and undergoes conformational changes upon binding ubiquitin. These conformational changes involve interactions between the CAT and the CTD domains.

The CTD contains five ubiquitin-like (Ubl) folds, each consisting of a β1β2αβ3β4 fold that is structurally similar to ubiquitin yet dissimilar in sequence to ubiquitin [56,57]. Structural analysis of USP7-CTD revealed that the Ubl folds engage in associations amongst each other, forming di-Ubl units, resulting in a 12-3-45 Ubl domain organization [56]. The last di-Ubl, Ubl45, is thought to be involved in USP7 activation by binding to a small loop near the active site termed the "switching loop" located in the CAT domain. The binding of Ubl45 to the "switching loop" enhances binding of ubiquitin and the catalytic activity of USP7 by 100-fold. In contrast, another group has suggested that only the C-terminal residues 1084-1102 bind the activation cleft located in the catalytic domain [58]. The binding of the C-terminal peptide was suggested to stabilize the active conformation of USP7. Interestingly, upon interaction with USP7's Ubl 12 domains, the protein GMPS (Guanine Monophosphate Synthetase) is able to allosterically activate USP7 and increase the efficiency of its catalytic activity [56]. Our group has shown the presence of hinges between the Ubl12 and Ubl45 dimers and Ubl3 [59], as well as a 26 amino-acid α-helical linker located between the CAT domain and the CTD [59,60]. These flexible regions allow USP7 to undergo rearrangements, permitting the enzyme to switch between active and inactive states.

To interact with proteins, USP7 has been shown to primarily utilize one of two domains, TRAF-like [55] or Ubl2 [59]. The TRAF-like domain possesses a ^{164}DWGF^{167} motif located in β-strand 7 that

binds interacting proteins containing a (P/A/E)XXS motif [61,62]. Structural analysis demonstrated that interacting proteins bind to a shallow groove on the surface of the NTD, and that the D164 and W165 residues in the ^{164}DWGF^{167} motif play an indispensable role in mediating interactions [63]. Among the first proteins shown to utilize the NTD interaction domain were the EBNA1 (Epstein-Barr Virus Nuclear Antigen 1) Epstein-Barr viral protein [55], as well as the cellular proteins p53, HDM2, HDMX [64–66]. Since then, crystal structures have been determined of NTD bound to MCM-BP (Minichromosome maintenance binding protein), UbE2E1 (Ubiquitin-conjugating enzyme E2 E1), and Kaposi's sarcoma herpesvirus (KSHV) proteins vIRF1 and vIRF4 [61–63,67].

The second interaction site is the ^{758}DELMDGD^{764} motif, a stable and negatively charged region located in a loop ahead of the last β (β4) strand of Ubl2 that interacts with proteins containing a highly conserved KxxxK or KxxxKxK motif [59]. The aspartate (D) residues in the ^{758}DELMDGD^{764} site are critical for the protein-protein interactions, forming salt bridges with the lysine (K) residues in the KxxxK motif. Occasionally, the KxxxK motif has been shown to be preceded by PR residues, known for strengthening the interaction. USP7-CTD has been structurally shown to interact with DNMT1 (DNA Methyl Transferase 1), ICP0, RNF169 (Ring finger protein 169), UHRF1 (Ubiquitin-like with PHD And Ring Finger Domains 1), and EZH2 (Enhancer of Zeste Homolog 2) [57,59,68–70].

Most recently, the crystal structure of USP7-CTD in complex with DNMT1 has shown the existence of a third interaction site located in Ubl45 [68]. Previous studies have also shown the interaction of Ubl45 with p53 and FOXO4 [71,72].

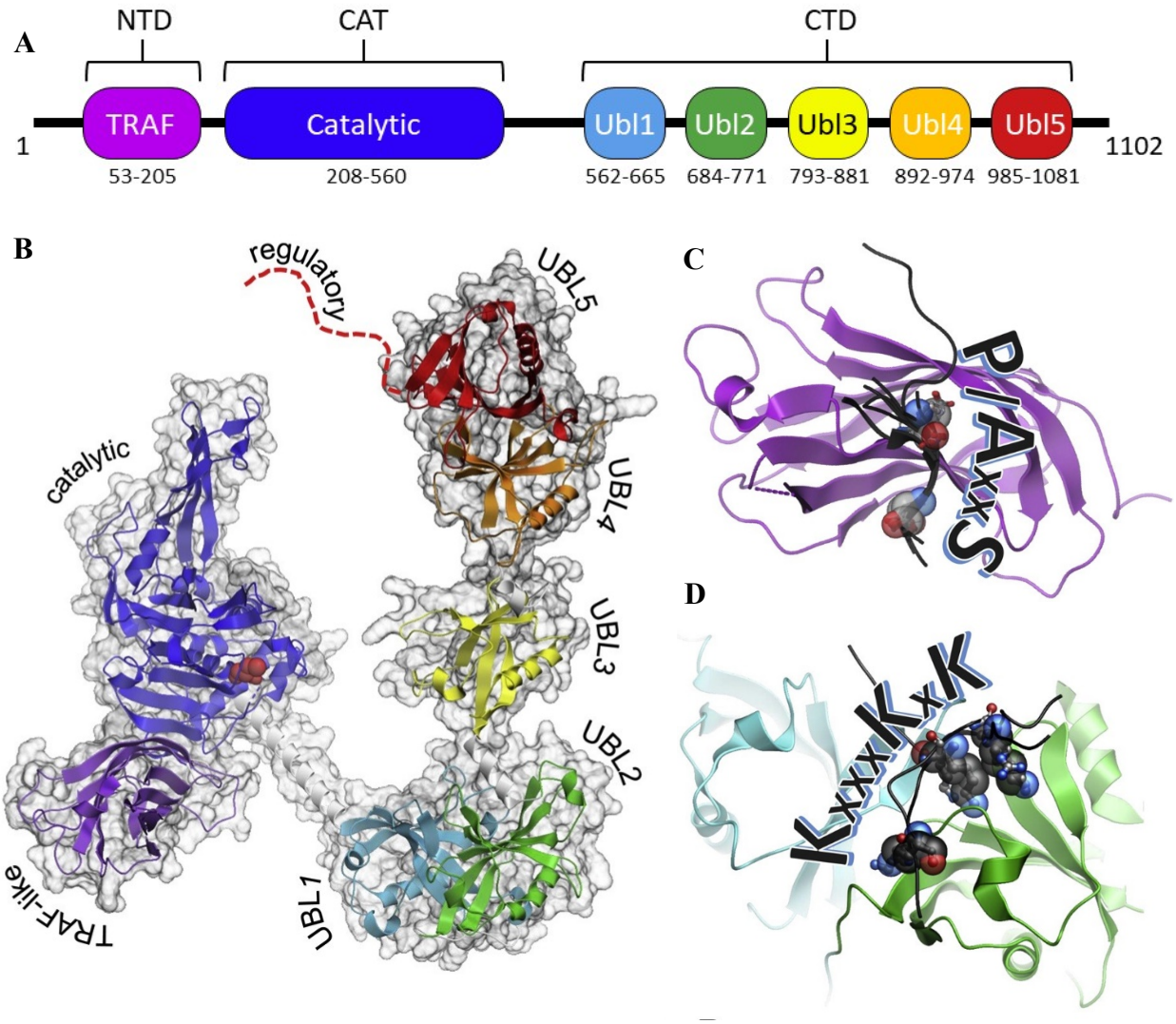

Figure 1-5. USP7 domain organization and structural characteristics. **A)** USP7 domain organization. USP7 possesses 3 notable domains including: The N terminal TRAF-like domain (NTD) shown in purple spanning residues 53-205, a catalytic domain (CAT) shown in blue encompassing residues 208-560, and a C terminal domain (CTD) containing five ubiquitin like domains: Ubl1 (562-665), Ubl2 (684-771), Ubl3 (793-881), Ubl4 (892-974), Ubl5 (985-1081). Each Ubl domain is depicted with a unique colour. Ubl1 and 2 associate with each other forming a di-Ubl unit. Likewise, Ubl4 and Ubl5 associate with each other. **B)** A predicted structural model of USP7 creating by superimposing overlapping structures of USP7 fragments, PDB IDs 2F1Z, 5FWI and 2YLM. The full-length USP7 model includes the TRAF-like domain, Catalytic domain, Ubl1-5, as well as the disordered C-terminus is depicted as a red dotted line. The colours of each domain correspond to the schematic in panel (A). **C)** A model of the TRAF-like domain (purple) recognizing a peptide (black) containing P/AxxS motif. **D)** The second interaction domain is located in Ubl2 (green) of the CTD. Ubl2 is shown in complex with a KxxxKxK peptide (black). Ubl2 binds proteins containing the KxxxK or KxxxKxK sequence. Panels **B)**, **C)** and **D)** were adapted from [41].

1.4 USP7's multifaceted role in the cell

Previous studies have demonstrated USP7 interacts with both cellular and viral proteins. From the cellular substrate perspective, USP7 has been shown to regulate critical transcription factors as well as proteins involved in DNA replication and cell division, epigenetic regulation, DNA damage response and repair, and immune response [41] (**Figure 1-6**). Intriguingly, a large number of the proteins USP7 interacts with are classified as E3 ligases [73] such as: MARCH7 [74], RNF220 [75], HDM2 [64], RING1B [76], RAD18 [77], TRIM27 [78], TRIM32 [79], UHRF1 [69], HLTF [80], CHFR [81], ICP0 [59], Mule [82], RNF169 [70] and RNF168 [83]. Many of the E3 ligase substrates are key players in the pathways listed above. Interestingly, numerous viral proteins have been demonstrated to interact with and deregulate USP7. The extensive roles of USP7 are discussed in the following sections.

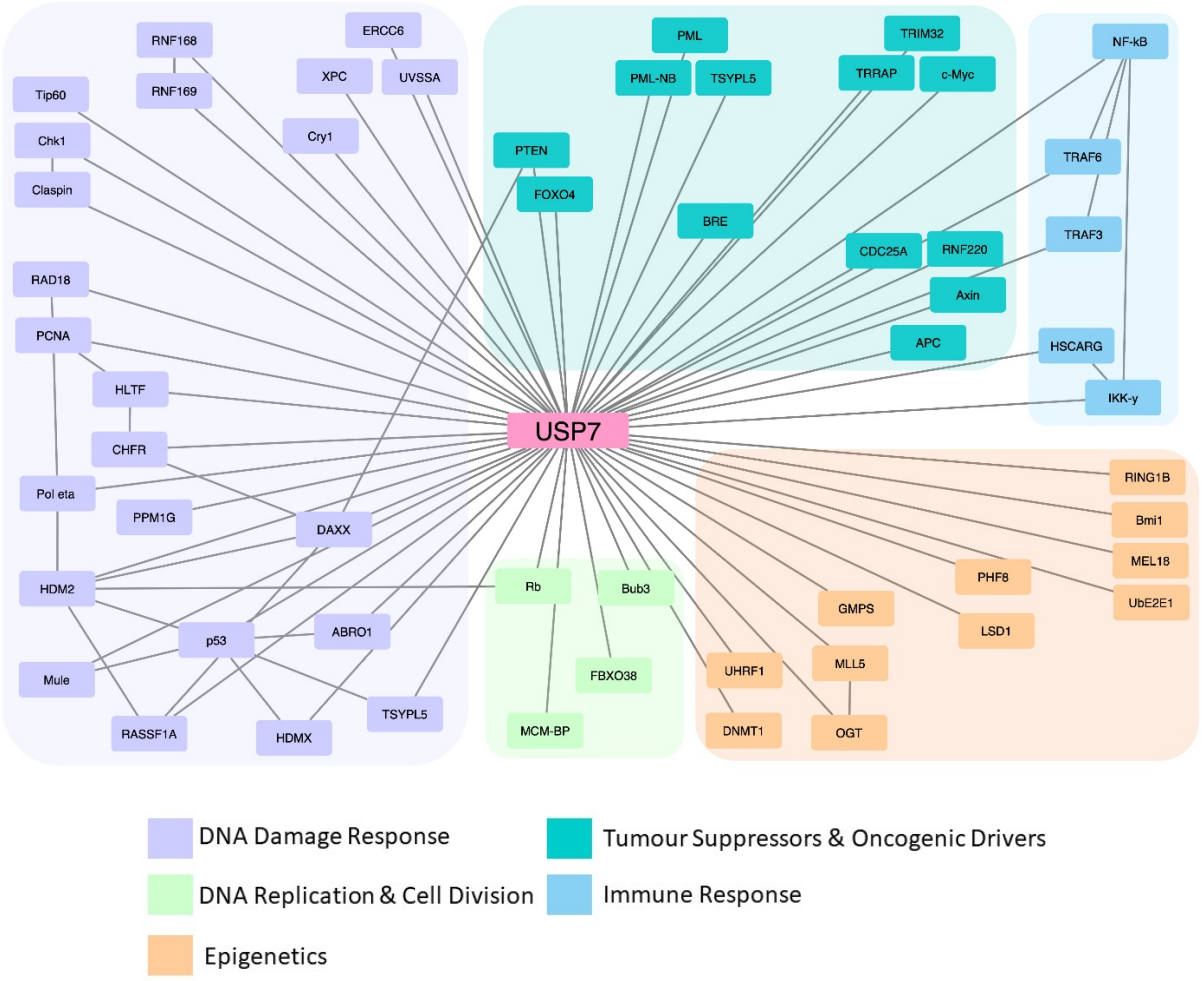

Figure 1-6. USP7 interactors have diverse cellular roles. Over 25 years of USP7 research has characterized numerous proteins regulated by USP7 that are involved in cellular functions that are indispensable for homeostasis. Many targets appear to be involved in maintaining genomic stability, on the level of DNA damage response, as well as DNA replication and cellular division. Furthermore, USP7 plays a role in regulating tumour suppressors, and oncogenic drivers. USP7 interaction partners are also involved in various cellular functions including immune response and epigenetics. Many of these interactors are interlinked, resulting in complex regulatory axes. This figure summarizes the interactors discussed in the following section.

1.4.1 USP7's role in DNA Damage Response

In the incidence of stress stimuli, it is imperative that our cells rapidly initiate the appropriate responses to either repair any incurred DNA damage or prevent further genomic insults [84]. These responses involve initiating expression of appropriate genes, recruitment of DNA repair factors and machinery, and initiating cell cycle arrest. If the damage incurred happens to be beyond repair, the cell may initiate apoptosis. USP7 is highly involved in DNA damage responses, regulating proteins involved in detecting, responding and repairing genomic insults.

The ATM-Chk2 and ATR-Chk1 pathways are critical kinase signaling cascades that coordinate cellular responses to DNA damage. The ATM-Chk2 and ATR-Chk1 pathways are activated by double stranded breaks and ssDNA respectively [85]. In the presence of DNA damage, the ATM and ATR pathways activate DNA damage checkpoints which cause cell cycle arrest and initiate either DNA repair mechanisms or apoptosis. Tip60 (Tat interactive protein 60) is a histone acetyltransferase that was found to be stabilized by USP7 [86,87]. Tip60 is responsible for acetylating nucleosomal histones, thereby having an important role in chromatin remodeling. Another critical function of Tip60 is the regulation of DNA damage responses by acetylating ATM which results in the activation of the ATM signaling cascade. Furthermore, ATF3 (activating transcription factor 3) binds Tip60 and stimulates its acetylase activity as well as promotes deubiquitination of Tip60 by USP7. USP7 was also shown to deubiquitinate key players in the ATR-Chk1 pathway, Checkpoint kinase 1 (Chk1) and its activator Claspin [88,89].

Upstream of the ATM signaling cascade, USP7 is responsible for stabilizing both RNF168 (Ring finger protein 168) and RNF169 (Ring finger protein 169). RNF168 is an E3 ligase that ubiquitinates histones, which acts as a signal to recruit DNA damage factors [83]. In contrast, RNF169 is a negative regulator of RNF168 function, by controlling the accumulation of DNA damage mediator proteins [70].

Downstream of the ATM/ATR signaling cascades, USP7 has been canonically characterized for its involvement in the p53-HDM2-HDMX axis acting as a DUB for p53, HDM2, and HDMX [65,90–92]. The tumour suppressor, p53, is a key player in DNA damage response, apoptosis, and senescence. Its primary inhibitor is HDM2, an E3 ligase that ubiquitinates both itself as well as

p53 and HDMX. Another regulator of p53 is HDMX, that inhibits p53-mediated transcriptional activation. Depending on the cellular state, USP7 has been shown to interact and stabilize p53, HDM2 and HDMX. Under normal conditions, p53 is maintained at low levels through an autoregulatory negative feedback loop with HDM2 [93]. In the absence of cellular stress, USP7 exhibits higher affinity for HDM2, saving it from auto-ubiquitination. If the cell is subjected to stress, activation of ATM signaling promotes the PPM1G-mediated dephosphorylation of USP7 and its subsequent inactivation, resulting in the destabilization of the USP7-HDM2 complex [93,94]. In turn, p53 can accumulate and promote cell cycle arrest or apoptosis. The complexity of the pathway has increased as more players have been added to the existing repertoire such as DAXX, RASSF1A, TSPYL5 and ABRO1.

DAXX (Death domain-associated protein) has been shown form a ternary complex with HDM2 and USP7 and facilitate the stabilization of both itself and HDM2 by USP7 [95,96]. In the presence of DNA damage, the interaction between USP7 and DAXX is disrupted, leading to the ubiquitination of HDM2 and subsequent p53 stabilization. In stressed cells, this complex is thought to be disrupted by the tumour suppressor RASSF1A (Ras Association Domain Family Member 1) [97]. When upregulated by ATM, RASSF1A associates with both HDM2 and DAXX, preventing USP7-dependent stabilization of HDM2 and DAXX.

Additionally, both TSPYL5 (testis-specific Y-encoded-like protein 5) and ABRO1 (Abraxas brother 1) have been shown to regulate p53 through interactions with USP7. In the presence of genotoxic stress, ABRO1 is translocated to the nucleus where it promotes the deubiquitination of p53 by USP7[98]. In contrast, TSPYL5 binds to USP7's NTD interaction domain, and prevents the rescue of p53 by USP7 [99].

USP7 is involved in the regulation of an additional p53 E3 ligase termed Mule (also known as ARF-BP1) [82]. In addition to ubiquitinating p53, Mule is also known to regulate DNA polymerases β and λ which are involved in base excision repair (BER) in response to DNA damage. A Ser-18 phosphorylated isoform of USP7, referred to as USP7S, was found to stabilize Mule.

Further expanding on USP7's role in DNA damage response, USP7 is involved in regulating nuclear excision repair (NER) by deubiquitinating XPC [100]. The XPC (xeroderma pigmentosum

complementation group C) protein is responsible for the detection of helix-distorting DNA lesions and subsequent initiation of NER. USP7 is thought to regulate two other proteins involved in transcription coupled-NER, UVSSA (UV-stimulated scaffold protein A) and ERCC6 (Excision Repair Cross-Complementation Group 6) [101,102].

If genomic damage occurs during replication, lesion bypass processes must be initiated to prevent the collapse of stalled replication forks which are a major cause of genomic loss [80]. The E3 ubiquitin ligase, Rad18, ensures the completion of replication by monoubiquitinating PCNA (Proliferating cell nuclear antigen) on K164, which promotes the recruitment of error-prone DNA polymerases that specialize in translesion DNA synthesis (TLS). Interestingly, USP7 was shown to both upregulate monoubiquitination of PCNA by stabilizing Rad18 [77], and downregulate it by deubiquitinating PCNA directly [103] (**Figure 1-7**). Furthermore, USP7 has been found to both directly and indirectly regulate the stability of a TLS polymerase, Polη (DNA polymerase eta)[104]. The indirect regulation involves HDM2, a previously defined substrate of USP7 and a Polη E3 ligase.

HLTF (Helicase-link transcription factor) is yet another PCNA E3 ligase that was identified to be regulated by USP7 [80]. Intriguingly, HLTF is known to be ubiquitinated by another USP7 substrate, CHFR (Checkpoint with forkhead and RING finger domain protein). In the presence of mitotic stress, CHFR is responsible for delaying cell cycle progression [81]. CHFR is a E3 ubiquitin ligase that targets mitotic proteins for proteasomal degradation. USP7 has been shown to stabilize CHFR, highlighting its role in regulating cell cycle progression and DNA damage response. Another example of DAXX functioning as adaptor protein has been observed in the USP7 stabilization of CHFR [105]. DAXX is thought to promote the USP7 deubiquitination of CHFR.

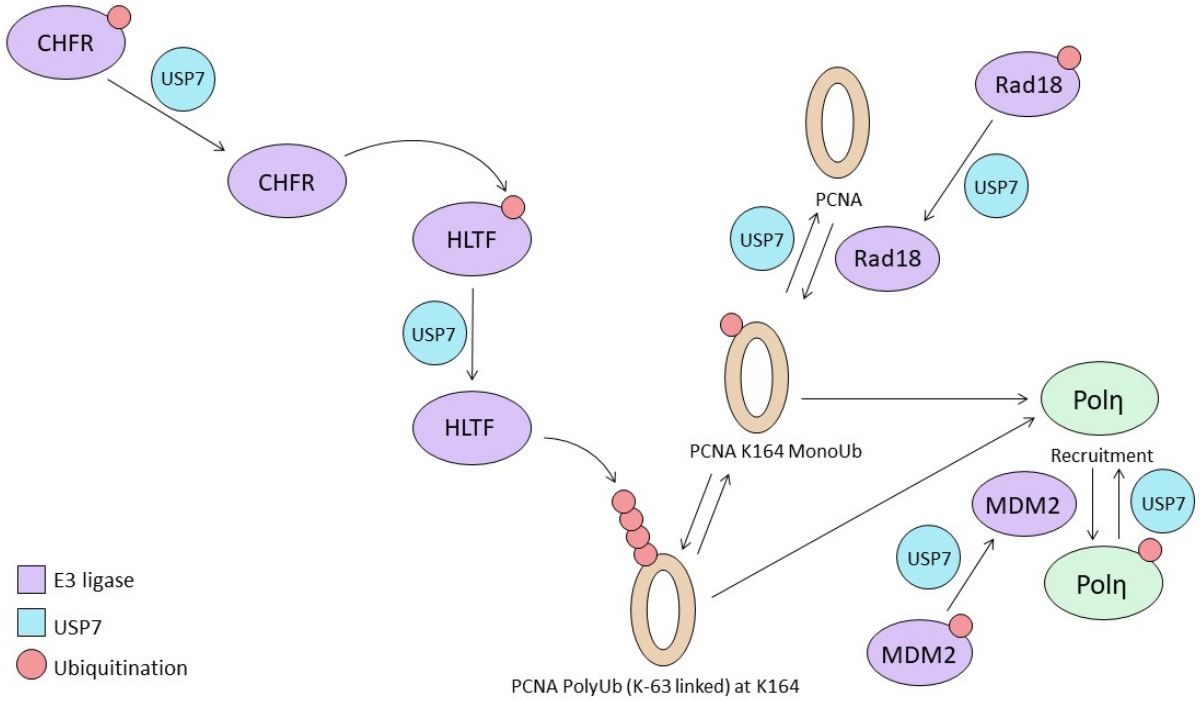

Figure 1-7. Translesional DNA synthesis pathways regulated by USP7. USP7 involvement in the regulation of translesional DNA synthesis is multifaceted. USP7 is known to stabilize key players that promote translesion DNA synthesis, such as HLTF, Rad18, Polη. Additionally, USP7 can antagonize translesional DNA synthesis by deubiquitinating PCNA or stabilizing E3 ubiquitin ligases CHFR and MDM2.

Circadian transcriptional repressors cryptochrome 1 (Cry1) and 2 (Cry2) are involved in the transcription of genes involved in DNA damage response [106]. In response to DNA damage, Cry1 undergoes phosphorylation and is deubiquitinated by USP7, while Cry2 is destabilized by FBXL3 (F-box and Leucine Rich Repeat protein 3). This increased ratio of Cry1 to Cry2 initiates the transcription of DNA damage response genes.

1.4.2 USP7's role in DNA Replication and Cell Division

In addition to playing a key role in DNA damage responses, USP7 is involved in maintaining genomic integrity by regulating proteins involved in DNA replication and cell division.

USP7 has been shown to play a critical role in promoting progression of DNA replication by deubiquitinating SUMOylated (Small Ubiquitin-like modifier) proteins at the replication fork [107].

Further underscoring USP7's role in regulating DNA replication, USP7 was found to interact with MCM-BP. After the conclusion of DNA replication, MCM-BP is responsible for unloading the MCM helicase complex from the DNA [67]. It was suggested that MCM-BP and USP7 work together to unload the MCM complex at the end of S-phase.

Moreover, USP7 has been shown to interact with several key players in the cell cycle. The tumour suppressor, Rb (Retinoblastoma-associated protein) is a critical regulator of the cell cycle, mediating the transition from G1 to S phase. Once phosphorylated, Rb becomes inactive, allowing E2F to propagate transition into S phase. Both USP7 and HDM2 are known to regulate Rb [108]. In this regulatory axis, HDM2 attenuates Rb levels while USP7 stabilizes them. In addition, USP7 appears to play a role in maintaining genomic stability during cell division by deubiquitinating the mitotic checkpoint, Bub3 [109]. Most recently, a novel role in cytokinesis was suggested for USP7 after it was found to stabilize FBXO38 (F-box only protein 38) [110]. Interestingly, FBXO38 was also found to interact with and regulate a kinesin 6 protein involved in cytokinesis, KIF20B (Kinesin Family Member 20B). In the absence of FBXO38 or USP7, KIF20B levels were significantly ablated.

1.4.3 USP7 in Oncogenesis

The role of USP7 in cancer has been termed 'context-dependent' due to its regulation of proteins that have roles in oncogenesis or tumour suppression [45]. Aside from p53 and Rb, the list of tumour suppressors USP7 regulates is extensive, including but not limited to PTEN, PML, and FOXO4.

PTEN (Phosphatase and tensin homolog) is a tumour suppressor whose localization is affected by its ubiquitination status [48]. Upon mono-ubiquitination, PTEN is shuttled to the nucleus, while its deubiquitinated form is known to localize to the cytoplasm. The nuclear exclusion of PTEN has been associated with cancer progression. The deubiquitination of PTEN is carried out by USP7 and promoted by DAXX. PML has been suggested to negatively regulate USP7-mediated PTEN nuclear exclusion through its adaptor protein, DAXX.

Similar to PTEN, the localization of the transcription factor FOXO4 (Forkhead box O4) is facilitated by USP7 [72]. In the presence of oxidative stress, FOXO4 undergoes monoubiquitination and translocations to the nucleus where it functions as a transcription factor. In the nucleus, USP7 inhibits FOXO4 by removing the ubiquitin moiety, promoting its nuclear exclusion.

PML (Promyelocytic leukemia) is a tumour suppressor protein that localizes to and nucleates membrane-less punctate structures interspersed between chromatin, termed PML nuclear bodies (PML-NB) [111]. PML-NBs are involved in numerous biological processes, such as maintaining genomic stability, antiviral responses, apoptosis and senescence [112]. USP7 is known to localize to PML-NB, where it attenuates levels of both PML and PML-NB. Interestingly, USP7 does not seem to require its catalytic activity to regulate the levels of PML and PML-NB [113].

Furthermore, USP7 has recently been shown to interact with TSYPL5 (testis-specific Y-encoded-like protein 5), a PML protein involved in telomere maintenance. Alternative lengthening of telomeres (ALT) is a mechanism, unique to cancer cells and immortalized cell lines, allowing the cells to maintain telomeres through the process of homologous recombination. ALT telomeres possess several defining features, such as is increased heterogeneity in both variant repeats and length, decreased nucleosome density, as well as their frequent association with PML-NB. The TSYPL5 protein has been found to be indispensable in ALT cells. Additionally, TSPYL5 was previously characterized as an inhibitor of USP7, impeding the DUB activity of USP7 towards p53 [99]. However, a recent study has identified TSPYL5 as a PML body component, responsible for stabilizing POT1 (protection of telomeres 1) and promoting cell survival [114]. TSPYL5 is thought to carry out the stabilization of POT1 by preventing USP7 from stabilizing E3 ligases that target POT1 for degradation.

USP7 has also been shown to regulate the proto-oncoprotein c-Myc. USP7 was found to deubiquitinate TRRAP (Transformation/Transcription Domain Associated Protein), a co-factor for c-Myc, E2F and Tip60 [115,116]. Upon overexpression of USP7, c-Myc experienced increased expression at both the mRNA and protein level along with the transactivation of c-Myc responsive genes. In neuronal stem cells, USP7 was shown to colocalize with both c-Myc and TRIM32 (Tripartite Motif Containing 32), its E3 ligase [79]. Additionally, USP7 appears to block neuronal differentiation by stabilizing c-Myc.

USP7 has been shown to promote cell survival of BRCA-deficient cells [117]. Upon DNA damage, BRE (Brain and Reproductive organ Expressed, also known as BRCC45) has been shown to recruit USP7 to stabilize the oncoprotein CDC25A (Cell Division Cycle 25A). CDC25A is phosphatase responsible for the progression of the cell cycle from G1 to S phase. In the occurrence of DNA damage, CDC25A undergoes degradation, preventing the progression of the cell cycle. BRE was suggested to function as an adaptor protein, forming a complex with CDC25A and USP7, promoting the deubiquitination of CDC25A by USP7.

Additionally, USP7 has been shown to regulate the Wnt/β-catenin oncogenic pathway. The Wnt/β-catenin pathway is a major signal transduction pathway regulating many cellular processes such as stemness, and cell fate decisions during development [118]. The deregulation of this pathway is implicated in numerous human pathologies. USP7 is involved in the regulation of the Wnt/β-catenin pathway via its interaction with the E3 ubiquitin ligase RNF220 (Ring Finger Protein 220) [75]. RNF220 is thought to interact with the TRAF-like domain of USP7, bridging USP7 with β-catenin in Wnt-stimulated colon cancer cells. The RNF220/USP7 interaction promotes the stabilization of β-catenin and Wnt signaling. USP7 was also found to promote activation of the Wnt pathway in the context of colorectal cancer [119]. APC (Adenomatous polyposis coli) is a tumour suppressor protein that is frequently truncated in colorectal cancers, resulting in continuous Wnt activation. It was discovered that APC lacking the β-catenin inhibitory domain (CID) allowed β-catenin deubiquitination by USP7 and subsequent Wnt signaling. A β-catenin 26-mer overlapping peptide array was used to map the USP7 binding site, identifying two P/A/ExxS binding sequences. Most recently, USP7 found to directly interact with and stabilize Axin through its TRAF-like domain [120]. Axin is a scaffolding protein of the β-catenin destruction complex. By stabilizing Axin, USP7 plays an important role as a negative regulator of the Wnt/β-catenin pathway. It is interesting to note that all the characterized interactors involved in Wnt/β-catenin signaling utilize the interaction site located in the TRAF-like domain of USP7.

1.4.4 USP7's role in Immune Response and Viral Infection

USP7 has been shown to play an extensive role in regulating immune response as well as involvement in viral infection. For instance, USP7 regulates the major immune transcription factor, NF-κB, a key regulator of proinflammatory signaling. In the absence of stimuli, NF-κB is sequestered and inhibited in the cytosol by the IκB proteins [121]. The presence of a stimulus, such as an infectious agent, initiates a signaling cascade that triggers the activation of the IκB kinase (IKK) complex, composed of IKK-α, IKK-β, and IKK-γ. When activated, IKK phosphorylates IκB, which leads to its degradation and release of NF-κB. Upon release, NF-κB is rapidly translocated to the nucleus where it promotes expression of genes involved in inflammation and immune response. It appears that USP7 has a role in promoting inflammatory signaling by promoting stabilization of NF-κB [122]. Additionally, USP7 has been found to indirectly suppress NF-κB signaling through its interaction with HSCARG [123]. The interaction with HSCARG facilitates USP7 in suppressing IKK-γ polyubiquitination which prevents the degradation of IκB. Furthermore, USP7 deubiquitinates the upstream transducing proteins TRAF3 (TNF Receptor Associated Factor 3) and TRAF6 (TNF Receptor Associated Factor 6) [124,125]. Ubiquitination of TRAF3 and TRAF6 is required for the transduction of NF-κB signaling. Thus, the USP7 dependent deubiquitination of TRAF3 and TRAF6 results in suppressed NF-κB signaling.

In addition to its roles in immune response, USP7 has been characterized to interact with numerous viral proteins and is frequently deregulated upon viral infection. As obligate intracellular parasites, viruses are highly reliant on host machinery for replication and propagation. The selective pressures of evolution have allowed viruses to develop mechanisms that subvert host cellular machinery and responses, promoting survival of the viral niche. The perturbation and manipulation of the ubiquitin proteasome system (UPS) has been significantly implicated in viral-host interactions [126]. Due to its extensive regulatory network, USP7 is a favorable target for dysregulation by viruses.

Interestingly, USP7 has been shown to be targeted by four members of the Herpesviridae family, including Herpes simplex virus-1 (HSV-1), EBV, Human cytomegalovirus (HCMV) and Kaposi's sarcoma-associated herpesvirus (KSHV). Other known viruses that harbour USP7-

interacting proteins include the Human immunodeficiency virus (HIV) [127], Ebola virus (EBOV) [128], Merkel cell polyomavirus (MCV) [129], and Adenovirus (ADV) [130]. Notably, several of these viruses are characterized as oncoviruses, including KSHV, MCV, and EBV. Oncoviruses are able to impart the hallmarks of cancer to infected cells by mass deregulation of host processes to promote viral propagation and immune evasion [131]. Considering the multifaceted roles USP7 possesses, it is evident why USP7 is a frequent target for deregulation by viruses.

The first protein USP7 was characterized to interact with is ICP0, a HSV-1 viral E3 ubiquitin ligase [43]. During HSV infection, USP7 is involved in the regulation of upstream NF-κB signaling [132]. ICP0 facilitates the translocation of USP7 from the nucleus to the cytoplasm. In the cytoplasm, USP7 acts as a suppressor of NF-κB signaling by deubiquitinating upstream effectors, TRAF6 and IKK-γ. The deubiquitination of TRAF6 and IKK-γ appears to ablate their activating potential of the NF-κB pathway.

Another example is the EBNA1 protein belonging to EBV and is critical for viral replication as well as latency persistence. EBNA1 interacts with USP7 and this interaction has been shown to trigger numerous effects that benefit EBV persistence [133]. For instance, EBNA1 recruits USP7 and its stimulating interaction partner, GMPS, to the viral episome [134]. At the viral episome, USP7 is thought to be involved regulating gene expression by stimulating the DNA binding activity of EBNA1 as well as deubiquitinating histone H2B. Additionally, EBNA1 attenuates USP7 mediated stabilization of p53 by outcompeting p53 for binding of USP7 [55]. The disruption of p53 stabilization prevents DNA-damage induced apoptosis, promoting viral persistence. Moreover, EBNA1 is involved in the disruption of PML-NB and is dependent on EBNA1 binding USP7 [135].

1.5 USP7 in Epigenetic Regulation

Among all the biological roles USP7 participates in the cell, this thesis will focus on USP7's role in epigenetic regulation. Epigenetic modifications are alterations that affect the expression of genes without modifying the genomic sequence. Epigenetic phenomena permit different cell types to exhibit unique gene expression profiles and maintain these unique profiles after

undergoing somatic division. The epigenome is comprised of DNA, RNA and proteins. Perturbations to the epigenome are significant events that facilitate cancer progression and metastasis as well as permit the development of resistance to immune surveillance and chemotherapy [136]. Using next-generation sequencing, it has been determined that more than 50% of human cancers possess mutations in enzymes related to chromatin organization.

In eukaryotes, the structural state of chromatin has been shown to play an important role in orchestrating gene expression [137]. The nucleosome, a basic building block of chromatin, consist of a histone octamer that wraps 147 base pairs (bp) of DNA [138]. A histone octamer is composed of two copies of each of the core histone proteins: H2A, H2B, H3 and H4. Each of the histone proteins have a characteristic globular domain and an unstructured tail [139]. This unstructured tail is the target of a variety of post-translational modifications (PTMs), such as: phosphorylation, methylation, acetylation, SUMOylation, and ubiquitination [140]. Histone tail PTMs influence chromatin compaction which in turn has important implications in cell cycle regulation, development, differentiation, gene expression, DNA replication and repair [137,141,142]. Additionally, histone modifications act as docking sites for chromatin binding effector proteins.

USP7 is involved in the regulation of both DNA methylation and histone ubiquitination through its interaction with UHRF1 and DNMT1. UHRF1 is an E3 ligase that targets H3K18 and H3K23 for monoubiquitination [69]. The monoubiquitination stimulates recruitment of DNMT1 to replicating chromatin and subsequent maintenance of DNA methylation [68]. USP7 has been shown to interact with and regulate both UHRF1 and DNMT1 using its Ubl domains, resulting in their stabilization and stimulation of activity [143]. The interaction between USP7 and DNMT1 was reported to be impaired upon acetylation of lysine residues in the DNMT1 interaction site [68]. Similarly, phosphorylation of S652 in UHRF1 attenuated interactions between USP7 and UHRF1 [144]. Additionally, USP7 binding to UHRF1 was found to allosterically regulate the chromatin binding ability of UHRF1. Upon binding of USP7, UHRF1 shifts to an open state, favouring chromatin binding and deubiquitination [69].

USP7 appears to have several roles in regulating transcriptional repression. GMPS was found to form a complex with USP7 and stimulate deubiquitination of monoubiquitin from Lysine 120 histone H2B, a modification associated with active transcription [145]. USP7 additionally stabilizes

the histone deacetylase, SIRT1 (Silent information regulator 1), by cleaving its K48-linked polyubiquitin chains [146].

Moreover, USP7 is extensively involved in modulating several proteins involved in the Polycomb repressive system. This epigenetic modifying system is a major regulator of developmental gene repression. Polycomb group proteins (PcG) are critical regulators of gene expression due to their role in directing embryogenesis, stem cell pluripotency as well as X chromosome inactivation [76,147]. There are two main complexes that regulate the repression of genomic loci, polycomb repressive complex (PRC) 1 and 2. PRC1 is recruited by the trimethylation of H3K27, which is catalyzed by PRC2. PRC1 is responsible for the ubiquitination of H2AK119 and is composed of the two core proteins: RING1A/B and one of six PcG Ring Finger proteins (PCGF1-6). The E3 ligase, RING1B is the catalytic subunit responsible for monoubiquitinating H2AK119. USP7 stabilizes both RING1B as well as two PCGF proteins, PCGF2/MEL18 and PCGF4/Bmi1 and has been shown to be critical for the ubiquitinating function of the PRC1 complex [76,148,149]. Moreover, USP7 interacts with and stabilizes UbE2E1, an E2 conjugating enzyme and PRC1 component [63]. The presence of both USP7 and UbE2E1 was found to be critical in the ubiquitination of H2AK119 [150].

Among the histone PTMs, histone methylation is of particular interest. Histone methylation is regulated by enzymes that 'read', 'write', and 'erase' the modification which can occur on basic residues (lysine, arginine, and histidine) [151–153]. These residues can be mono-, di-, or tri-methylated by histone methyltransferases, the 'writer' enzymes. Focusing on histone lysine methylation, the modification can signal either the activation or repression of gene expression depending on both the degree and site of methylation. For instance, methylation on H3K9, H3K27, or H4K20 is associated with gene silencing, while methylation of H3K4, H3K36, and H3K79 is coupled with transcriptionally active genes [139]. However, these associations are a generalization and the methylation of certain residues has been associated with both activation and silencing. An example of this is the di- or tri- methylation of H3K4, generally linked with transcriptional activation, has also been associated with transcriptional repression. The association of H3K4 methylation with transcriptional repression is observed upon the binding of ING2 (inhibitor of growth family member 2). ING2 is thought to function as a co-repressor protein by stabilizing a histone deacetylase complex [154]. Interestingly, simultaneous methylation

of certain residues has been shown to have a combinatorial effect. For instance, simultaneous tri-methylation of H3K4 and H3K27 is associated with transcriptional activation; while individually H3K4 and H3K27 methylation is associated with activation and repression respectively [155]. Histone methyl-modifying enzymes are also known to elicit combinatorial effects. An example of this is the co-association of the UTX histone demethylase and the MLL2-MLL3 histone methyltransferase, both associated with activation of gene expression [156]. The co-association is thought to provide an additive effect, permitting the optimization of active gene expression. Additionally, histone lysine methylations can coordinate with DNA methylation and other histone modifications allowing for a high degree of gene expression regulation [157,158]. Histone modifying enzymes are imperative in modulating appropriate gene expression and mutation or dysregulation of these enzymes has been heavily implicated in numerous pathologies [137].

USP7 has been shown to deubiquitinate histone demethylases PHF8 (plant homeodomain finger-containing protein 8, also known as KDM7B) and LSD1 (Lysine-specific demethylase 1) [49,159]. USP7 has also been shown to deubiquitinate the histone methyltransferase MLL5 (Mixed lineage leukemia 5) [160]. MLL5 is regulated by both OGT (O-GlcNAc tranferase) and USP7 and thought to form a stable ternary complex.

Bearing in mind the intricacy of histone lysine methylation and its multifaceted level of regulating gene expression, there remains much to be explored in USP7's role modulating histone methylases and demethylases.

1.6 Thesis Rationale

The focus of this thesis was to identify and characterize novel interactions between USP7 and the histone methylase Enhancer of Zeste Homolog 2 (EZH2), and the histone demethylase Retinoblastoma Binding Protein 2 (RBP2, also known as KDM5A or JARID1A). The contents of Chapter 2 focus on exploring the interactions between USP7 and EZH2. We characterize the interaction in human cell lines and *in vitro* as well as determine the critical residues involved in mediating the interaction. Furthermore, our data demonstrates that USP7 deubiquitinates EHZ2 and that this relationship mediates the downstream function of EZH2.

The focus of Chapter 3 is identifying and characterizing the interaction between USP7 and the demethylating enzyme RBP2. We identified the novel interaction and regulatory relationship of USP7 and RBP2 in mammalian cell lines. We characterized residues which play a key role in mediating this interaction, as well as the role of USP7 on the downstream function of RBP2.

CHAPTER 2 : EZH2 and USP7

Certain contents of this chapter have been reprinted in [57].

2.1 INTRODUCTION

There are three distinct families of histone methyltransferases (HMT): SET-domain-containing proteins, Disruptor of telomeric silencing 1-like (DOT1-like) proteins, and protein arginine N-methyltransferase 1 (PRMT1) [139]. The first HMT identified was SUV39H1 (Suppressor Of Variegation 3-9 Homolog 1), a SET-domain containing H3K9 HMT [161]. Since the discovery of SUV39H1, numerous histone methyltransferases have been identified, some shown to methylate chromatin bound histones as well as free histones and even non-histone proteins [162]. HMTs are able to catalyze the attachment of a methyl group to a given residue using methyl groups donated by S-adenosylmethionine (SAM), resulting in mono-, di-, or tri-methylation of a lysine residue [152] (**Figure 2-1**).

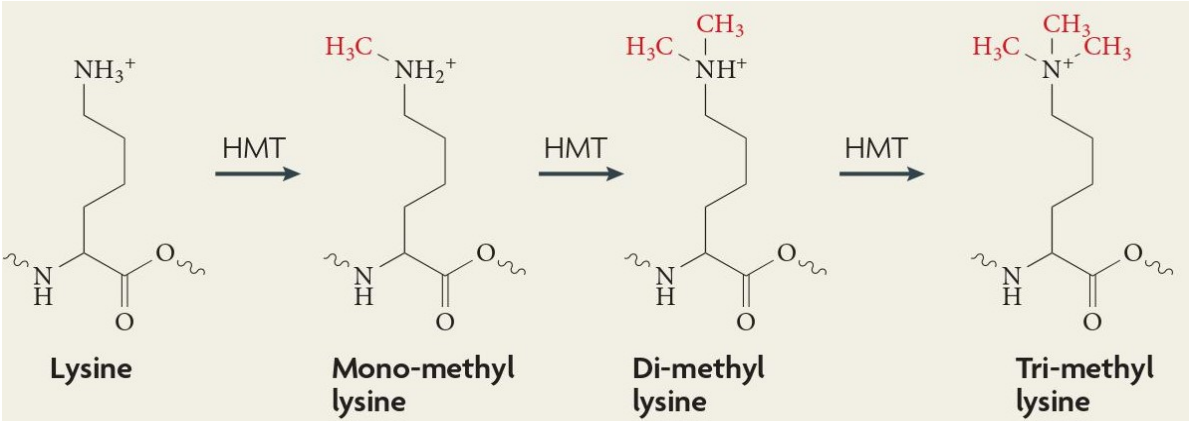

Figure 2-1. Histone Lysine methyltransferase mechanism. This mechanism depicts the mono-, di-, and tri-methylation of lysine residues by histone methyl transferases (HMT). Adapted from [163].

2.1.1 EZH2 and the PRC2 Complex

Enhancer of zeste homolog 2 (EZH2; also known as KMT6) is a SET-domain-containing histone methyltransferase whose homolog in *Drosophila Melanogaster* is E(Z) [164]. The EZH2 gene is

located on the long arm of chromosome 7 at 7q36.1, and codes for a 751 amino acid nuclear protein (86 kDa). EZH2 is the catalytic subunit of the Polycomb repressive complex 2 (PRC2), which is responsible for repressing gene expression by methylating H3K27 (**Figure 2-3**). Additionally, EZH1 is a homolog of EZH2 and associated with non-canonical PRC2 [165]. The PRC2 complex is a transcriptional repressor of genes involved in differentiation and development, including HOX, WNT, NANOG and SOX [166,167]. The high degree of conservation the PRC2 complex exhibits is evident by its presence in plants, insects and mammals [168]. The PRC2 complex can add up to three methyl groups to H3K27. Due to the inability of EZH2 to perform enzymatic functions by itself, it must be complexed with at least two noncatalytic partners, EED (Embryonic Ectoterm Development) and SUZ12 (Suppressor of Zeste 12) [164]. The N-terminal of EZH2 contains a WD-40 binding domain (WDB) which EZH2 uses to bind to the WD-40 domain containing PRC2 core partner, EED [169] (**Figure 2-2**). The Stimulation Response Motif (SRM, residues 141-158) precedes SANT1 (residues 159-250) and SANT2 (residues 428-467). SRM stabilizes SANT1, a histone reader domain with recently discovered specificity for unmodified histone H4 N-terminal tail [170]. Both SANT domains confer EZH2 histone binding ability. The C-terminal region contains the cysteine-rich CXC (residues 555-592) and SET (residues 612-733) domains which are required for the histone methyltransferase activity of EZH2 [171]. The catalytic active site of EZH2 is the SET domain, containing a SAM binding site as well as a methyl acceptor lysine binding site [172].

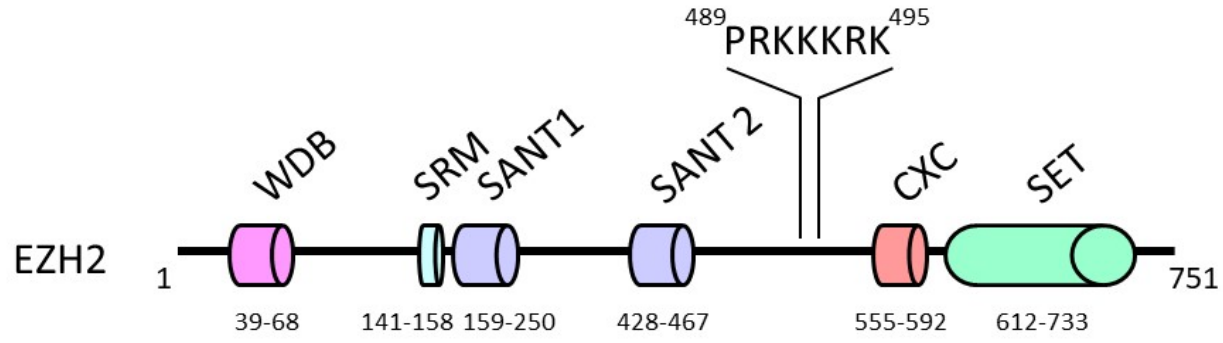

Figure 2-2. Domain architecture of EZH2. The N-terminal region WDB domain contains a binding region for the non-catalytic partner EED. The SRM domain stabilizes the SANT1 domain. Both SANT1 (residues 159-250) and SANT2 (residues 428-467) confer histone binding. The CTD of EZH2 contains a cysteine-rich CXC domain (residues 555-592) and an adjacent SET-domain (residues 612-733) which are necessary for the histone methyltransferase activity of

EZH2. The [489]PRKKKRK[495] sequence is the predicted USP7 interaction sequence. (SRM, stimulation response motif; EED, Ectoterm Development; WDB, WD-40 binding domain).

The core human PRC2 complex can include an additional subunit, RBBP4 (Rb binding protein 4) or RBBP7 (Rb binding protein 7). The combination of EED, SUZ12, RBBP4/7 and EZH2 forms the core PRC2 complex (**Figure 2-3**). The EED subunit harbours five WD40 domain repeats and binds H3K27me3. The binding of EED to H3K27me3 is thought to allosterically activate the methyltransferase activity of the PRC2 complex [173,174]. The C-terminal VEFS domain of SUZ12 is essential for interacting with EZH2 and stabilizing the PRC2 complex [175]. Additionally, it has been suggested that the N-terminal domain of SUZ12 binds to CpG islands and is vital in maintaining appropriate H3K27 methylation patterns. The RBBP4/7 subunit is not essential for maintaining the histone methyltransferase function of EZH2 but contributes to histone binding, interacting with unmodified H3K4 [168]. Additionally, the PRC2 complex can exist in several forms including PRC2.1 and PRC2.2, defined by the accessory units associating with it [176]. The PRC2.1 subcomplex includes the additional constituents: EPOP/PALI and PCL1/2/3. In contrast, PRC2.2 includes JARID2 and AEBP2 [177].

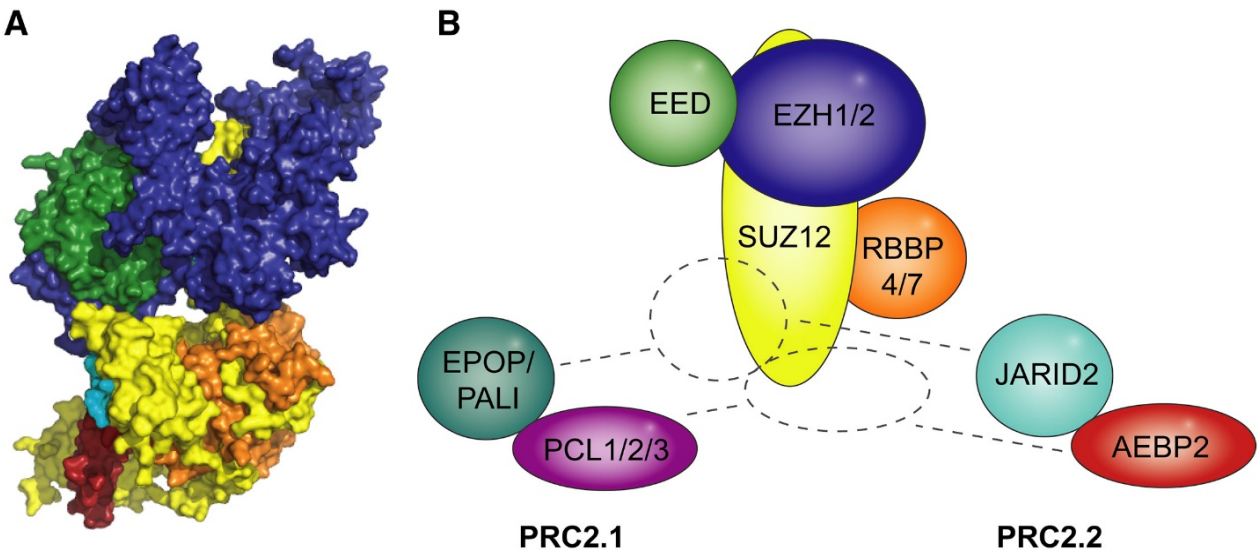

Figure 2-3. Human PRC2 complex constituents. (A) This structural depiction of PRC2 superimposed the crystal structures of PDB ID: 5WAI [178] and PDB ID: 5LS6 [179] onto a structure determined using cryo-EM PDB ID: 6C23 [180]. The colours correspond to the subunits shown in sub-panel **(B)**, (SUZ12, yellow; EED, green; and EZH2, blue) as well as AEBP2 (red) and JARID2 (turquoise) fragments. **(B)** A depiction of the PRC2 complex organization. The core PRC2 complex includes the subunits EZH2, SUZ12, EED, and RBBP4/7. EZH2's non-catalytic partners include EED and SUZ12 are indispensable for EZH2's catalytic function. PRC can form subcomplexes PRC2.1 and PRC2.2 by associating with additional subunits EPOP/PALI and PCL1/2/3 or JARID2 and AEBP2 respectively. Adapted from [177].

2.1.2 PRC2-mediated H3K27 methylation

Before catalyzing the addition of methyl groups to H3K27, PRC2 must undergo recruitment to the appropriate site of methylation. PRC2 binding sites have a few defining characteristics. For instance, PRC2 binding sites are enriched in un-methylated CpG islands, and the binding sites are typically transcriptionally inactive [181,182].

The addition of methyl groups to H3K27 by PRC2 can result in mono-, di- and trimethylation. Each degree of methylation is associated with distinct genomic spatial distribution. In mouse embryonic stem cells, the most abundant methylation state is H3K27me2, existing in 50-70% of histone H3 [175]. In comparison, H3K27me1 and H3K27me3 are each responsible for 10-15% of

histone H3 methylation. Monomethylation of H3K27 is enriched in the body of active genes and stimulates the transcription of the genes [183]. H3K27me1 is involved in 'cross-talk' by its association with the SETD2-dependent trimethylation of H3K36. H3K36me3 regulates H3K27 methylation by inhibiting the conversion of H3K27me1 to H3K27me2. Another example of the complexity of H3K27 methylation is its relationship with H3K27 acetylation. Located in intragenic and intergenic regions, H3K27me2 plays a role in averting the acetylation of H3K27 in enhancers by histone acetyltransferases. The acetylation of H3K27 is associated with the activation of poised enhancers. Therefore, it was suggested that widespread deposition of H3K27me2 may prevent the firing of non-cell-type-specific enhancers. Lastly, H3K27me3 is found at promoters and gene bodies of silenced genes, as well as CpG islands. Additionally, the H3K27me3 modification itself plays a role in propagating the H3K27me3 epigenetic mark in proliferating cells, ensuring appropriate gene expression and the preservation of cellular identity. During DNA replication, the H3K27me3 mark recruits and binds the PRC2 complex, allowing for subsequent trimethylation of H3K27 on the daughter strands.

Moreover, *in vitro* experiments demonstrated that PRC2 methylation efficiency is dependent on the degree of modification. For instance, PRC2 has a 10-fold higher catalytic efficiency in generating H3K27me1 and H3K27me2 compared to H3K27me3 [184]. Interestingly, H3K27me1 and H3K27me2 modifications are thought to occur in a more rapid manner and involve a transient nucleosome-PRC2 interactions [183]. In comparison H3K27me3 is facilitated by stable PRC2 binding which occurs through specific association with CpG islands.

The trimethylation of H3K27 is extensively associated with transcriptional repression and several mechanisms by which PcG complexes contribute to transcriptional silencing have been proposed (**Figure 2-3**). For instance, EZH2 functions as a recruitment platform for DNA methyltransferases to target genes, resulting in transcriptional silencing [185]. The H3K27me3 modification recruits PRC1, resulting in H2AK119 ubiquitination and subsequent transcriptional repression [186]. PRC1 was also found to prevent the binding of the chromatin remodeling complex SWI/SNF, whose activity favours the open chromatin state [187]. PcG complexes are thought to inhibit transcription by preventing the assembly of the initiation complex [188,189]. Additionally, experiments *in vitro* have demonstrated that PRC1 inhibits transcription by RNA polymerase II [190].

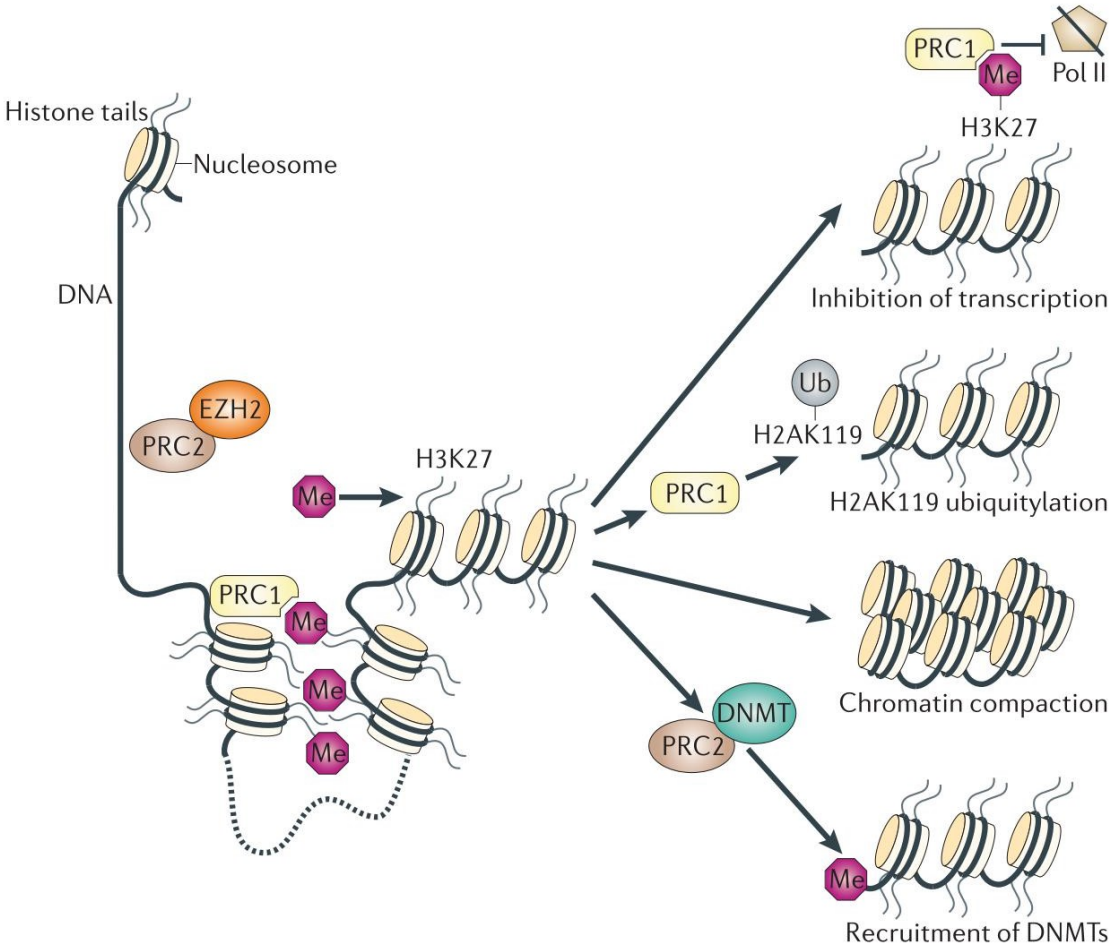

Figure 2-4. PcG components and H3K27me3 promote transcriptional repression. The trimethylation of H3K27 is associated with transcriptional repression. Several mechanisms by which PcG complexes contribute to gene silencing have been proposed. For instance, H3K27me3 recruits PRC1 resulting in the deposition of the repressive mark, H2AK119Ub. PcG complexes are thought to inhibit transcription by preventing the assembly of the initiation complex. Furthermore, it has been proposed that PRC1 inhibits the transcriptional activity of RNA Polymerase II (Pol II) *in vitro*. PRC1 has also been shown to prevent the binding of the SWI/SNF chromatin remodeling complex whose activity is associated with the open chromatin state. EZH2 has been shown to play a role in recruitment of DNA methyltransferases (DNMTs) whose activity promotes transcriptional repression. [191].

2.1.3 EZH2 dysregulation in Cancer

By methylating H3K27, EZH2 functions as a transcriptional repressor known to silence over 200 tumour suppressor genes [164]. Overexpression of EZH2 results in inappropriate hypersilencing of tumour suppressor genes which are responsible for promoting differentiation and restraining proliferation. Due to its heavy implication in cancer, EZH2 presents itself as a promising early biomarker for precancerous tissues [192]. Abnormally elevated levels of EZH2 have been implicated in several forms of cancer including breast, bladder, colon, liver, prostate cancer, melanoma and lymphomas [193–199].

Interestingly, a major target of PcG-mediated repression is the INK4a/ARF locus, encoding the tumour suppressors $p16^{INK4a}$ and $p14^{ARF}$ respectively [200,201]. The $p16^{INK4a}$ tumour suppressor activates the Rb signaling pathway, while $p14^{ARF}$ promotes p53 signaling by inhibiting MDM2. Thus, in this context overexpression of EZH2 would result in inappropriate silencing of both the Rb and p53 tumour suppressor pathways, both of which suppress proliferation. In fact, compared to proliferating cells, stressed and senescent cells exhibited decreased expression of EZH2 [200].

It is not clear whether EZH2 is an oncogene or a tumour suppressor, as contradictory findings have observed EZH2 behaving as both. In the context of lymphomas, EZH2 was found to harbor activating point mutations, suggesting EZH2 is an oncogene [196]. In contrast, mutations abrogating the methyltransferase activity of EZH2 have been identified in myeloid malignancies, suggesting EZH2 is a tumour suppressor [202]. These contradictory observations can be explained by considering the different contexts. As mentioned previously, the methylation of H3K27 is generally associated with repression of gene transcription. However, the genes that are targeted for repression may vary between cell types.

Due to the extensive involvement of EZH2 in tumorigenesis, efforts are currently underway to develop inhibitor treatments that target EZH2 and its associating components [203]. Preliminary data has been providing promising results. For instance, EZH2 inhibition in colorectal cancer cells inducts autophagy and apoptosis and has anti-metastatic effects in triple-negative breast cancer [204,205].

Aside from cancer, EZH2 is found to be decreased in female patients with Hutchinson-Gilford progeria syndrome along with decreased H3K27me3 on the inactive X chromosome [206].

2.1.4 Rationale

The contents of this chapter investigate the regulatory relationship between USP7 and EZH2. We hypothesized that USP7 and EZH2 would interact after identifying a conserved KxxxK interaction sequence in EZH2. The conserved KxxxK motif shared sequence similarity with previously defined USP7 interactors, as well as a high degree of conservation amongst species. Our group predicted that EZH2 utilizes the KxxxK motif to interact with the ^{761}MDGD^{764} interaction site in USP7. We aimed to demonstrate the interaction between EZH2 and USP7 in both mammalian cell lines as well as *in vitro*. Furthermore, using pull-down experiments we characterized the nature of the interaction by comparing the interaction of wild-type and interaction site mutants. We sought out to determine whether EZH2 is a substrate of USP7 using a deubiquitination assay. Our final query was determining if USP7 plays a role in regulating the downstream histone-methylating activity of EZH2.

Previous findings by other groups have provided preliminary data corroborating our hypothesis. The stability of EZH2 appears to be dependent on the UPS as several E3 ubiquitin ligases have been reported to ubiquitinate EZH2 including Smurf2, β-TRCP, FBXW7, PJA1, FOXP3, CHIP, and MDM2/MDMX [207–213]. Moreover, USP7 knock-down coincides with a loss of PRC2 deposition at the INK4a locus along with de-repression of transcription [149]. Considering a major repression target of PcG complexes is the INK4a/ARF locus, this suggested USP7 has a role in regulating the function of PRC2. Several additional papers have reported interactions between USP7 and EZH2 using a GST pulldown as well as a high-throughput PRC2 interactome study in pluripotent NT2 embryonal cell line [76,214].

The preliminary findings in our lab as well as data collected by other groups strengthen our hypothesis that EZH2 and USP7 interact [215–219]. The extensive implication of both proteins in numerous human pathologies underscores the significance of investigating this interaction.

2.2 MATERIALS AND METHODS

2.2.1 Plasmids

The plasmids used for bacterial transformation and expression are listed in (**Table 2-1**). The pGEX-EZH2$^{450\text{-}500}$ was cloned previously from pGEX-EZH2 (Addgene plasmid # 28060) by [215]. The plasmids used for mammalian transfection were: pcDNA3/HA-Ub, pCAN/Myc-USP7, pcDNA3.1/FLAG, pcDNA3/FLAG-EZH2, pcDNA3/FLAG-EZH2$^{\Delta\text{-}MUT}$, pcDNA3/FLAG-EZH2$^{TR\text{-}MUT}$. The pcDNA3/FLAG-EZH2$^{\Delta\text{-}MUT}$ has a deletion of the interaction sequence ^{491}KKKRK^{495}, and the pcDNA3/FLAG-EZH2$^{TR\text{-}MUT}$ is truncated at residue 490. Both pcDNA3/ FLAG-EZH2$^{\Delta\text{-}MUT}$ and pcDNA3/ FLAG-EZH2$^{TR\text{-}MUT}$ were made by ACGT Corporation (Toronto, Canada).

Table 2-1. **Plasmid Constructs used for bacterial transformation and expression.** The constructs in the pGEX-2TK backbone contain a Glutathione-S-transferase (GST) tag while the constructs in a pET15B backbone contain a 6xHistidine (His) tag.

Protein	Backbone	Residues
GST	pGEX-2TK	
GST-EZH2$^{450\text{-}500}$	pGEX-2TK	450-500
6xHis-CTD USP7 (WT)	pET15b	535-1102
6xHis-CTD$^{D762R/D764R}$ USP7 (MRGR)	pET15b	535-1102
6xHis-CTD^{D762A} USP7 (MAGD)	pET15b	535-1102
6xHis-CTD$^{D762A/D764A}$ USP7 (MAGA)	pET15b	535-1102

2.2.2 Bacterial Transformation

1 µL of plasmid was added to 50 µL of thawed chemically-competent DH5α or BL21 (DE3) mgk *Escherichia coli* and incubated on ice for 10 minutes. The cells were then heat-shocked for 45 seconds at 42°C and incubated on ice for 2 minutes. Afterwards, 100µL of SOC was added and the cells were incubated for 30 minutes at 37°C and then plated on Luria Broth (LB) agar containing the required antibiotic (100 µg/ml Ampicillin and/or 50 µg/ml Kanamycin). The plates were then incubated overnight, and a single colony was chosen to inoculate 5 mL of LB which was incubated in a shaker overnight at 37°C (200 rpm) (Innova 43R, New Brunswick Scientific). An aliquot was used to make a glycerol stock.

2.2.3 Bacterial Expression of Recombinant Protein

A freshly transformed colony was inoculated into 100 mL of LB media with 100 µg/ml Ampicillin and 50 µg/ml Kanamycin and grown at 37°C at 200 rpm until the OD_{600nm} of the media reached 0.8-1 (Innova 43R, New Brunswick Scientific). At this point the culture was induced with 0.4 mM of Isopropyl β-D-1 thiogalactopyranoside (IPTG) (Bioshop) and incubated overnight at 16°C (200 rpm). The cells were pelleted by centrifugation at 5,000 x g for 10 minutes with a JLA 16.250 Beckman rotor (Beckman Coulter Avanti J-E centrifuge).

2.2.4 Nickel Affinity Chromatography

The cell pellet was resuspended in 15 mL of Binding Buffer (500 mM NaCl, 50 mM Tris [pH 7.5], 5 mM Imidazole, 1 X Protease inhibitor cocktail (0.001 M Benzamidine and 0.0005 M PMSF in ethanol) and 1X Protease inhibitor tablet (cOmplete EDTA-Free, Roche). The cells were sonicated on ice at 35% amplitude for 4 minutes (10 seconds ON, 15 seconds OFF, Branson Digital Sonifier D450). The soluble fraction was collected by centrifuging the cell lysate for 30 minutes at 30,000 x g at 4°C with a JA-25.50 Beckman rotor (Beckman Coulter Avanti J-E centrifuge). The clarified cell lysate was then incubated at 4°C on the rotator with 1 mL of Ni^{2+}-NTA-Agarose (Qiagen) for 1 hour. The resin was washed eight times with 5 mL of wash buffer (50 mM Tris [pH 7.5], 500 mM NaCl, 20 mM Imidazole, and 5% Glycerol). The His-

tagged proteins were eluted from the resin by adding 5 mL of elution buffer (20 mM Tris [pH 8.0], 500 mM NaCl, 500 mM Imidazole, 10% glycerol) and incubating for 5 minutes with rotation at 4°C. The eluted fraction was dialyzed overnight against (50 mM Tris [pH 8.0], 100 mM NaCl, 5 mM DTT, 10% glycerol).

2.2.5 GST Purification and Pull-down

The cell pellet was resuspended in 15 mL of 1X PBS (4.3 mM Na_2HPO_4, 1.47 mM KH_2PO_4, 137 mM NaCl, 2.7 mM KCl, pH 7.4) with 1 X Protease inhibitor cocktail and 1 X Protease inhibitor tablet (cOmplete ULTRA Tablets, Roche). The cells were sonicated on ice at 35% amplitude for 4 minutes (10 seconds ON, 15 seconds OFF, Branson Digital Sonifier). To collect the soluble fraction, the cell lysate was centrifuged at 30,000 x g for 20 minutes at 4°C with a JA-25.50 Beckman rotor (Beckman Coulter Avanti J-E centrifuge). The clarified cell lysate was incubated with 150 µL of Glutathione Sepharose 4B (GE Healthcare) and incubated at 4°C for 1 hour with rotation. The beads were then washed five times with 5 mL of 1X PBS.

40 µL (dry bead volume) of GST or GST-$EZH2^{450-500}$ bound glutathione beads were combined with 100 µg of purified 6xHis-USP7 protein (6xHis-CTD, 6xHis-$CTD^{D762R/D764R}$, 6xHis-CTD^{D762A}, 6xHis-$CTD^{D762A/D764A}$) and 1X GST interaction buffer (50 mM Tris pH 8, 100 mM NaCl, 5% Glycerol, 5 mM DTT, 0.1 mM Benzamidine, 0.05 mM PMSF) for a total volume of 500 µL in the tube. The pull-down reactions were incubated overnight at 4°C with rotation. Afterwards, the glutathione beads were washed five times with 100 µL of 1X GST interaction buffer (50 mM Tris pH 8, 100 mM NaCl, 5% Glycerol) and elution samples were made by boiling 16 µL of beads with 4 µL of 5X SDS loading dye (5% β-mercaptoethanol, 10% SDS, 30% glycerol, 250 mM Tris-HCl [pH 6.8], 0.02% Bromophenol blue). The 5% input (6xHis-USP7 protein) and 20 µL of elution sample were resolved on a 12% SDS-polyacrylamide gel and stained with Coomassie Blue.

2.2.6 Mammalian Cell Culture and Transfections

Human osteosarcoma U2OS, colorectal carcinoma HCT116 parental (John Hopkins University School of Medicine, Cell line #8 40-16), and HCT116 USP7$^{-/-}$ (HAUSP -/-, 4HAUSP2-4, John Hopkins University School of Medicine Cell line #89) cells were grown on McCoy's (Wisent) media containing 10% fetal bovine serum (FBS, Gibco) and 1 mg/ml Penicillin-Streptomycin (Wisent). Human cervical adenocarcinoma cell line HeLa was grown on Dulbecco's Modified Eagle Medium (DMEM, Wisent) media containing 10% FBS and 1 mg/ml Penicillin-Streptomycin. All cell lines were incubated at 37°C, 5% CO2. The cells were transfected using Polyjet^{TM} In Vitro DNA transfection reagent (SignaGen Laboratories) according to the manufacturer's protocol. To obtain cell lysates, cell pellets were resuspended in RIPA lysis buffer (150 mM NaCl, 50 mM Tris [pH 8.0], 1% NP-40, 0.5% sodium deoxycholate, 0.1% SDS, with 1X Protease inhibitor cocktail and 1X Protease inhibitor tablet (Roche cOmplete ULTRA Tablets)). After incubating the resuspended pellets on ice for 15 min, the samples were sonicated at 10% amplitude for 0.5 seconds ON and 5 seconds OFF for a total ON time of 1.5 seconds (Sonic Dismembrator Model 500, Fisher Scientific). To obtain the soluble fraction, the lysates were centrifuged at 17,000 x g for 15 minutes at 4ºC. The supernatant was recovered, and samples were prepared by boiling the lysate with 1X SDS loading dye.

2.2.7 Antibodies and Immunoblotting

The following antibodies were used for immunoblotting and immunoprecipitating: anti-EZH2 mouse (Cell-signaling, AC22), anti-EZH2 rabbit (Cell-signaling, d2c9), anti-H3K27me3 rabbit (Millipore, ABE44), anti-USP7 rabbit (Bethyl, A300-033A), anti-USP7 mouse (Millipore, 05-1946), anti-GAPDH mouse (Santa-Cruz, sc047723), anti-ECS (FLAG) (Bethyl, A190-102A), anti-HA rabbit (Cell-signaling, C29F4), normal rabbit IgG (Santa Cruz, sc-2027).

After resolving protein samples using SDS-PAGE (SDS-polyacrylamide gel electrophoresis), the gel was transferred to a 0.45 µm Immobilon-P PVDF membrane (Millipore) activated according to the manufacturer's instructions. The transfers were typically ran at 30V overnight at 4°C or 90V for 2.5 hours on ice using 1X Western Transfer Buffer (25 mM Tris [pH 8.3], 192 mM Glycine, and 20% methanol). Following transfer, the PVDF membrane was blocked in 5% non-

fat milk in 1X PBST for 1 hour at RT with rocking. The PVDF membrane was then probed with primary antibodies overnight at 4°C. After primary antibody incubation, the membrane was washed three times with 1X PBS-T in 5 min intervals. After primary antibody incubation, the membrane was washed three times with 1X PBS-T in 5 min intervals. Secondary antibody incubation was carried out for 1 hour at RT with the following antibodies: anti-mouse IgG HRP-conjugated goat polyclonal (ThermoFisher, 31430) or anti-rabbit IgG HRP-conjugated goat polyclonal (Bethyl, A120-101P). Afterwards, the membrane was washed four times with 1X PBS-T in 15 min intervals. The PVDF membrane was incubated for 5 minutes with Amersham ECL Prime Western Blotting Detection Reagent (GE Healthcare) according to the manufacturer's protocol. The immunoblot was imaged using a Microchemi® (DNR-IS) or was exposed to film and a processed through a developer (SX101A Konica).

2.2.8 MG132 Proteasomal Inhibition

HCT116 USP7$^{+/+}$ and HCT116 USP7$^{-/-}$ were incubated with DMSO or 40 μM of MG132 for 1 hour and harvested. 30 ug of sample was resolved on a 10% SDS-polyacrylamide gel, transferred to a PVDF membrane at 30V overnight at 4ºC. The membrane was blocked at room temperature (RT) for 1 hr with 5% non-fat milk in 1X PBS-T (1X PBS, 0.1% Tween-20) and blotted with the following antibodies overnight at 4ºC: 1:3000 USP7 rabbit, 1:1000 EZH2 mouse, 1:2000 GAPDH mouse.

2.2.9 Endogenous Co-immunoprecipitation

U2OS pellet was resuspended in NP-40 buffer (150 mM NaCl, 1% NP-40, 50 mM Tris-HCl [pH 8.0], with 1X Protease inhibitor cocktail and 1 X Protease inhibitor tablet (Roche cOmplete ULTRA Tablets)) and incubated on a nutator for 30 min at 4ºC to lyse the cells. The lysate was centrifuged at 17,000 x g for 10 minutes, and the clarified lysate was recovered and quantified (Pierce™ BCA Protein Assay Kit). The lysate was precleared by incubation with 20 μL of Protein A/G-PLUS Agarose (Santa Cruz, sc-2003) and 1 μg of normal rabbit IgG at 4ºC for 30 min. The beads were pelleted by centrifugation at 1,000 x g for 5 min at 4ºC, and the precleared lysate was collected. The following antibodies were used for the immunoprecipitation: 2 μg

normal rabbit IgG, 3 µL anti-USP7 rabbit. To set up the immunoprecipitation reactions, 1 mg of lysate was combined with the respective antibody, 1X Protease inhibitor cocktail and 1 X Protease inhibitor tablet, and NP-40 lysis buffer to adjust the final volume of each reaction to a total of 500 µL. The immunoprecipitation reactions were incubated overnight on a nutator at 4ºC. The next day, 50 µL of Protein A/G-PLUS Agarose (Santa Cruz, sc-2003) was washed with 500 µL of 1X PBS three times and then blocked with 5% BSA in PBS for 30 min at 4°C. The beads were then equilibrated by washing with 500 µL of NP-40 lysis buffer three times. The equilibrated beads were then added to the antibody and lysate reaction and incubated for 1 hour at 4°C. The beads were washed three times using 500 µL of 1X PBS. To prepare the samples, 35 µL of 1X SDS was added to the beads and boiled for 5 minutes. The input (5%) and 25 µL of elution were resolved on a 10% SDS-polyacrylamide gel and transferred to a PVDF membrane at 30V overnight at 4ºC and botted with 1:2000 anti-USP7 mouse, 1:1000 anti-EZH2 mouse.

2.2.10 FLAG-EZH2 and USP7 Co-immunoprecipitations

Using 20 µL of Polyjet^{TM}, U2OS cells in a 15 cm tissue culture dish were transfected with 10 µg of either: pcDNA3.1/FLAG, pcDNA3/FLAG-EZH2, pcDNA3/FLAG-EZH2$^{\Delta\text{-MUT}}$, or pcDNA3/FLAG-EZH2$^{TR\text{-MUT}}$. The cells were harvested 24 hours post-transfection and the pellets were resuspended in M2 Lysis buffer (50 mM Tris HCl [pH 7.4], 150 mM NaCl, 1 mM EDTA, 1% Triton X-100, 1 X Protease inhibitor cocktail and 1 X Protease inhibitor tablet (Roche cOmplete ULTRA Tablets) and incubated on a nutator for 30 min at 4ºC. The lysate was centrifuged at 17,000 x g for 15 minutes, and the clarified lysate was recovered and quantified (Pierce™ BCA Protein Assay Kit). To immunoprecipitate FLAG-EZH2, 1 mg of cell lysate was combined with 40 µL of resuspended ANTI-FLAG M2 Affinity Gel (Sigma-Aldrich, A2220) equilibrated following the manufacturer's directions and incubated overnight at 4ºC with agitation. The following day, the reactions were washed four times with 500 µL of M2 Lysis buffer, and the beads were boiled with 20 µL 2X SDS loading dye. 2% input and 20 µL of each elution was resolved on a 10% SDS-polyacrylamide gel and transferred to a PVDF membrane at 90V on ice for 2.5 hours. The PVDF membrane was blocked at RT for 1 hr with 5% milk in PBS-T and blotted with the following antibodies overnight at 4ºC: 1:4000 USP7 rabbit (Bethyl, A300-033A), 1:2000 anti-ECS (FLAG) (Bethyl, A190-102A).

2.2.11 *In Vivo* Deubiquitination Assay

HeLa cells in a 10 cm tissue culture dish were transiently transfected with 5 µg of FLAG-EZH2, or 3 µg of FLAG-EZH2 and 3 µg of HA-Ub, or 3 µg of each: FLAG-EZH2, HA-Ub and Myc-USP7. The cells were treated with 40 µM of MG132 8 hrs before harvest. The cells were harvested 24 hours post-transfection and resuspended in 100 µL of Denaturing Ubiquitination Buffer (50 mM Tris-HCl [pH 8.0], 5 mM DTT, 1% SDS) and boiled for 10 minutes, and then cooled on ice for 10 minutes. Afterwards, the lysates were sonicated at 10% amplitude (0.5 sec ON and 5 seconds OFF, for a total ON time of 1.5 sec) (Sonic Dismembrator Model 500, Fisher Scientific). The lysates were centrifuged for 15 min at 17,000 x g at 4°C and the supernatant was isolated. The lysate was diluted with 900 µL of dilution buffer (5 0mM Tris-HCl [pH 8.0], 150 mM KCl, 5% Glycerol, 0.4% NP-40, 1 X Protease inhibitor cocktail and 1 X Protease inhibitor tablet (Roche cOmplete ULTRA Tablets) and the lysate was quantified (Pierce™ BCA Protein Assay Kit). To immunoprecipitate FLAG-EZH2, 750 µg of cell lysate was combined with 40 µL of resuspended ANTI-FLAG M2 Affinity Gel (Sigma-Aldrich, A2220) equilibrated according to the manufacturer's directions and incubated overnight at 4ºC with agitation. The immunoprecipitation was conducted according to the manufacturer's protocol. To elute the protein, the beads were boiled with 20 µL 2X SDS loading dye. Following elution, 1.33% input and 20 µL of each elution was resolved on separate 10% SDS-polyacrylamide gels and transferred to a PVDF membrane at 90V on ice for 2.5 hours. The PVDF membrane was blocked at RT for 1 hr with 5% milk in PBS-T and blotted with the following antibodies overnight at 4ºC: 1:2000 anti-USP7 rabbit (Bethyl, A300-033A), 1:2000 anti-ECS (FLAG) (Bethyl, A190-102A), 1:1000 anti-GAPDH mouse (Santa-Cruz, sc047723), 1:1000 anti-HA rabbit (Cell-signaling, C29F4).

2.3 RESULTS

2.3.1 Predicting the EZH2 interaction site

EZH2 was identified as a predicted interactor of USP7 on the basis on a conserved motif located in the EZH2 sequence (**Figure 2-5**). Using a combination of BLAST, Prosite, Eukaryotic Linear Motif as well as Phyre2, our group discovered the ^{489}PRKKKRK^{495} interaction site in EZH2. This site was strongly predicted to participate in interactions with the ^{761}MDGD^{764} sequence in USP7 as it shared the conserved KxxxK sequence with previously defined USP7-CTD interactors including ICP0, GMPS, UHRF1, DNMT1, and RNF169 [57]. Additionally, EZH2 exhibited the conservation of two additional residues ^{489}PR^{490} present in ICP0 and GMPS. Further substantiating our prediction, the KxxxK motif is situated in an unstructured region and is conserved in EZH2's homologue EZH1. Our lab extensively characterized the interaction between USP7 and EZH2 as well as PRC2 constituents using co-immunoprecipitations, *in vitro* pull-downs, fluorescence polarization, siRNA knock-down, mammalian cell work [57,215]. I further conducted experiments that corroborated the USP7-EZH2 interaction and relationship. This was achieved using deubiquitination assays, pull-downs, co-immunoprecipitations, and mammalian cell work.

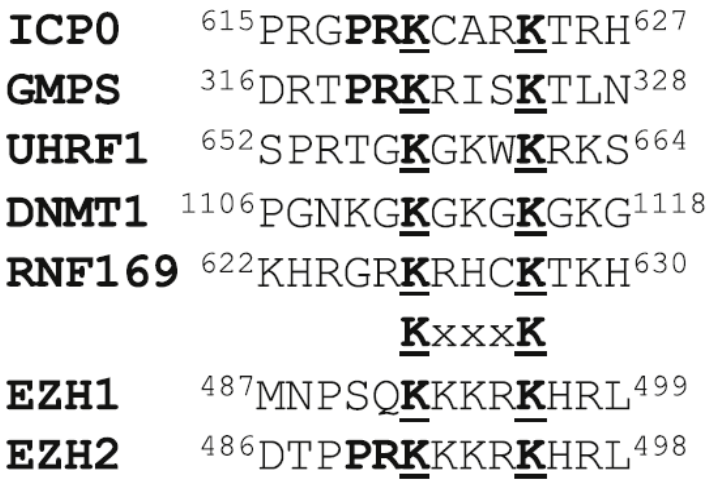

Figure 2-5. Sequence alignment of the EZH2 ^{489}PRKKKRK^{495}. Using BLAST, Prosite, Eukaryotic Linear Motif as well as Phyre2 our group predicted that the ^{489}PRKKKRK^{495} sequence will interact with the ^{761}MDGD^{764} sequence in USP7. The predicted EZH2 interaction site was

aligned with previously defined USP7 Ubl2 interactors such as ICP0, GMPS, UHRF1, DNMT1, and RNF169. EZH2 shares the conserved K residues separated by any three amino acids. EZH2 shares an additional two residues (PR) with ICP0 and GMPS. Moreover, the K residues are conserved in EZH1 as well and the sequence is located in an unstructured region Adapted from [57].

2.3.2 EZH2 stability is UPS dependent

To determine if the stability of EZH2 is dependent on the UPS, we compared the cell lysates of USP7$^{+/+}$ and USP7$^{-/-}$ HCT116 cells treated with the proteasomal inhibitor MG132 or DMSO (control) (**Figure 2-6**). Notably, EZH2 was more abundant in the USP7$^{+/+}$ cells compared to the USP7$^{-/-}$. In both cell lines treated with MG132, EZH2 levels were increased compared to the DMSO controls, suggesting the involvement of the UPS system.

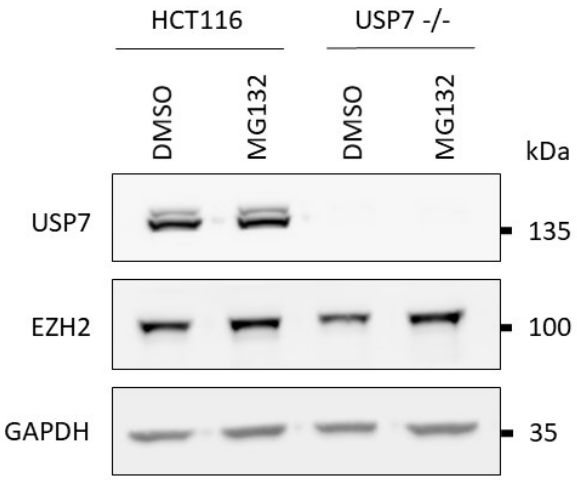

Figure 2-6. EZH2 stability is Ubiquitination Dependent. Immunoblot of HCT116 and HCT116 USP7$^{-/-}$ cells treated with the proteasomal inhibitor MG132. HCT116 USP7$^{+/+}$ and HCT116 USP7$^{-/-}$ were treated with 40 μM of MG132 or DMSO (control) for 1 hour before harvesting. Cellular lysates (30 μg) resolved on a 10% SDS-polyacrylamide gel subjected to immunoblotting with anti-USP7 rabbit, anti-EZH2 mouse and anti-GAPDH mouse antibodies.

2.3.3 Endogenous EZH2 and USP7 interact

To determine if USP7 and EZH2 interact, we performed endogenous co-immunoprecipitations in U2OS cells using IgG (control), anti-USP7, and anti-EZH2 (**Figure 2-7**). EZH2 was found to strongly co-immunoprecipitate with USP7, suggesting an interaction.

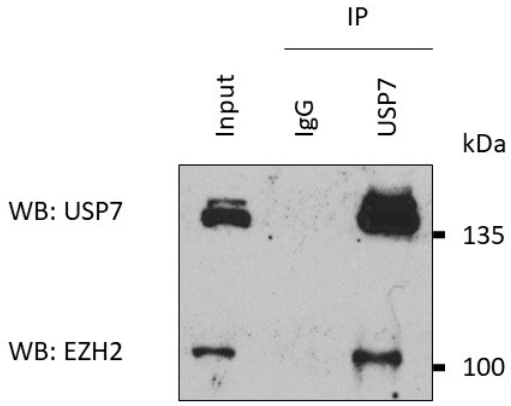

Figure 2-7. Endogenous EZH2 and USP7 interact. Endogenous USP7-EZH2 co-immunoprecipitation in U2OS cells. USP7 and EZH2 were immunoprecipitated with anti-USP7 rabbit using Protein A/G beads. The control for the immunoprecipitation was normal rabbit IgG. The input (5%) and elutions (25 μL) were resolved on a 10% SDS-polyacrylamide gel and subjected to immunoblotting with anti-USP7 mouse and anti-EZH2 mouse antibodies.

2.3.4 Direct interaction between USP7 and EZH2

The peptide GST-EZH2 450-500 containing the predicted interaction sequence ^{489}PRKKKRK^{495} was expressed and purified in BL21 MGK *E. coli* to perform GST pull-downs with His-USP7 constructs (**Figure 2-8**). To determine if the USP7-EZH2 interaction is dependent on the ^{761}MDGD^{764} sequence in USP7, we expressed and purified His-USP7 CTD encompassing Ubl1-5 (residues 535-1102) constructs: wildtype (WT, MDGD), and mutants MRGR D762R/D764R, MAGD D762A, and MAGA D762A/D764A. To conduct the GST pull-down, GST-EZH2 450-500 bound to glutathione agarose was incubated with purified Ubl1-5 constructs. In comparison to the empty GST beads (negative control), wild-type Ubl1-5^{WT} eluted from the GST-EZH2 450-500 bound beads and not from the GST alone (**Figure 2-8, A**). The Ubl1-5^{MRGR} mutant did not appear to interact as strongly as the wild-type. Furthermore, when the interaction of the single

mutant Ubl1-5^{MAGD} versus Ubl1-5^{MAGA} is compared, the interaction of the double mutant with GST-EZH2 450-500 appeared to be severely attenuated in comparison to the single mutant (**Figure 2-8, B**).

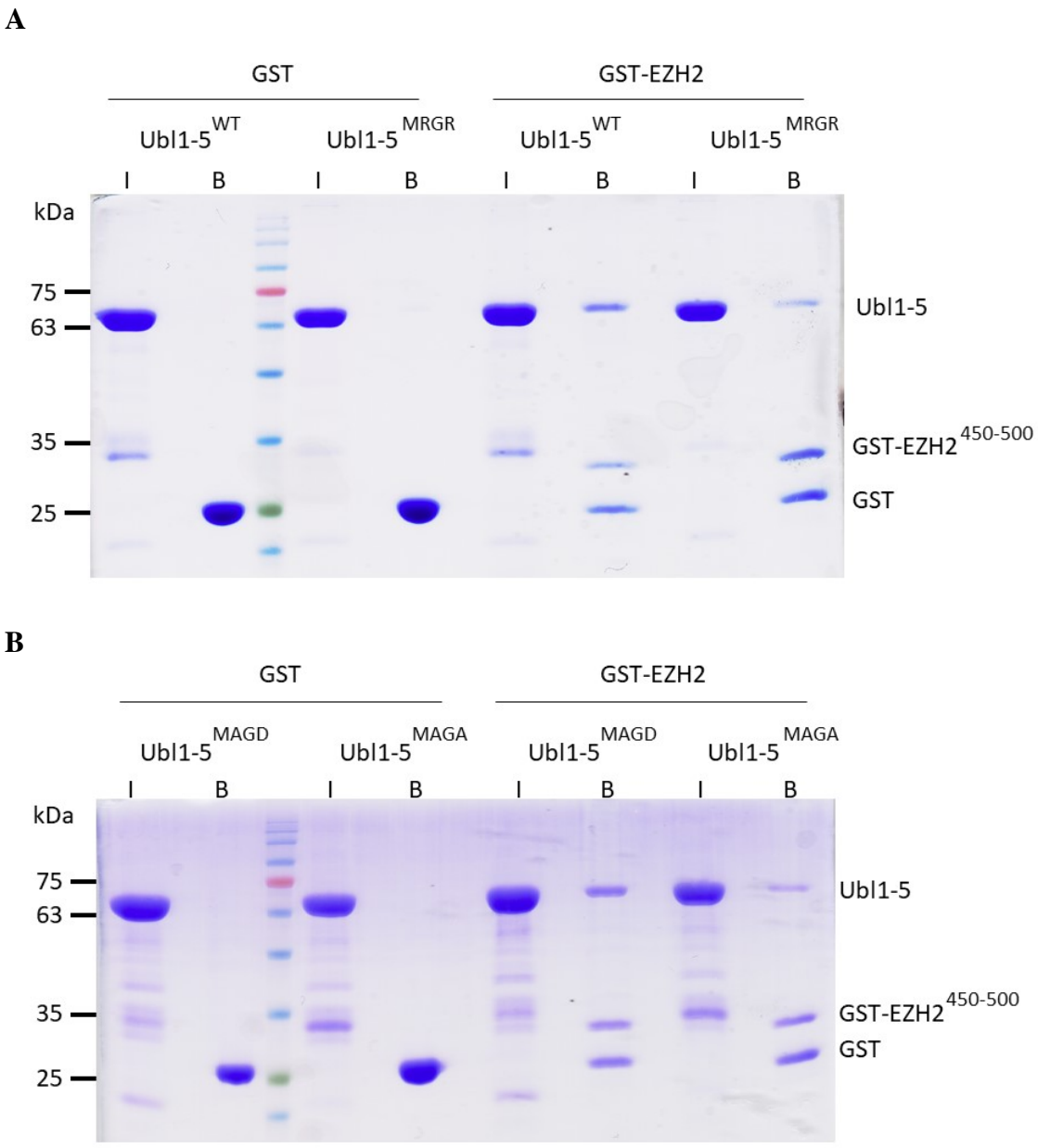

Figure 2-8. EZH2 interacts with USP7-CTD via MDGD *In Vitro*. GST-Pulldown of GST-EZH2$^{450-500}$ and 6xHis-USP7-CTD (Ubl 1-5) WT and mutants (MRGR, MAGD, MAGA). Ubl1-5 was incubated with GST or GST-EZH2$^{450-500}$ bound to GSH-agarose. The 5% input (I) and 20 μL bead (B) fractions were resolved on a 12% SDS-polyacrylamide gel and stained with Coomassie

Blue. **(A)** GST pull-down of GST and GST-EZH2$^{450\text{-}500}$ with Ubl1-5^{WT} or UBl1-5^{MRGR} **(B)** GST pull-down of GST and GST-EZH2$^{450\text{-}500}$ with Ubl1-5^{MAGD} or UBl1-5^{MAGA}.

2.3.5 EZH2 interacts with USP7 using a KxxxK motif

Additionally, FLAG-EZH2 mutants were utilized to perform a co-immunoprecipitation in U2OS cells with endogenous USP7 (**Figure 2-9**). U2OS cells were transfected with either: pcDNA3.1-FLAG, wild-type FLAG-EZH2, or mutant FLAG-EZH2. Two FLAG-EZH2 mutants were generated, the FLAG-EZH2$^{\Delta\text{-MUT}}$ deletion mutant lacking ^{491}KKKRK^{495} and FLAG-EZH2$^{TR\text{-MUT}}$ truncated at residue 490. The largest amount of USP7 co-immunoprecipitated with wild-type FLAG-EZH2 compared to the empty vector control and both the FLAG-EZH2 mutants. It should be noted that there is a high background, evident by the appearance of USP7 in the empty vector control.

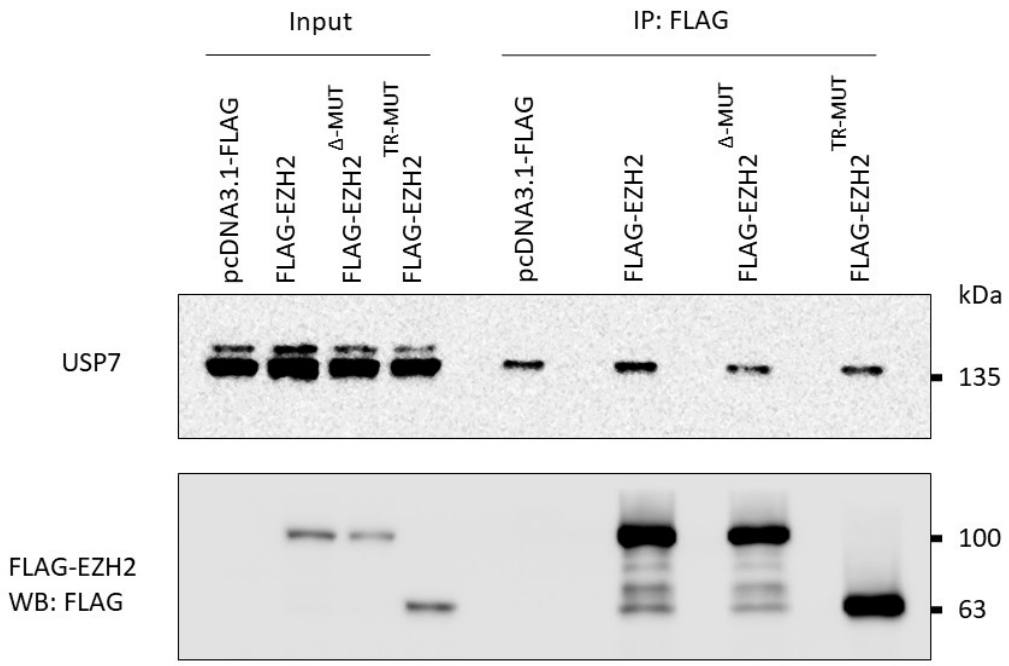

Figure 2-9. USP7-EZH2 interaction dependent on KKKRK. FLAG-EZH2 and endogenous USP7 co-immunoprecipitation in U2OS cells. U2OS cells transfected with 10 μg of pcDNA3.1-FLAG, FLAG-EZH2, FLAG-EZH2$^{\Delta\text{-MUT}}$, or FLAG-EZH2$^{TR\text{-MUT}}$. FLAG-EZH2 was immunoprecipitated using anti-FLAG agarose resin. The inputs (2%) and elutions (20 μL) were resolved on a 10% SDS-polyacrylamide gel immunoblotted with anti-ECS (FLAG) and anti-USP7 rabbit antibodies.

2.3.6 USP7 deubiquitinates EZH2

After characterizing the interaction between EZH2 and USP7, we sought to identify whether USP7 deubiquitinates EZH2 by performing a deubiquitination assay (**Figure 2-10**). HeLa cells were transfected with either FLAG-EZH2, FLAG-EZH2 and HA-Ub, or FLAG-EZH2 and HA-Ub with Myc-USP7. FLAG-EZH2 was immunoprecipitated, and the elution was probed using anti-HA to detect ubiquitination of FLAG-EZH2. When HA-Ub and FLAG-EZH2 were co-transfected, FLAG-EZH2 was ubiquitinated indicated by the presence of a smear. Upon the co-transfection of HA-Ub, FLAG-EZH2 and Myc-USP7, the intensity of the smear is greatly diminished. This suggested that USP7 deubiquitinates FLAG-EZH2.

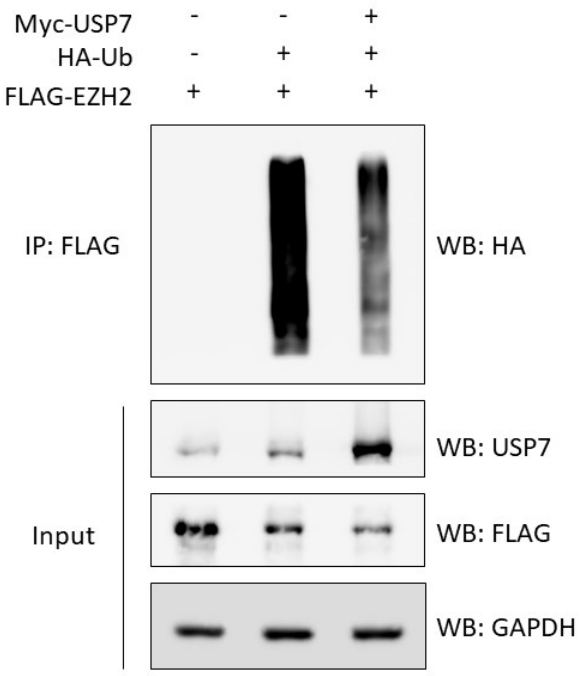

Figure 2-10. USP7 Deubiquitinates EZH2. EZH2-USP7 Deubiquitination assay in HeLa cells. HeLa cells transfected with FLAG-EZH2, HA-Ub and FLAG-EZH2, or HA-Ub, FLAG-EZH2 and Myc-USP7 were treated with 20 μM of MG132 8 hours before harvest. The cells were harvested 24 hours post-transfection and the cell lysates were immunoprecipitated with anti-FLAG M2 agarose to purify FLAG-EZH2. The inputs (1.33%) and elutions (20 μL) were resolved on separate 10% polyacrylamide gels and subjected to immunoblotting with: anti-USP7 rabbit, anti-ECS (FLAG), anti-GAPDH mouse, anti-HA rabbit antibodies.

2.3.7 USP7 mediates EZH2 function

Lastly, to determine the effect of USP7 on the downstream function of EZH2 we compared parental HCT116 cells with a HCT116 USP7$^{-/-}$ cell line (**Figure 2-11**). In comparison to the parental cell line, the USP7$^{-/-}$ cells exhibited a decrease in both EZH2 as well as H3K27me3.

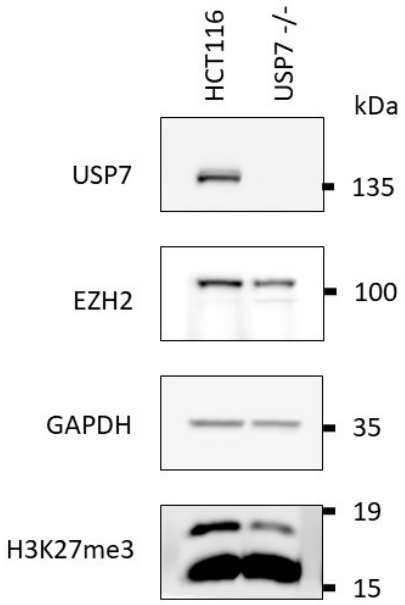

Figure 2-11. USP7 Mediates EZH2 Function. Immunoblot of HCT116 USP7$^{+/+}$ and HCT116 USP7$^{-/-}$. 10 μg of cell lysates resolved on a 12% SDS-polyacrylamide gel, immunoblotted with anti-USP7 rabbit, anti-EZH2 mouse, anti-GAPDH mouse, anti-H3K27me3 rabbit antibodies.

2.4 DISCUSSION

This project revolved around characterizing the interaction and regulatory relationship between USP7 and EZH2. I expanded on previous work in our lab that suggested the ^{761}MDGD^{764} interaction site located in the CTD of USP7 interacts with the ^{491}KKKRK^{495} sequence of EZH2. To enhance the understanding of EZH2 regulation, we queried whether the stability of EZH2 is dependent on the UPS system and the involvement of USP7. Next we determined whether EZH2 and USP7 interact in a physiologically relevant manner and the key residues involved in this interaction. Lastly, we aimed to elucidate whether EZH2 is a substrate of USP7 and whether this interaction affects the downstream function of EZH2. Most recently, four other papers similarly reported the USP7-EZH2 interaction [216–219]. The findings of their work are discussed and compared in this section.

2.4.1 EZH2 stability is UPS dependent

To determine if EZH2 stability is dependent on the UPS system we treated HCT116 USP7$^{+/+}$ cells and USP7$^{-/-}$ cells with a proteasomal inhibitor and investigated the effect on EZH2 stability (**Figure 2-6**). Upon proteasomal inhibition, EZH2 was increased in both USP7$^{+/+}$ and USP7$^{-/-}$ cells, suggesting that EZH2 stability is regulated by a deubiquitinating enzyme. The increase of EZH2 levels appeared to be more drastic in the USP7$^{-/-}$ cells. This data implied that USP7 regulates EZH2. In fact, this is corroborated by the comparison of EZH2 in HCT116 USP7$^{+/+}$ cells versus the USP7$^{-/-}$ cells. The EZH2 levels appear to be lower in the USP7$^{-/-}$ cells. Further supporting our findings, similar experiments in prostate (DU145, PC3), embryonic (293T), melanoma (A375), and colorectal (SW480) cell lines observed the increase of EZH2 levels upon treatment with a proteasomal inhibitor [216,217,219]. Additional experiments conducted by our lab have shown overexpression of USP7 results in increased levels of USP7 and USP7 knock-down results in EZH2 reduction [57]. Altogether, this data persuasively suggests the stability of EZH2 is dependent on USP7.

2.4.2 USP7 and EZH2 interact in Human Osteosarcoma cells

We performed an endogenous EZH2-USP7 co-immunoprecipitation to determine if the interaction is biologically valid (**Figure 2-7**). We were able to co-immunoprecipitate EZH2 with USP7, which supported our hypothesis that EZH2 and USP7 interact. The endogenous interaction was also demonstrated in melanoma (A375) and embryonic (HEK293T) cell lines [216,217]. Previous experiments by our lab have additionally shown that USP7 and EZH2 interact by overexpressing Myc-USP7 and FLAG-EZH2 and co-immunoprecipitating both proteins [215]. Additionally, another group performed a co-immunoprecipitation of USP7-EZH2 in 293T and DU145 cell lines overexpressing FLAG-EZH2 or FLAG-USP7 [219]. Likewise, the group observed the co-immunoprecipitation of USP7-EZH2.

2.4.3 USP7 interacts with EZH2 via ^{761}MDGD^{764}

We further sought out to characterize the interaction sites and residues involved in facilitating the interaction using an *in vitro* pull-down experiment. By analyzing the EZH2 sequence, we had predicted that ^{489}PRKKKRK^{495} would interact with the ^{761}MDGD^{764} USP7 interaction site. To test this hypothesis previous members of our lab performed a GST pull-down with GST-EZH2$^{487\text{-}498}$ and His-Ubl1-5. The results suggested GST-EZH2$^{487\text{-}498}$ interacted with wild-type Ubl1-5 and Ubl1-3, but lacked interaction with Ubl1-5^{MAGD}, and Ubl1-3^{MAGA} mutants [215]. To further explore this interaction I performed a pull-down with a longer EZH2 peptide, GST-EZH2$^{450\text{-}500}$ and His-Ubl1-5^{WT}, as well as the mutants His-Ubl1-5^{MRGR}, His-Ubl1-5^{MAGD}, and His-Ubl1-5^{MAGA} (**Figure 2-8**). The mutants harboured a substitution of the negatively charged D762/764 residues to either R, a positively charged amino acid, or A, an un-charged, smaller amino acid. In comparison to wild-type Ubl1-5, the MRGR mutant exhibited an attenuated interaction with GST-EZH2$^{450\text{-}500}$ (**Figure 2-8, A**). This experiment supported our hypothesis that USP7 and EZH2 interact via the predicted sequences and emphasized the importance of aspartate residues in the ^{761}MDGD^{764} domain. Furthermore, a pull-down with GST-EZH2$^{450\text{-}500}$ and MAGD and MAGA mutants showed that both aspartate residues are required to mediate the interaction (**Figure 2-8, B**). When comparing the elution fractions for MAGD and MAGA, it is evident that mutation of both residues causes a significant reduction in binding. However,

mutation of both aspartate residues does not completely abolish the interaction, as both MRGR and MAGA mutants appear to retain binding. This implies the possibility of additional residues in mediating the interaction. The *in vitro* pull-down also suggests that the USP7-EZH2 interaction is a direct interaction, as opposed to an indirect interaction via a complex.

To explore the importance of the K residues in the predicted ^{489}PRKKKRK^{495} interaction sequence, our group had previously conducted *in vitro* pull-down experiments. In comparison to wild-type, K495A GST-EZH2$^{487-498}$ exhibited a significant loss of interaction between Ubl1-5 [215]. We wanted to further characterize this interaction in mammalian cells by immunoprecipitating FLAG-EZH2, FLAG-EZH2$^{\Delta\text{-MUT}}$ (deletion mutant lacking ^{491}KKKRK^{495}), or FLAG-EZH2$^{\text{TR-MUT}}$ (truncated at residue 490) (**Figure 2-9**). Endogenous USP7 was found to co-immunoprecipitate the strongest with wild-type FLAG-EZH2. The mutant FLAG-EZH2 interactions displayed USP7 co-immunoprecipitation comparable to that of the control. These findings corroborated our previous data on the significance of the ^{491}KKKRK^{495} sequence in mediating USP7 interactions. This experiment was limited by the presence of high background in the elution sample of the control; thus, it should be repeated with more stringent washes.

Our group's collective data has provided extensive evidence corroborating the EZH2-USP7 interaction. In addition to the data in this chapter, our group has co-crystallized the ^{487}TPPRKKKRKHRL^{498} EZH2 peptide with Ubl123, a USP7-CTD construct, determining the structure of the complex and characterizing the nature of the interaction [57]. As predicted the KxxxK motif in highly involved in the interaction, EZH2 residues K491 and K495 form salt bridges with D762 and D764 in Ubl123. The R490 and K492 residues in the EZH2 peptide participated in interactions with the Ubl123 residues D754 and L760. Moreover, our group used fluorescence polarization assays to demonstrate that the EZH2$^{487-498}$ peptide interacts with Ubl123, but not the NTD of USP7.

Interestingly, EZH2 T345 and T487 have been found to undergo phosphorylation by the mitotic kinase, CDK1 (cyclin dependent kinase) [220,221]. The phosphorylation of EZH2 at these residues is found to be enhanced at mitosis and is thought to promote ubiquitination and destabilization of EZH2 [221]. It is interesting to note the proximity of the T487 residue to the predicted ^{489}PRKKKRK^{495} interaction motif. Considering this finding, the question arises of whether USP7

can bind EZH2 and prevent T487 phosphorylation and subsequent ubiquitination, and whether this potential mode of regulation is dependent on the cell cycle. This presents an additional potentially unexplored avenue of EZH2 regulation by USP7.

In contrast to our proposed interaction, Su et al. suggested EZH2 interacts with the TRAF domain of USP7 [216]. An *in vitro* pull down of full-length GST-EZH2 and His-USP7 constructs (TRAF, Catalytic domain, Ubl1-5) suggested interaction via the TRAF domain. Furthermore, pulldowns of full-length FLAG-USP7 and GST-EZH2 constructs (EZH2 N1 (1-173), N2 (174-340), C1(341-559), and C2 (560-751)) mapped the interaction site to N1. As our results suggested, the interaction between EZH2 and USP7 may involve multiple interaction sites. If this is the case, it would not be unique to the EZH2-USP7 interaction. In fact, USP7 substrates p53 and HDM2 have both been characterized to interact with both the N-terminal and C-terminal domains of USP7 [64,71].

2.4.4 USP7 deubiquitinates EZH2

To determine if EZH2 is a USP7 substrate, we performed a deubiquitination assay. HeLa cells were transfected with FLAG-EZH2, FLAG-EZH2 and HA-Ub with and without Myc-USP7 and treated with a proteasomal inhibitor. FLAG-EZH2 was immunoprecipitated and the immunoprecipitated FLAG-EZH2 was probed for ubiquitination (**Figure 2-10**). Transfection of FLAG-EZH2 and HA-Ub presented as a dark smear, indicating the accumulation of ubiquitinated and polyubiquitinated FLAG-EZH2. In contrast, the transfection of FLAG-EZH2, HA-Ub and Myc-USP7 resulted in decreased smear intensity, indicating a reduction in ubiquitinated FLAG-EZH2. Indeed, EZH2 appears to be deubiquitinated by USP7 and this result was replicated by [216,219]. Zheng et al., performed a deubiquitination assay with catalytically inactive C223S USP7 mutant and observed the attenuation of EZH2 deubiquitination by USP7. Additionally, Su et al. demonstrated that USP7 can deubiquitinate K48-linked polyubiquitin chains from EZH2 but not K63-linked polyubiquitin chains. As mentioned previously K48-linkages are associated with proteasomal degradation while K63-linkages are UPS independent.

Curiously, HDM2/HDMX has been recently identified as a novel EZH2 E3 ubiquitin ligase, mediating cell sensitivity to DNA damage [213]. The authors suggested the chromatin condensation

promoted by EZH2 enhances cellular resistance to DNA damage. From a clinical perspective, the authors propose the use of HDM2/HDMX inhibitors to protect renewable tissues from DNA damage induced by chemo-/radiotherapy. Considering that HDM2/HDMX are well defined USP7 substrates, it would be fascinating to investigate if USP7 plays a role in this regulatory axis [90].

2.4.5 USP7 affects EZH2 downstream function

Finally, we sought out to determine if USP7 regulates the downstream function of EZH2 by affecting H3K27me3 (**Figure 2-11**). Our previous data suggested USP7 stabilizes EZH2, thus we expected $USP7^{-/-}$ cells to exhibit reduced levels of EZH2 and H3K27me3 compared to the HCT116 $USP7^{+/+}$ cells. Indeed, as we anticipated, $USP7^{-/-}$ cells possessed attenuated levels of EZH2 as well as H3K27me3. In agreeance with our findings, another group had demonstrated the loss of H3K27me3 in response to USP7 knock-down or knock-out in melanoma cell lines [216]. Interestingly, the authors suggested that the loading of the PRC2 complex is preceded by deubiquitination of H2BK120 by USP7. As previously stated, USP7 has been characterized to deubiquitinate monoubiquitinated H2BK120 [145]. Su et al. showed that knock-down of USP7 coincided with increased H2BK120Ub and decreased H3K27me3 levels despite overexpression of EZH2 in three melanoma cell lines.

2.4.6 USP7-EZH2 mechanisms and clinical relevance

Several groups have now defined the USP7-EZH2 interaction in neural progenitor cells as well as laryngeal squamous cell carcinoma (LSCC), melanoma, and prostate cancer.

In the context of LSCC, elevated levels of USP7 were correlated with high levels of EZH2 and poor prognosis [218]. The authors used immunohistochemical staining to determine the expression of USP7 and EZH2 in normal laryngeal tissues and LSCC, identifying USP7 and EZH2 as biomarkers for LSCC. Likewise, USP7 and EZH2 expression correlates with both the grade and prognosis of melanoma patients [216]. Further corroborating our findings, USP7 was found to associate with the PRC2 complex and stabilize EZH2 in melanoma cells. In prostate cancer cells,

the overexpression of USP7 resulted in enhanced proliferation, migration and invasion [219]. These effects were attenuated with co-transfection of USP7 and EZH2-shRNA, indicating that USP7 promotes prostate carcinogenesis via EZH2 stabilization. *In vivo* mouse xenograft experiments showed that deletion of USP7 decreased EZH2 and repressed prostate tumorigenesis. Clinical prostate cancer tissues were shown to correlate with increased levels of USP7 and EZH2.

In the context of melanoma, the USP7-EZH2 regulatory axis was found to affect the regulation of the FOXO1 (Forkhead Box O1) transcription factor [216]. FOXO1 is responsible for regulating the expression of genes for gluconeogenesis. Interestingly, USP7 was found to deubiquitinate FOXO1 and prevent its association with the promoters of gluconeogenic genes [222]. In melanoma cells, EZH2 was found to be enriched at USP7 binding regions, such as the promoter of FOXO1 [216]. Upon knock-down of USP7 or EZH2, the expression of both FOXO1 mRNA and protein was increased. Su et al. showed that the inhibition of USP7 and EZH2 in melanoma cells and xenografted mice resulted in repressed cell proliferation due to the upregulation of FOXO1. The comparison of normal human tissue with clinical melanoma samples revealed elevated levels of USP7 and EZH2, as well as reduced levels of FOXO1 expression. The increased levels of EZH2 and USP7 as well as a reduction in FOXO1 were correlated with the histological grade of the melanoma. Furthermore, enhanced expression of USP7 correlated with poor prognosis of melanoma patients. This fascinating axis should be further investigated in other forms of cancer. In fact, FOXO1 is known to be downregulated in breast and prostate cancer [223]. It would be interesting to investigate whether USP7 and EZH2 are involved in the downregulation of FOXO1 in these forms of neoplasms.

Additionally, the USP7-EZH2 axis was found to be essential in promoting cancer and neural stemness [217]. Lei et al. proposed a model in which USP7 is recruited by EZH2, to stabilize EZH2 as well as DNMT1, HDAC1, LSD1, β-catenin, SMAD2/4. The stabilization of these factors prevented neuronal differentiation of progenitor cells by repressing the expression of neuronal-specific genes. In contrast, the inhibition of EZH2 or USP7 promoted differentiation and resulted in a loss of stemness in neural progenitor cells. These findings underscore the importance of USP7-EZH2 regulatory axis in maintaining key proteins that promote tumorigenesis.

CHAPTER 3 : RBP2 and USP7

3.1 INTRODUCTION

Histone methylation was once thought to be irreversible until the discovery of Lysine-specific demethylase 1 (LSD1) [224]. LSD1 is responsible for demethylating mono- and di-methylated H3K4. There are two groups of histone demethylases: LSD demethylases and jumonji C (JmjC) domain containing demethylases [225]. LSD demethylases include LSD1 and LSD2, and are dependent on flavin adenine dinucleotide (FAD) to demethylate mono- and di-methylated lysines (**Figure 3-1, A**). The JmjC family contains 30 members in humans, and require Fe(II) and α-ketoglutarate for the demethylating function (**Figure 3-1, B**) [226]. While flavin-dependent demethylases act on mono- and di-methylated residues, JmjC domain containing demethylases act on mono-, di-, and tri-methylated residues. However, limited information exists on the mechanisms that control the activities of histone lysine demethylases.

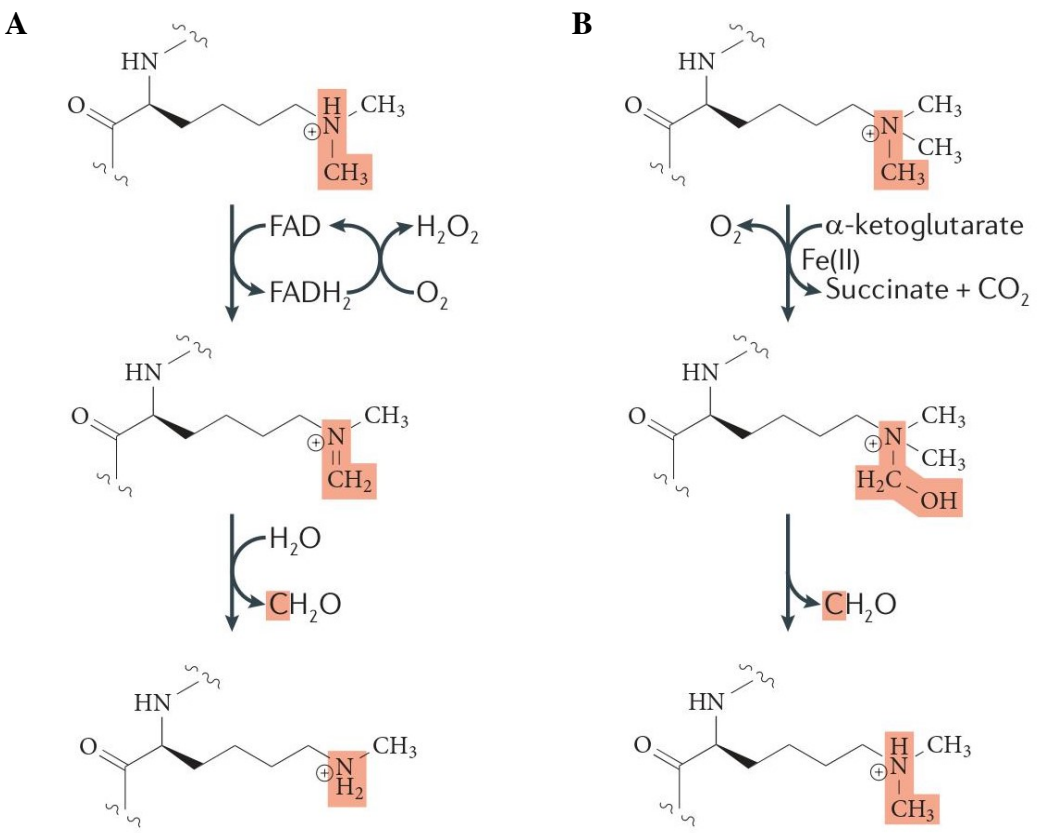

Figure 3-1. Catalytic mechanisms of Histone demethylases. There are two groups of histone demethylases, LSD demethylases and jumonji C (JmjC) domain containing demethylases. These two groups use distinctive reaction mechanisms to catalyze the removal of methyl groups from histone lysine residues. A) LSD1 and LSD2 demethylases are dependent on flavin adenine dinucleotide (FAD) to demethylate mono- and di-methylated lysines. B) In contrast, JmjC demethylases require Fe(II) and α-ketogluterate are required for the demethylating function and are able to act on mono-, di-, and tri-methylated residues. Adapted from [227].

3.1.1 The KDM5 demethylase subfamily

The KDM5 subfamily of histone demethylases consists of four members KDM5A, KDM5B, KDM5C, and KDM5D [228]. KDM5 histone demethylases are conserved among species, and the members of the family share a high degree similarity in domain architecture (**Figure 3-2**). All KDM5 subfamily members possess a Jumonji N Domain (JmjN), an AT-rich interacting domain (ARID) for DNA binding, at least two plant homeodomain (PHD) domains required for histone recognition, the catalytic Jumonji C Domain (JmJC), and a C5HC2 zinc-finger domain (C5HC2)

[228,229]. KDM5A and KDM5B both have a third PHD domain (PHD3). It has been reported that KDM5 proteins possess regulatory roles that are independent of their demethylase function, suggested to involve PHD3 domains [230].

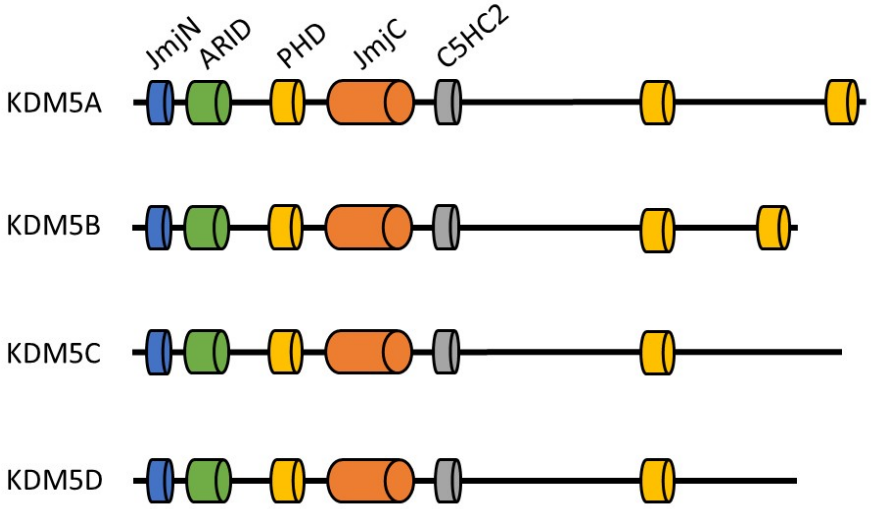

Figure 3-2. Domain organization of KDM5 family proteins. The KDM5 family of proteins consist of KDM5A, KDM5B, KDM5C, and KDM5D in humans. The members of the KDM5 family share similar domain organization, all harbouring JmjN, Jumonji N Domain; ARID, AT-rich interacting domain; PHD, plant homeodomain; JmJC, Jumonji C Domain; C5HC2, C5HC2 zinc-finger domain. KDM5A and KDM5B both have a third PHD domain (PHD3).

This family of histone demethylases catalyzes the removal of dimethyl (Me2) and trimethyl (Me3) modifications from H3K4. The methylation of H3K4 is evolutionarily conserved and associated with transcriptional activation [231]. Depending on the degree H3K4 methylation, the location of the histone methylation can vary, as well as the effect the modification imposes on the genomic region. For instance, H3K4me1 was found to be enriched at enhancers, and depleted at active promoters [232]. In comparison, H3K4me2 has been observed to be present at both promoters and enhancers, as well as the 5'end of transcribing genes [232,233]. The dimethylation of H3K4 has been shown to occur at both inactive and active euchromatic genes and is associated with repressed nucleosome acetylation and remodeling [233,234]. Interestingly, promoters are marked with H3K4me3 and the presence of this mark coincides with increased acetylation and decreased nucleosome density at promoters [232,233].

There has been an increasing amount of evidence from primary tumours, as well as knock-out mouse models that have established KDM5 members as key players in human cancer and disease. Particularly, KDM5A and KDM5B are considered to be oncogenic drivers due to their frequent mutation in a plethora of human cancers [229]. KDM5A and KDM5B are promising therapeutic targets and efforts are currently underway to develop enzymatic inhibitors. Dysregulation of KDM5C have been linked with X-linked mental retardation, Huntington disease and renal cell carcinoma.

3.1.2 RBP2 role in a cell

The focus of our project is the ubiquitously expressed demethylase KDM5A, also known as the Retinoblastoma-Binding Protein 2 (RBP2). RBP2 was originally isolated as a binding partner of Rb [235]. Rb is a tumour suppressor protein that has been found to be frequently inactivated in various forms of cancer [236]. Rb is responsible for cell cycle arrest, inhibiting entry into S-phase until the cell is ready to divide, as well as promoting differentiation and senescence of cells. The ability of Rb to promote differentiation and senescence is associated with its interaction with RBP2 [237]. By interacting with RBP2, Rb prevents RBP2 from repressing genes required for differentiation. Apart from RBP2's interaction with Rb, the majority of RBP2's genomic targets are involved in cellular differentiation [238–241]. RBP2 gene targets are not solely restricted to genes involved in cellular differentiation. RBP2 represses expression of the progesterone receptor in the MCF-7 human breast cancer cell line [242], Additionally, RBP2 has also been shown to play an essential role in mitochondrial biogenesis by regulating mitochondrial genes [243]. RBP2 has been shown to silence the telomerase reverse transcriptase (hTERT) gene, which is widely activated in cancerous cells [244]. Loss of RBP2 resulted in a significant increase in hTERT expression in EBV-immortalized cells. Moreover, RBP2 has also been involved in regulation gene-expression in a demethylase-independent manner [245]. By inhibiting histone deacetylase (HDAC) mediated repression, RBP2 promotes the cyclic transcription of circadian genes by CLOCK-BMAL1.

3.1.3 RBP2 domain organization

RBP2 is a 1690 amino acid protein that has two isoforms, isoform 1 and isoform 2. Beginning at the N terminus, RBP2 harbours a JmjN domain (residues 25-59), followed by the ARID domain (residues 85-170) (**Figure 3-3**) [225]. The ARID domain is involved in DNA binding and has been shown to bind a CCGCCC motif and is essential in regulating transcription [246]. Residues 295-343 encompass the first PHD domain. The PHD domain can bind to certain methylated residues and allows for the recruitment of HDACs. The first PHD domain preferentially binds unmethylated H3K4 histone tail and this binding stimulates the catalytic activity of RBP2 [225]. This is followed by the catalytic domain, the JmjC domain (residues 470-586). The C5HC2 zinc finger domain (ZF) is located between residues 676-729. Finally, towards the C terminus of the protein, RBP2 possesses two more PHD domains (PHD2 and PHD3).

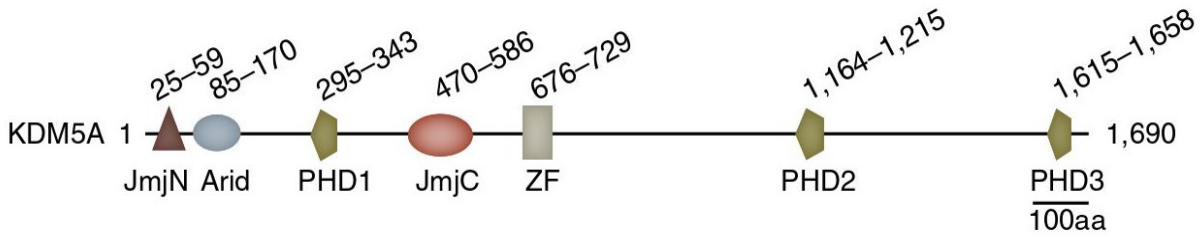

Figure 3-3. RBP2 Domain Organization. JmjN, Jumonji N Domain; ARID, AT-rich interacting domain; PHD, plant homeodomain; JmjC, Jumonji C Domain; ZF, C5HC2 zinc finger domain [225].

3.1.4 RBP2 in human disease

RBP2 is a critical regulator in the expression of loci linked to development, differentiation, circadian rhythm, mitochondrial function, and oncogenesis. The importance of RBP2 was demonstrated by RBP2's extensive implication in human pathologies. RBP2 dysregulation is associated with various forms of cancer such as cervical cancer [247], lung cancer [248], melanoma [249],

breast cancer [250], renal cell carcinoma [251], neuroendocrine tumours [252,253], leukemia [254], and gastric cancer [255].

RBP2 has been linked with acute myeloid leukemia [254,256]. Patients with acute myeloid leukemia express a fusion protein between NUP98 (nucleoporin-98) and the C-terminal PHD3 finger of RBP2 [254]. The resulting NUP98-PHD3 fusion protein specifically recognizes H3K4me2/3 marks but lacks the demethylase domain of RBP2. Thus, NUP98-PHD3 is able to bind and prevent the removal of H3K4me3, resulting in a lack of gene silencing. The NUP98-PH3 fusion protein was found to be critical for leukaemogenesis. Its aberrant function causes developmental loci to 'locked' in an active chromatin state.

In gastric cancer RBP2 levels were found to be elevated, and inhibition of RBP2 triggered cell senescence [255]. Furthermore, RBP2 plays a role in promoting metastasis and epithelial-to-mesenchymal transition by repressing E-cadherin, as well as promoting angiogenesis by enhancing VEGF expression [257,258]. Interestingly, the bacterium *Helicobacter pylori*, closely associated with the development of gastric cancer, was found to induce RBP2 expression [259]. This induction was mediated by the *H. pylori* virulence factor, CagA which is known to activate the PI3K/AKT-Sp1 pathway. Enhanced expression of Sp1 induced by the PI3K/AKT signaling pathway binds the promoter of RBP2 and stimulates its expression. The knockdown of RBP2 was shown to inhibit gastric cancer *in vivo*.

Interestingly, RBP2 was found to be related to susceptibility and severity of ankylosing spondylitis, an inflammatory disease that typically targets the sacroiliac joints and the spine [260,261].

Collectively, these findings present RBP2 as an ideal target for cancer therapy and efforts are currently underway to develop small molecule inhibitors [262].

3.1.5 Project Rational

USP7 plays a critical role in many cellular functions and has been involved in epigenetic regulation. Our group was interested to investigate if USP7 plays a role in regulating RBP2. The dysregulation of both RBP2 and USP7 has been associated with numerous human pathologies.

Developing a better understanding of their respective functions and roles in a cell may aid in the understanding of mechanisms underlying certain human pathologies.

On the basis of our previous work and literature, we analyzed the RBP2 sequence and identified numerous potential interaction motifs, including KxxxK as well as P/A/ExxS motifs. We hypothesized that RBP2 and USP7 interact, and that USP7 may play a regulatory role in RBP2 stability. We aimed to investigate the potential regulatory role of USP7 on RBP2 in mammalian cells. Once our data suggested USP7 stabilizes RBP2, we characterized the interaction between USP7 and RBP2 in mammalian cells and *in vitro*. Lastly, we intended to further elucidate the USP7-RBP2 regulatory axis by investigating the effect on RBP2 downstream H3K4 demethylating function in mammalian cells.

3.2 MATERIALS AND METHODS

3.2.1 Plasmids

The plasmids used for bacterial transformation and expression were: pGEX-2TK, pGEX-2TK/CTD-USP7$^{535\text{-}1102}$. The plasmids used for mammalian transfection were: pcDNA3, pCAN/Myc-USP7, pCAN/Myc-USP7^{C223S}, pCAN/Myc-USP7^{MRGR}, pCAN/Myc-USP7$^{DW\text{-}MRGR}$, pcDNA3.1/FLAG, pcDNA3/HA-FLAG-RBP2. pcDNA3/HA-FLAG-RBP2 was a gift from William Kaelin (Addgene plasmid # 14800)

3.2.2 Bacterial Transformation

1 µL of plasmid was added to 50 µL of thawed chemi-competent DH5α cells or BL21 (DE3) mgk *Escherichia coli* and incubated on ice for 10 minutes. The cells were then heat-shocked for 45 seconds at 42°C and incubated on ice for 2 minutes. Afterwards, 100µL of SOC was added and the cells were incubated for 30 minutes at 37°C and then plated on LB agar containing the required antibiotic (100 µg/ml Ampicillin and/or 50 µg/ml Kanamycin). The plates were then incubated overnight, and a single colony was chosen to inoculate 5 mL of LB which was incubated in a shaker overnight at 37°C (200 rpm) (Innova 43R, New Brunswick Scientific). An aliquot was used to make a glycerol stock.

3.2.3 Bacterial Expression of GST-Ubl1-5

BL21 (DE3) mgk *E. coli* were transformed with either pGEX-2TK or pGEX-2TK/CTD-USP7$^{535\text{-}1102}$ and a colony was picked and inoculated into 100 mL of LB media with 100 µg/ml Ampicillin and 50 µg/ml Kanamycin and grown at 37°C at 200 rpm until the OD_{600nm} of the media reached 0.8-1 (Innova 43R, New Brunswick Scientific). Once the OD_{600nm} reached 0.8-1 the culture was induced with 0.4mM of IPTG (Bioshop) and incubated overnight at 16°C at 200 rpm. The cells were pelleted by centrifugation at 5,000 x g for 10 minutes with a JLA 16.250 Beckman rotor (Beckman Coulter Avanti J-E centrifuge).

3.2.4 GST Purification of GST-Ubl1-5

The bacterial cell pellet expressing was resuspended in 15 mL of 1X PBS (pH 7.4) with 1X Protease inhibitor cocktail and 1X Protease inhibitor tablet (cOmplete ULTRA Tablets, Roche). The cells were sonicated on ice at 35% amplitude for 4 minutes (10 seconds ON, 15 seconds OFF, Branson Digital Sonifier). To collect the soluble fraction, the cell lysate was centrifuged at 30,000 x g for 20 minutes at 4°C with a JA-25.50 Beckman rotor (Beckman Coulter Avanti J-E centrifuge). The clarified cell lysate was incubated with 150 µL of Glutathione Sepharose 4B (GE Healthcare) and incubated at 4°C for 1 hour with rotation. The beads were then washed five times with 5 mL of 1X PBS.

3.2.5 GST-Ubl1-5 and FLAG-RBP2 pulldown

HeLa cells P39 (15 cm tissue culture dish) were transiently transfected with 10 µg of either pcDNA3.1/FLAG or pcDNA3/HA-FLAG-RBP2 using PolyJet™. The cells were harvested 24 hours post-transfection and resuspended in M2 Lysis buffer (50 mM Tris HCl [pH 7.4], 150 mM NaCl, 1 mM EDTA, 1% Triton X-100, 1X Protease inhibitor cocktail and 1X Protease inhibitor tablet (Roche cOmplete ULTRA Tablets) and incubated at 4°C with agitation for 30 min. The lysate was clarified by centrifugation at 17,000 x g for 15 min at 4°C (Sorvall Legend Micro 17 R, Thermo Scientific) and the supernatant was collected and quantified (Pierce™ BCA Protein Assay Kit). To conduct the GST-pulldown, 25 µL (dry bead volume) of GST or GST-Ubl1-5 USP7 bound glutathione beads were combined with 700 µg of HeLa lysates transiently expressing pcDNA3.1/FLAG or pcDNA3/HA-FLAG-RBP2 and 1X GST interaction buffer (50 mM Tris [pH 8], 100 mM NaCl, 5% Glycerol, 5 mM DTT, 0.1 mM Benzamidine, 0.05 mM PMSF) for a total volume of 500 µL in the tube. The pull-down reactions were incubated for 2 hours at 4°C with agitation. Afterwards, the glutathione beads were washed five times with 1 mL of 1X PBS. Elution samples were made by boiling the beads with 80 µL of 1X SDS loading dye. The 3.4% input (HeLa lysate expressing pcDNA3.1/FLAG or pcDNA3/HA-FLAG-RBP2) and 20 µL of elution sample were resolved on a 4-20% Mini-PROTEAN® TGX™ Precast Protein Gel (BioRad) and transferred to a PVDF membrane 30V, overnight at 4°C. The following day

the PVDF membrane was blocked and blotted with the following antibodies: 1:4000 anti-JARID1A rabbit (Cell-signaling, D28B10), 1:4000 anti-GST mouse (Millipore,71097-3).

3.2.6 Mammalian Cell Culture, Transfection and Sample Preparation

Human osteosarcoma U2OS cells, colorectal carcinoma cell line HCT116 parental (John Hopkins University School of Medicine, Cell line #8 40-16), and HCT116 HAUSP -/- (4HAUSP2-4, John Hopkins University School of Medicine Cell line #89) were grown on McCoy's (Wisent) media containing 10% fetal bovine serum (FBS) and 1 mg/ml Penicillin-Streptomycin. Human cervical adenocarcinoma cell line HeLa was grown on Dulbecco's Modified Eagle Medium (DMEM, Wisent) media containing 10% FBS and 1 mg/ml Penicillin-Streptomycin. All cell lines were incubated at 37°C, 5% CO2. The cells were transfected using Polyjet^{TM} In Vitro DNA transfection reagent (SignaGen Laboratories) according to the manufacturer's protocol. To obtain cell lysates, cell pellets were resuspended in RIPA lysis buffer (150 mM NaCl, 50 mM Tris [pH 8.0], 1% NP-40, 0.5% sodium deoxycholate, 0.1% SDS, with 1X Protease inhibitor cocktail and 1X Protease inhibitor tablet (Roche cOmplete ULTRA Tablets)). After incubating the resuspended pellets on ice for 15 min, the samples were sonicated at 10% amplitude for 0.5 seconds ON and 5 seconds OFF for a total ON time of 1.5 seconds (Sonic Dismembrator Model 500, Fisher Scientific). To obtain the soluble fraction, the lysates were centrifuged for at 13,000 x g for 15 minutes at 4ºC. The supernatant was recovered, and samples were prepared by boiling the lysate with 1XSDS loading dye.

3.2.7 Antibodies and Immunoblotting

The following primary antibodies were used for immunoblotting: anti-USP7 rabbit (Bethyl, A300-033A), anti-USP7 mouse (Millipore, 05-1946), anti-GAPDH mouse (Santa-Cruz, sc047723), anti-ECS (FLAG) (Bethyl, A190-102A), anti-JARID1A (RBP2) rabbit (Cell-signaling, D28B10), anti-Myc HRP (Cell-signaling, 14038s), anti-Myc mouse (Millipore, 05-724), anti-H3K4me3 rabbit (Actif Motif, 39-60), anti-GST mouse (Millipore, 71097-3). For immunoprecipitation normal mouse IgG (Santa-Cruz, sc2025) was used.

After resolving protein samples on a SDS-polyacrylamide gel using SDS-PAGE, the gel would be transferred to a 0.45 µm Immobilon-P PVDF membrane (Millipore) activated according to the manufacturer's instructions. The transfers would typically be run 30V overnight at 4°C or 90V for 2.5 hours on ice using 1X Western Transfer Buffer (25 mM Tris [pH 8.3], 192 mM Glycine, and 20% methanol). Following transfer, the PVDF membrane would be blocked in 5% non-fat milk in 1X PBST for 1 hour at RT with rocking. The PVDF membrane would then be probed with primary antibodies overnight at 4°C. After primary antibody incubation, the membrane was washed three times with 1X PBS-T in 5 min intervals. Secondary antibody incubation was carried out for 1 hour at RT with the following antibodies: anti-mouse IgG HRP-conjugated goat polyclonal (ThermoFisher, 31430) or anti-rabbit IgG HRP-conjugated goat polyclonal (Bethyl, A120-101P). Afterwards, the membrane was washed four times with 1X PBS-T in 15 min intervals. The PVDF membrane was incubated for 5 minutes with Amersham ECL Prime Western Blotting Detection Reagent (GE Healthcare) according to the manufacturer's protocol. The immunoblot was imaged using a Microchemi® (DNR-IS) or the immunoblot was exposed to film and a processed through a developer.

3.2.8 Proteasomal Inhibition Using MG132

HCT116 USP7$^{+/+}$ and HCT116 USP7 $^{-/-}$ were incubated with DMSO or 40 µM of MG132 for 1 hour and harvested. 30 µg of sample was resolved on a 10% SDS-polyacrylamide gel, transferred to a PVDF membrane at 30V overnight at 4ºC. The membrane was blocked and blotted with the following antibodies: 1:3000 USP7 rabbit (Bethyl, A300-033A-M), 1:2000 anti-JARID1A rabbit (Cell-signaling, D28B10), 1:2000 GAPDH mouse (Santa-Cruz, sc047723).

3.2.9 RBP2 and USP7 Co-immunoprecipitation

To conduct the endogenous RBP2-USP7 co-immunoprecipitation, HeLa cell pellets were resuspended in RIPA lysis buffer (150 mM NaCl, 50 mM Tris [pH 8.0], 1% NP-40, 0.5% sodium deoxycholate, 0.1% SDS, with 1X Protease inhibitor cocktail and 1X Protease inhibitor tablet (Roche cOmplete ULTRA Tablets)) and incubated on ice with agitation for 15 minutes. The cell lysates were clarified by centrifugation at 17,000 x g for 15 min at 4°C, and the

supernatant was recovered. For the co-immunoprecipitation, 400 µg of cell lysate was combined with either normal mouse IgG (Santa-Cruz, sc2025) or anti-USP7 mouse (Millipore, 05-1946) and incubated at 4°C for 1 hour with agitation. 20 µL of Protein A/G-PLUS Agarose (sc-2003) was washed with 500 µL of 1X PBS three times and then blocked with 5% BSA in PBS for 30 min at 4°C. The beads were then equilibrated by washing with 500 µL of lysis buffer three times. Afterwards, 20 µL of Protein A/G-PLUS Agarose (sc-2003) was added to the antibody-cell lysate reaction the reactions were incubated overnight. The following day, the reactions were washed three times using 500 µL of 1X PBS. To prepare the samples, 40 µL of 1X SDS was added to the beads and boiled for 5 minutes. 10% (50 µg) of input and 20 µL of the beads were resolved on a 10% SDS-polyacrylamide gel and transferred to a PVDF membrane at 90V on ice for 2.5 hours. The PVDF membrane was blocked and blotted with the following antibodies: 1:2000 USP7 rabbit (Bethyl, A300-033A), 1:1000 anti-JARID1A/RBP2 rabbit (Cell-signaling, D28B10).

A second co-immunoprecipitation was done to show the interaction between exogenously expressed FLAG-RBP2 and endogenous USP7. HeLa P12 (10 cm) were transfected with 5 µg of either pcDNA3.1/FLAG or pcDNA3/HA-FLAG-RBP2 using 15 µL of PolyJet™. 24 hours after transfection, the HeLa cells were washed with two times with cold 1X PBS. 700 µL of M2 Lysis buffer (50 mM Tris HCl [pH 7.4], 150 mM NaCl, 1 mM EDTA, 1% Triton X-100, 1X Protease inhibitor cocktail and 1X Protease inhibitor tablet (Roche cOmplete ULTRA Tablets) was added to the tissue culture dish and incubated on ice for 30 minutes with agitation. Afterwards, the plated HeLa cells were scraped off the tissue culture dish and collected. The cell lysate was centrifuged at 17,000 x g for 15 min at 4°C and the clarified supernatant was recovered and quantified (Pierce™ BCA Protein Assay Kit). To set up the immunoprecipitation reaction, 700 µg of cell lysate was combined with 40 µL of resuspended ANTI-FLAG M2 Affinity Gel (Sigma-Aldrich, A2220) equilibrated to the manufacturer's directions and incubated overnight at 4ºC with agitation. The following day, the reactions were washed four times with 500 µL of M2 Lysis buffer, and the beads were boiled with 20 µL 2X SDS loading dye. 1.14% (8 µg) input and 10 µL of boiled bead sample were resolved on a 10% SDS-polyacrylamide gel and transferred to a PVDF membrane at 80V on ice for 3 hours. The PVDF membrane was blocked and blotted

with the following antibodies: 1:3000 USP7 rabbit (Bethyl, A300-033A), 1:1000 anti-ECS (FLAG) (Bethyl, A190-102A).

3.2.10 RBP2 and USP7 Interaction Site Mutant Co-immunoprecipitations

HeLa cells (10 cm tissue culture dish) were co-transfected with 2.5 µg of pcDNA3/HA-FLAG-RBP2 and 2.5 µg of either pCAN/Myc-USP7, pCAN/Myc-USP7^{MRGR}, or pCAN/Myc-USP7$^{DW-MRGR}$ using 15 µL of PolyJet™. The cells were harvested 24 hours after transfection and resuspended in of M2 Lysis buffer (50 mM Tris HCl [pH 7.4], 150 mM NaCl, 1 mM EDTA, 1% Triton X-100, 1X Protease inhibitor cocktail and 1X Protease inhibitor tablet (Roche cOmplete ULTRA Tablets) and incubated at 4°C for 30 min with agitation. The lysate was clarified by centrifugation at 17,000 x g for 15 min at 4°C and the supernatant was recovered and quantified (Pierce™ BCA Protein Assay Kit). 40 µL of resuspended ANTI-FLAG M2 Affinity Gel (Sigma-Aldrich, A2220) equilibrated to the manufacturer's directions. The immunoprecipitation was set up overnight at 4ºC with agitation with 200 µg of lysate combined with 40 µL of equilibrated ANTI-FLAG M2 Affinity Gel and Lysis buffer to equal a total volume of 1 mL. The following day, reactions were washed four times with 500 µL of 1X TBS (50 mM Tris-HCl [pH 7.4], 150 mM NaCl), and the beads were boiled with 20 µL 2X SDS loading dye. 4% (8 µg) input and 20 µL of boiled bead sample were resolved on a 10% SDS-polyacrylamide gel and transferred to a PVDF membrane at 90V on ice for 2.5 hours. The PVDF membrane was blocked and blotted with the following antibodies: 1:3000 anti-USP7 rabbit (Bethyl, A300-033A), 1:1000 anti-ECS (FLAG) (Bethyl, A190-102A). The USP7 membrane was stripped and re-probed with 1:1000 anti-Myc mouse (Millipore, 05-724).

The reciprocal of the co-immunoprecipitation was done in HeLa cells (15 cm) co-transfected with 5 µg of pcDNA3/HA-FLAG-RBP2 and 5 µg of either pcDNA3, pCAN/Myc-USP7, pCAN/Myc-USP7^{MRGR}, or pCAN/Myc-USP7$^{DW-MRGR}$ using 30 µL of PolyJet™. The cells were harvested 24 hours after transfection and the cell lysate was obtained as described above. 50 µL of Pierce Anti-c-Myc Agarose (Thermo Scientific) was equilibrated according to the manufacturer's directions. The immunoprecipitations were set up with 900 µg of lysate, 50 µL of equilibrated Pierce Anti-c-Myc Agarose and 1X TBS to equal a total volume of 200 µL. The co-

immunoprecipitation reactions were incubated overnight at 4°C with agitation. The following day, the resin was washed three times with 500 µL of 1X TBS-T (0.05%) and boiled with 50 µL of 2X SDS. The input (10 µg) and 20 µL elution were resolved on a 10% SDS-polyacrylamide gel and transferred to a PVDF membrane at 30V overnight at 4°C. The PVDF membrane was blocked and blotted with the following antibodies: 1:1000 anti-Myc HRP (Cell-signaling, 14038s), 1:2000 anti-JARID1A rabbit (Cell-signaling, D28B10).

3.2.11 USP7 Reconstitution in USP7$^{-/-}$ Cells

HCT116 USP7$^{-/-}$ cells were transfected with 10 µg of either pcDNA3, pCAN/Myc-USP7, pCAN/Myc-USP7^{C223S}, pCAN/Myc-USP7^{MRGR}, or pCAN/Myc-USP7$^{DW\text{-}MRGR}$ using 20 µL of PolyJet^{TM}. The transfected cells were treated with 40 µM of MG132 1 hour prior to harvesting to inhibit the proteasome. The cells were harvested 24 hours after transfection. Additionally, two plates of cells were treated with either DMSO or 40 µM MG132 for 1 hour and served as the un-transfected controls. The cell pellets were resuspended in RIPA lysis buffer (150 mM NaCl, 50 mM Tris [pH 8.0], 1% NP-40, 0.5% sodium deoxycholate, 0.1% SDS, with 1X Protease inhibitor cocktail and 1X Protease inhibitor tablet (Roche cOmplete ULTRA Tablets)) and lysed using sonication (0.5 sec ON and 4 sec OFF repeated three times, 10% amplitude) (Sonic Dismembrator Model 500, Fisher Scientific). The cell lysates were boiled with 1X SDS, and 30 µg of each sample was resolved on a Novex^{TM} 4-20% Tris-Glycine Plus Midi Gel 20-Well (ThermoFisher) and a 4-20% Mini-PROTEAN® TGX^{TM} Precast Protein Gel (BioRad). Before transfer, the Novex^{TM} 4-20% gel was equilibrated in 1X Western Blot Transfer Buffer (12 mM Tris [pH 8.3,] 96 mM Glycine, 10% methanol) supplemented with 0.1% SDS for 15 minutes. Afterwards, the Novex^{TM} 4-20% gel was transferred to a PVDF membrane in 1X Western Transfer Buffer without 0.1% SDS for 1.5 hours at 30V on ice. The PVDF membrane was blocked and probed with 1:1000 anti-Myc HRP (Cell-signaling, 14038s), 1:2000 anti-JARID1A rabbit (Cell-signaling, D28B10), 1:2000 anti-GAPDH mouse (Santa-Cruz, sc047723). The 4-20% gel (BioRad) was transferred to a PVDF membrane with 1X Western Transfer Buffer (25 mM Tris [pH 8.3], 192 mM Glycine, and 20% methanol) at 90V for 2.5 hours on ice. The PVDF membrane was blocked and probed with 1:4000 anti-GAPDH mouse (Santa-Cruz, sc047723), and 1:5000 anti-H3K4me3 rabbit (Actif Motif, 39-60).

3.2.12 USP7 siRNA Knockdown Assay

The siRNA mediated knockdown of USP7 was performed using siUSP7 and siNC (negative control) (Shanghai GenePharma) for which the double stranded siRNA sequences are shown (**Table 3-1**). To transfect the siRNA, Lipojet™ In Vitro DNA and siRNA Transfection Kit (SignaGen) was used according to the manufacturer's instructions.

Table 3-1. Double stranded siRNA Sequences. The siRNA molecules were transiently transfected into mammalian cell lines using Lipojet™ In Vitro DNA and siRNA Transfection Kit (SignaGen). siNC is a negative control. siUSP7 was used to knock-down USP7.

siRNA USP7	CCCAAAUUAUUCCGCGGCAAATT UUUGCCGCGGAAUAAUUUGGGTT
siNC	UUC UCC GAA CGU GUC ACG UTT ACG UGA CAC GUU CGG AGA ATT

An siRNA knock-down of USP7 was performed in HeLa cells to determine the effect on RBP2. 10 cm plates of HeLa cells were transfected with 20 nM of siNC or siUSP7 using 20 µL of Lipojet™ and harvested 96 hours post-transfection. The cell pellets were resuspended in RIPA lysis buffer (150 mM NaCl, 50 mM Tris [pH 8.0], 1% NP-40, 0.5% sodium deoxycholate, 0.1% SDS, with 1X Protease inhibitor cocktail and 1X Protease inhibitor tablet (Roche cOmplete ULTRA Tablets)) and lysed using sonication (1 sec ON and 4 sec OFF repeated three times, 10% amplitude) (Sonic Dismembrator Model 500, Fisher Scientific). The samples were made by boiling cell lysate with 1X SDS. 50 µg of each sample was resolved on a 10% SDS-polyacrylamide gel and transferred to a PVDF membrane at 30V overnight at 4°C. The PVDF membrane was blocked and blotted with 1:2000 anti-JARID1A rabbit (Cell-signaling, D28B10), 1:1000 anti-GAPDH mouse (Santa-Cruz, sc047723), 1:1000 anti-USP7 mouse (Millipore, 05-1946).

Additionally, an siUSP7 knock-down was conducted in HeLa and HCT116 cells to determine the effect of USP7 silencing on both RBP2 and H3K4me3. 6 cm plates of HeLa and HCT116 cells were transfected with 50 nM of siNC or siUSP7 using LipoJet™ and the cells were harvested 48 hours after siRNA transfection. The cell pellets were resuspended in RIPA lysis buffer (150 mM NaCl, 50 mM Tris [pH 8.0], 1% NP-40, 0.5% sodium deoxycholate, 0.1% SDS, with 1X Protease inhibitor cocktail and 1X Protease inhibitor tablet (Roche cOmplete ULTRA Tablets)) and lysed using sonication (0.5 sec ON and 10 sec OFF repeated three times, 10% amplitude) (Sonic Dismembrator Model 500, Fisher Scientific). The samples were made by boiling cell lysate with 1X SDS. 40 µg of HCT116 siRNA knock-downs, as well as 25 µg of HeLa siRNA knock-downs were resolved on a 4-20% Mini-PROTEAN® TGX™ Precast Protein Gel (BioRad) and transferred to a PVDF membrane at 30V overnight at 4°C. The PVDF membrane was blocked and blotted with 1:2000 anti-JARID1A rabbit (Cell-signaling, D28B10), 1:2000 anti-GAPDH mouse (Santa-Cruz, sc047723), 1:5000 anti-H3K4me3 rabbit (Actif Motif, 39-60), 1:3000 USP7 rabbit (Bethyl, A300-033A).

3.3 RESULTS

3.3.1 RBP2 sequence analysis

Based on previous studies, KxxxK and P/A/ExxS are putative motifs that confer interaction with USP7. Bioinformatics analyses were performed using the ICP0 sequence (PRKxxRK) searching to identify novel proteins that interact with USP7. RBP2 was identified with strong similarities. There was only one PRKxxxK candidate, ^{1416}PRKQPRK^{1422}, but many other KxxxK sequences (**Appendix B**) (**Table 3-2**). Further analyses performed with Eukaryotic Linear Motif (ELM) and Phyre2 revealed additional prospective interaction sequences were determined. Considering the conservation of the sites and location in the predicted secondary structure, a couple candidate sequences present themselves as likely interactors. Out of two potential P/A/ExxS interaction sequences, ^{1401}AYSSA^{1405} is the most probable candidate due to its high degree of conservation among species (**Appendix B**) (**Table 3-2**). While ^{1380}PIKSE^{1384} is highly conserved, it is located in a more disordered region than ^{1401}AYSSA^{140}.

Table 3-2. RBP2 candidate sequences. The potential interaction sequences were identified using a combination of Eukaryotic Linear Motif (ELM), Prosite, and Phyre2.

Interaction motif	Candidate Interaction Sequences
P/A/ExxS	^{1401}AYSSA^{1405} ^{1380}PIKSE^{1384}
PRKxxxK	^{1416}PRKQPRK^{1422}

3.3.2 RBP2 stability is USP7 dependent

The initial question that we posed was whether RBP2 stability is dependent on the UPS system, and whether USP7 plays a role in its stability. We approached this query by investigating the endogenous protein levels of RBP2 in HCT116 (human colorectal carcinoma) cell lines in

response to inhibition of the proteasome. Parental HCT116 cells (USP7$^{+/+}$) and HCT116 USP7$^{-/-}$ knockout cells were treated with either DMSO or the proteasomal inhibitor MG132 (**Figure 3-3**). In the HCT116 cells, RBP2 increased upon MG132 treatment in comparison to DMSO. The USP7$^{-/-}$ HCT116 cells treated with DMSO appeared to have minimal levels of ubiquitinated RBP2, indicated by several bands with increased molecular weight. When treated with MG132, RBP2 levels increased significantly indicated by the presence of a dark smear. The presence of a smear rather than a single band suggested that the RBP2 present in the USP7$^{-/-}$ cells treated with a proteasomal inhibitor that RBP2 is polyubiquitinated.

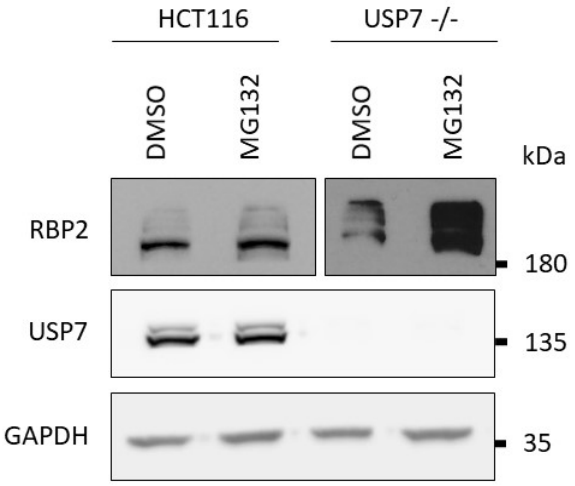

Figure 3-4. RBP2 Stability is DUB dependent. Immunoblot of HCT116 USP7$^{+/+}$ and HCT116 USP7$^{-/-}$ cells treated with the proteasomal inhibitor MG132. HCT116 USP7$^{+/+}$ and HCT116 USP7$^{-/-}$ were treated with 40 μM of MG132 or DMSO (control) for 1 hour before harvesting. Cellular lysates (30 μg) resolved on a 10% SDS-polyacrylamide gel were subjected to immunoblotting with anti-USP7 rabbit, anti-RBP2 rabbit and anti-GAPDH mouse antibodies.

Furthermore, we investigated the regulatory relationship between USP7 and RBP2 by probing endogenous RBP2 levels in wild-type and USP7 knock-out cells as well as the abundance of RBP2 under overexpression or knock-down of USP7. The levels of USP7 and RBP2 were compared in U2OS, HCT116 USP7$^{+/+}$ and HCT116 USP7$^{-/-}$ cells (**Figure 3-5, A**). RBP2 was most abundant in U2OS and HCT116 cells and appeared to be absent from the USP7$^{-/-}$ cells. To further investigate the relationship between USP7 and RBP2, HeLa cells were transfected with either pcDNA3, Myc-USP7, or catalytically inactive C223S Myc-USP7 (**Figure 3-5, B**). The

cells overexpressing wild-type Myc-USP7 exhibited increased levels of RBP2. The cells transfected with pcDNA3 or C223S Myc-USP7 displayed similar levels of RBP2. To probe what residues are involved in the interaction, HeLa cells were co-transfected with FLAG-RBP2 and pcDNA3, or Myc-USP7, or a Myc-USP7 MRGR or DW-MRGR mutant (**Figure 3-5, C**). Interestingly, the cells co-transfected with FLAG-RBP2 and pcDNA3 exhibited the lowest abundance of RBP2. In contrast, cells transfected with FLAG-RBP2 and Myc-USP7 wild-type or MRGR mutant showed increased levels of RBP2 compared to the cells transfected with FLAG-RBP2 and empty vector control. Additionally, the cells transfected with Myc-USP7 or Myc-USP7 MRGR mutant displayed similar RBP2 levels. The cells co-transfected with FLAG-RBP2 and Myc-USP7 DW-MRGR mutant exhibited attenuated levels of RBP2 compared to the cells transfected with Myc-USP7 or Myc-USP7 MRGR. To further explore USP7's regulatory role on RBP2, an siRNA knock-down of USP7 was conducted in HeLa cells (**Figure 3-5, D**). In the absence of USP7, RBP2 levels were noticeably decreased compared to the siNC control.

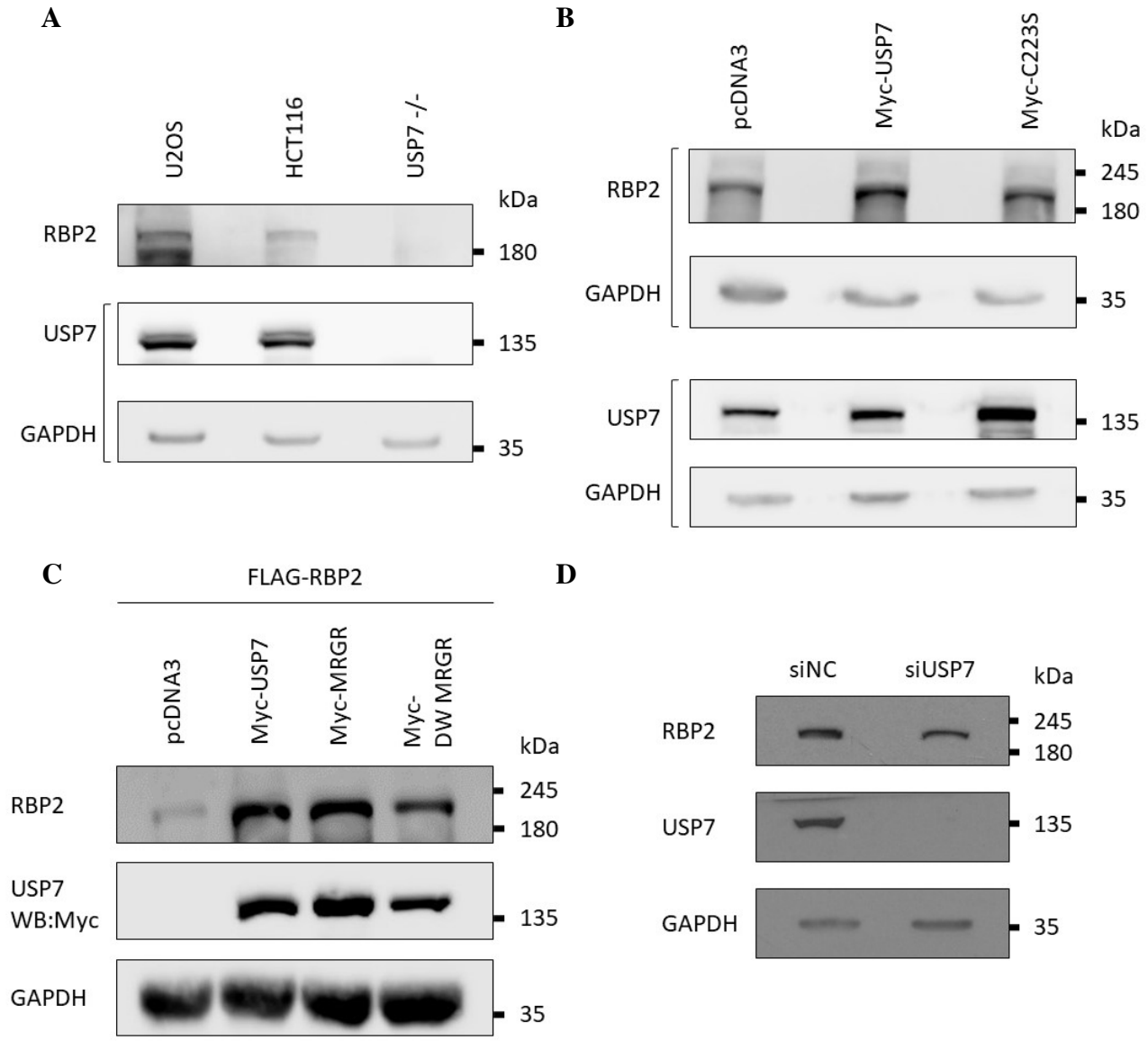

Figure 3-5. USP7 regulates RBP2 stability. (A) Immunoblot of U2OS, HCT116 USP7$^{+/+}$ and HCT116 USP7$^{-/-}$ cell lysates. Cell lysates (40 µg) were resolved on 7.5% and 12% SDS-polyacrylamide gels and subjected to immunoblotting. After transfer to a PVDF membrane, the 7.5% gel was blotted with anti-RBP2 rabbit antibodies. The 12% SDS-polyacrylamide gel was blotted with anti-USP7 rabbit, anti-GAPDH mouse antibodies. **(B)** Immunoblot of HeLa cells lysates transfected with 5 µg pcDNA3, Myc-USP7, or Myc-USP7^{C223S} harvested 24 hours after transfection. Cell lysates (40 µg) were resolved on 7.5% and 12% SDS-polyacrylamide gels immunoblotted with RBP2 rabbit and anti-GAPDH mouse, anti-USP7 rabbit and anti-GAPDH mouse respectively. **(C)** Immunoblot of HeLa cells co-transfected with 5 µg of FLAG-RBP2 and 5 µg of either pcDNA3, Myc-USP7, Myc-USP7^{MRGR}, or Myc-USP7$^{DW\text{-}MRGR}$ harvested 24 hours post-transfection. The cell lysates (20 µg) were resolved on a 10% SDS-polyacrylamide gel and immunoblotted with anti-RBP2 rabbit, anti-Myc HRP, and anti-GAPDH mouse antibodies. **(D)** Immunoblot of USP7 knock-down in HeLa cells. The cells were treated with 20 nM of siNC

(control) or siUSP7 and harvested 96 hours post-transfection. The cell lysates (50 µg) were resolved on a 10% SDS-polyacrylamide gel and immunoblotted with anti-RBP2 rabbit, anti-USP7 mouse, anti-GAPDH mouse antibodies.

3.3.3 USP7 and RBP2 interact

To investigate whether USP7 interacts with RBP2, an endogenous co-immunoprecipitation was performed in HeLa cells (**Figure 3-6, A**). IgG was used as a negative control. RBP2 appeared to co-immunoprecipitate with USP7 but not with the IgG. Furthermore, a reciprocal co-immunoprecipitation was performed in HeLa cells overexpressing either pcDNA3.1-FLAG or HA-FLAG-RBP2 (**Figure 3-6, B**). Using M2 affinity resin, FLAG-RBP2 was immunoprecipitated and endogenous USP7 was found to strongly associate with the FLAG-RBP2 bound beads in comparison to FLAG bound beads.

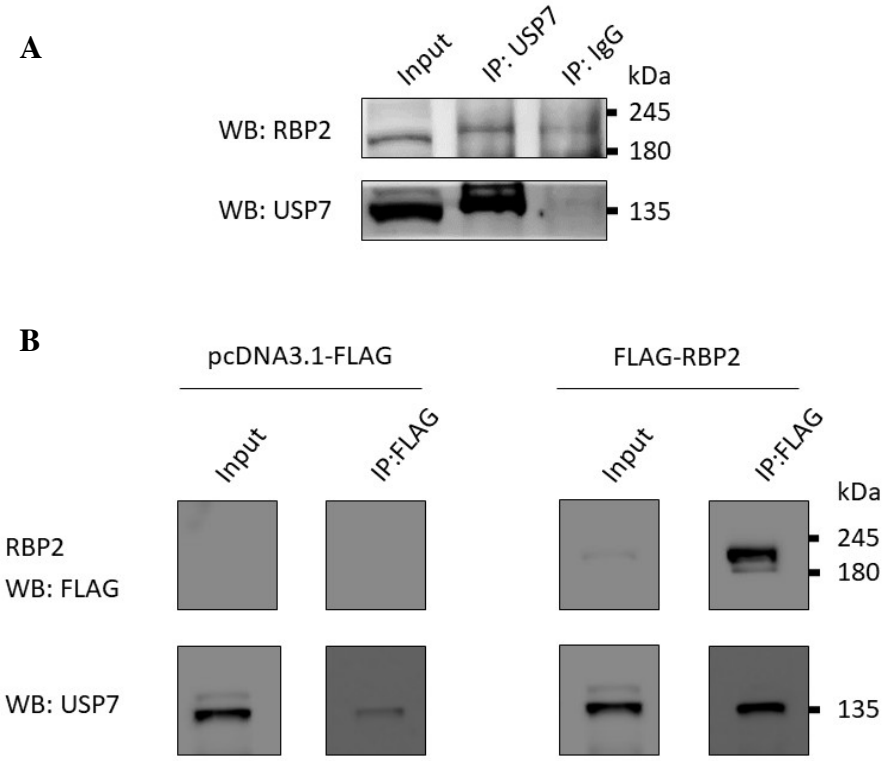

Figure 3-6. USP7 and RBP2 interact. (A) Endogenous USP7 and RBP2 co-IP in HeLa cells. USP7 was immunoprecipitated with anti-USP7 mouse and protein A/G agarose. Normal mouse IgG was used as the control. The input (10%) and elution (20 μL) were resolved on a 10% SDS-polyacrylamide gel and immunoblotted with anti-USP7 rabbit and anti-RBP2 rabbit antibodies. **(B)** Co-immunoprecipitation of FLAG-RBP2 and endogenous USP7 in HeLa cells. The cells were transfected with 5μg of pcDNA3.1-FLAG or FLAG-RBP2 and harvested 24 hours post-transfection. FLAG-RBP2 was immunoprecipitated with anti-FLAG M2 affinity gel. The input (1%) and elution (10 μL) were resolved on a 10% SDS-polyacrylamide gel and immunoblotted with anti-ECS (FLAG), and anti-USP7 rabbit antibodies.

The question of whether RBP2 interacts with the CTD of USP7 was investigated by performing a GST-pulldown. Using BL21 *E. coli*, GST and GST-Ubl1-5 were expressed and purified using glutathione affinity purification. Afterwards, HeLa cells exogenously expressing pcDNA3.1-FLAG or FLAG-RBP2 were incubated with the GST or GST-Ubl1-5 bound glutathione beads to conduct the pull-down. FLAG-RBP2 appeared to strongly interact with the GST-Ubl1-5 and not the GST bound beads (**Figure 3-7**).

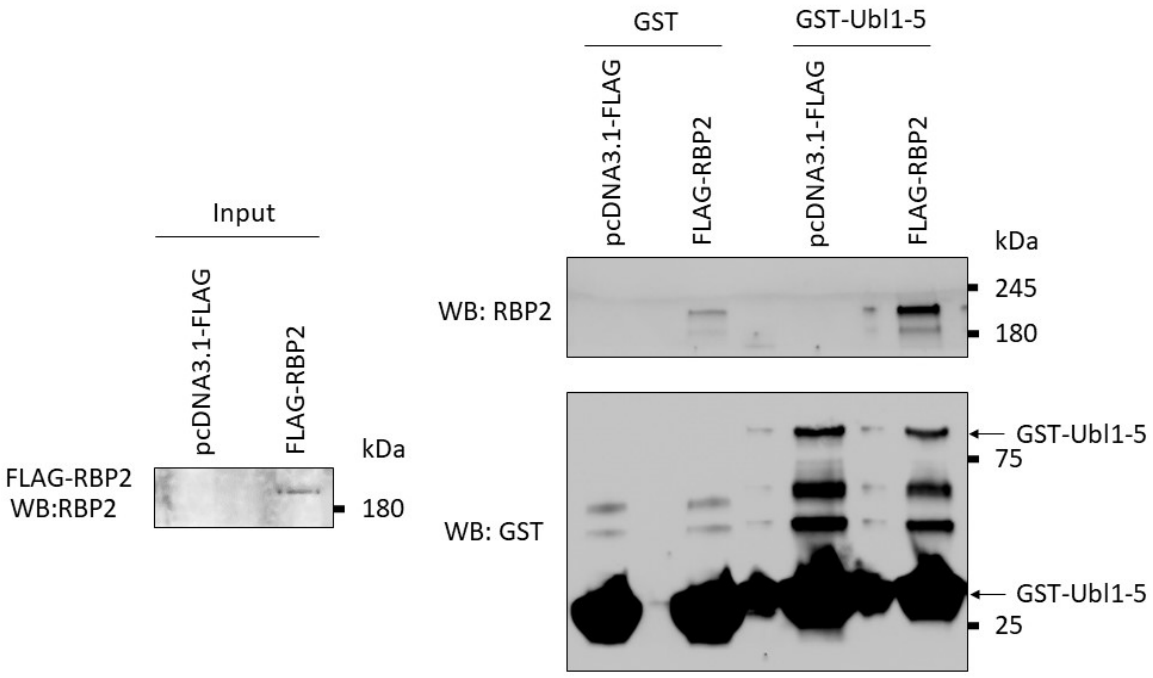

Figure 3-7. RBP2 interacts with USP7-Ubl1-5. A GST Pull-down of FLAG-RBP2 with GST-Ubl1-5 USP7. HeLa cells transfected with 10 μg of pcDNA3.1-FLAG or HA-FLAG RBP2 were lysed and the cell lysate was incubated with GST or GST-Ubl1-5 bound glutathione-agarose beads. The input HeLa cell lysates (3.4%) and GST pull-down elutions (20 μL) were resolved on a 4-20% SDS-polyacrylamide gel and immunoblotted with anti-RBP2 rabbit and anti-GST mouse antibodies.

To further determine the nature of the interaction, co-immunoprecipitations of FLAG-RBP2 were conducted with Myc-USP7 wild-type, MRGR and DW-MRGR interaction site mutants. FLAG-RBP2 was immunoprecipitated using M2 beads and the elution fractions were probed for the presence of USP7. Both Myc-USP7 wild-type and MRGR mutant appeared to interact with FLAG-RBP2 (**Figure 3-8, A**). The DW-MRGR Myc-USP7 mutant did not appear to interact with FLAG-RBP2. Additionally, a reciprocal interaction study was performed by immunoprecipitating Myc-USP7 using anti-Myc agarose. FLAG-RBP2 appeared to co-immunoprecipitate strongly with Myc-USP7 wild-type (**Figure 3-8, B**). In comparison, it appeared that a diminished amount of FLAG-RBP2 interacted with Myc-USP7 MRGR. FLAG-RBP2 did not appear to interact with the empty beads nor with Myc-USP7 DW-MRGR.

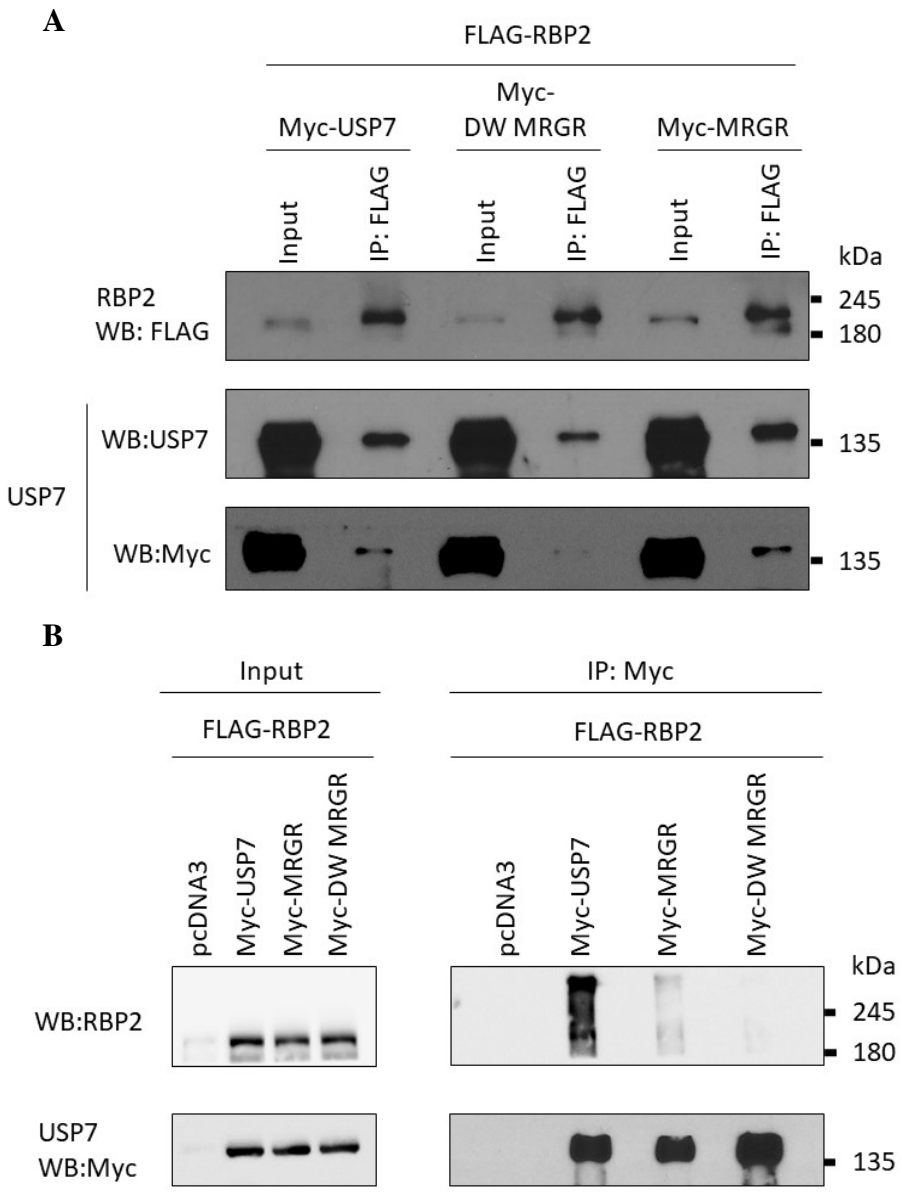

Figure 3-8. RBP2-USP7 interaction is dependent on DWGF and MDGD. **(A)** FLAG-RBP2 and Myc-USP7 co-immunoprecipitation in HeLa cells. HeLa cells transfected with 2.5 μg of FLAG-RBP2 and 2.5 μg of Myc-USP7, Myc-USP7$^{DW\text{-}MRGR}$, or Myc-USP7^{MRGR}. The cells were harvested 24 hours post-transfection, and FLAG-RBP2 was immunoprecipitated with anti-FLAG M2 affinity gel. The inputs (4%) and elutions (20 μL) were resolved on a 10% SDS-polyacrylamide gel and immunoblotted with anti-ECS (FLAG) rabbit, anti-USP7 rabbit, anti-Myc mouse antibodies. **(B)** FLAG-RBP2 and Myc-USP7 co-immunoprecipitation in HeLa cells. HeLa cells transfected with 5 μg FLAG-RBP2 and 5 μg of pcDNA3, Myc-USP7, Myc-USP7$^{DW\text{-}MRGR}$, or Myc-USP7^{MRGR}. Myc-USP7 was immunoprecipitated with anti-c-Myc agarose. The input (1.11%) and elution (20 μL) were resolved on a 10% SDS-polyacrylamide gel and immunoblotted for anti-RBP2 rabbit, anti-Myc HRP antibodies.

3.3.4 The USP7-RBP2 interaction mediates H3K4me3 demethylation by RBP2

Lastly, our goal was to investigate the effects of the interaction between USP7 and RBP2 by examining the H3K4me3 in response to USP7 perturbation. In comparison to the wild-type parental cell line, USP7$^{-/-}$ HCT116 cells appeared to lack RBP2 and demonstrate an increase in H3K4me3 (**Figure 3-9**).

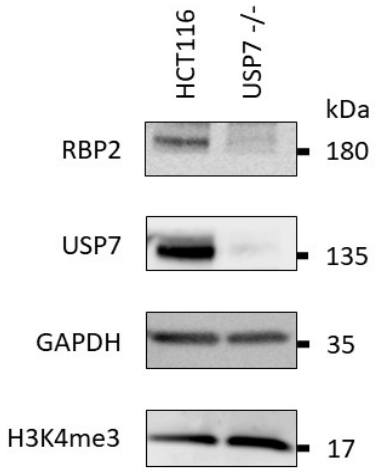

Figure 3-9. USP7 regulates RBP2 and H3K4me3. Immunoblot of HCT116 USP7$^{+/+}$, HCT116 USP7$^{-/-}$ cell lysates. The cell lysates (40 μg) HCT116 USP7$^{+/+}$ and USP7$^{-/-}$ were electrophoresed on a 4-20% SDS-polyacrylamide gel. The gel was immunoblotted with anti-RBP2 rabbit, anti-USP7 rabbit, anti-GAPDH mouse and anti-H3K4me3 rabbit antibodies.

3.4 DISCUSSION

Based on sequence analysis of RBP2 and comparison to previously identified interactors, we hypothesized that USP7 interacts with RBP2. The aim of our research was to identify if USP7 interacts with and regulates RBP2. Additionally, we investigated whether the USP7-RBP2 relationship has downstream effects on RBP2 demethylation activity.

3.4.1 USP7 regulates RBP2 stability

We initially approached this question by determining if RBP2 stability is dependent on the proteasome by treating HCT116 $USP7^{+/+}$ and $USP7^{-/-}$ cells with a proteasomal inhibitor (**Figure 3-4**). In both cases, polyubiquitinated RBP2 accumulated in the mammalian cells treated with the proteasomal inhibitor, indicating that RBP2 stability is dependent on the UPS system. Interestingly, the $USP7^{-/-}$ cells treated with a proteasomal inhibitor exhibited a marked increase in RBP2 levels compared to control $USP7^{-/-}$ cells, suggesting that in the absence of USP7, RBP2 is unstable and degraded by the UPS. It appears that $USP7^{-/-}$ cells possess minimal RBP2 levels in comparison to U2OS and HCT116 $USP7^{+/+}$, further suggesting RBP2 stability is dependent on USP7 (**Figure 3-5, A**). RBP2 is present in HeLa cells and appears to be stabilized upon the overexpression of Myc-$USP7^{WT}$, but not its catalytically inactive mutant Myc-$USP7^{C223S}$ (**Figure 3-5, B**). This suggested that the catalytic ability of USP7 is required for the stabilization of RBP2. To explore this regulatory relationship further, we exogenously expressed Myc-$USP7^{WT}$ and its MRGR and DW-MRGR interaction site mutants to determine if the regulatory effect USP7 has on RBP2 was dependent on the ^{164}DWGF^{167} and/or ^{761}MDGD^{764} interaction sites (**Figure 3-5, C**). Overexpression of Myc-$USP7^{WT}$ led to an increase in RBP2 levels compared to empty vector. Overexpression of Myc-$USP7^{MRGR}$ resulted in similar RBP2 levels as cells transfected with Myc-$USP7^{WT}$, suggesting that the ^{761}MDGD^{764} site may not have a primary role in mediating RBP2 stability. In contrast, transfection of Myc-$USP7^{DW\text{-}MRGR}$ resulted in a significant decrease of RBP2. This finding proposed that the USP7 ^{164}DWGF^{167} site may be important in regulating RBP2 stability. Unexpectedly, the RBP2 levels in the $USP7^{DW\text{-}MRGR}$ transfection were higher than the empty vector transfected cells. It could be inferred that there

may be other USP7 interaction sites or that USP7 is having a stabilization effect independent of its catalytic function. In fact, several additional residues in the CTD of USP7 were discovered to mediate interactions with substrates [68]. Additionally, the knock-down of USP7 in HeLa cells, corroborated our previous data that USP7 regulates RBP2 stability. Upon USP7 knock-down, RBP2 levels appear to be attenuated compared to the control (**Figure 3-5, D**).

3.4.2 USP7 interacts with RBP2

After exploring the regulatory relationship of RBP2 and USP7 in mammalian cells, we pursued the question of whether USP7 and RBP2 interact. To ensure the interaction is direct, we performed a endogenous co-immunoprecipitation and were able to see RBP2 co-immunoprecipitating with USP7 (**Figure 3-6, A**). While the interaction was shown, this experiment was limited by a low abundance of RBP2 protein in the input lysate. This could be due to the reported retention of RBP2 in salt-sensitive nuclei, requiring high concentration of salt for release [237]. Thus, we repeated the RBP2-USP7 co-immunoprecipitation with cells overexpressing FLAG-RBP2 and observed USP7 to strongly co-immunoprecipitate with RBP2 compared to the control (**Figure 3-6, B**). Since overexpression of Myc-USP7^{MRGR} did not attenuate RBP2 levels (**Figure 3-5, C**), we aimed to determine if the CTD of USP7 was involved in the RBP2-USP7 interaction using a GST pull-down (**Figure 3-7**). RBP2 was found to strongly co-elute with the CTD of USP7 compared to GST control. To our surprise, RBP2 interacts with the CTD of USP7, but perhaps the interaction is independent of the ^{761}MDGD^{764} interaction site. To further determine the nature of the interaction, such as what interaction sites and residues are involved, co-immunoprecipitations were performed using USP7 interaction domain mutants. The cells were co-transfected with FLAG-RBP2 and Myc-USP7^{WT}, Myc-USP7^{MRGR}, or Myc-USP7$^{DW\text{-}MRGR}$, and FLAG-RBP2 was immunoprecipitated (**Figure 3-8, A**). Wild-type Myc-USP7 as well as the MRGR mutant co-immunoprecipitated with FLAG-RBP2, suggesting additional interaction sites aside from the MDGD motif. In agreement with our other experiments, the DW-MRGR USP7 mutant experienced attenuated interaction with RBP2. In the reciprocal co-immunoprecipitation similar results were observed (**Figure 3-8, B**). The immunoprecipitation of Myc-USP7^{WT} exhibited the highest amount of interacting RBP2 compared to the control and interaction mutants. Interestingly, the RBP2 interaction appeared to

be diminished in the MRGR mutant co-immunoprecipitation, and completely absent in the DW-MRGR mutant. This finding was unexpected, as the reciprocal MRGR USP7 mutant co-immunoprecipitation did not demonstrate the same degree of attenuation in interaction. Thus, it would be beneficial to perform an *in vitro* interaction study using purified USP7 CTD, wild-type and MDGD mutants. Altogether, these data suggest that the RBP2-USP7 interaction is dependent on the ^{164}DWGF^{167} site in USP7, and possibly the ^{761}MDGD^{764} site. Yet further studies need to be conducted to confirm the latter.

3.4.3 USP7 affects RBP2-mediated H3K4 demethylation

After showing that USP7 interacts with and regulates RBP2, we sought out to determine if the USP7-RBP2 relationship has downstream effects on H3K4 methylation. We predicted that if USP7 stabilizes RBP2, in the absence or reduction of USP7 we should see a reduction of RBP2 as well as a reduction in demethylation of H3K4. Due to the decrease of RBP2 demethylating activity, we would expect to see an increase in H3K4me3 or H3K4me2. When comparing HCT116 USP7$^{+/+}$ cells with HCT116 USP7$^{-/-}$, H3K4me3 appears to increase in the HCT116 USP7$^{-/-}$ cells (**Figure 3-9**). As expected, the increase in H3K4me3 coincided with the absence of RBP2 in HCT116 USP7$^{-/-}$ cells, suggesting that USP7 affects the downstream activity of RBP2.

A limitation of our experiment is that only H3K4me3 levels were studied, while RBP2 is known to deubiquitinate H3K4me3 and H3K4me2. To investigate this relationship in greater detail, the experiment should be repeated and H3K4me1, H3K4me2, and HK4me3 should be probed for. Additional histone modifications can be probed for as well to obtain a deeper understanding of the regulation of H3K4 methylation. For instance, H2B ubiquitination has been demonstrated to stimulate di- and trimethylation of H3K4 by SET1 [157]. As previously mentioned, USP7 has been characterized to form a complex with GMPS and deubiquitinate H2BK120me1 [263]. It would be interesting to conduct experiments investigating whether USP7 has additional indirect roles of regulating H3K4 methylation.

Additionally, USP7 has been shown to stabilize the H3K4 demethylases LSD1 [159] and KDM2B [264] and the methylase MLL5 [160]. Thus, the H3K4me3 levels observed may not be a direct

representation of RBP2 activity. The list of demethylases and methylases that target H3K4 is extensive and may include potential USP7-interactors that have not yet been identified (**Table 3-3**).

Table 3-3. H3K4 modifying enzymes. Adapted from [265] * Methylases and demethylases that have been characterized to directly interact with USP7.

Demethylases	**Methylases**
LSD1(KDM1A)*	MLL1 (KMT2A)
LSD2 (KDM1B)	MLL2 (KMT2B)
JHDM1A (KDM2A)	MLL3 (KMT2C)
JHDM1B (KDM2B)*	MLL4 (KMT2D)
JARID1A (KDM5A, RBP2)	MLL5 (KMT2E)*
JARID1B (KDM5B)	SET1A (KMT2F)
JARID1C (KDM5C)	SET1B (KMT2G)
JARID1D (KDM5D)	ASH1 (KMT2H)
NO66	SMYD1 (KMT3D)
	SMYD2 (KMT3C)
	SMYD3 (KMT3E)
	SET7/9 (KMT7)

The regulatory relationship between USP7 and RBP2 and the downstream effect on H3K4me3 may involve additional regulatory proteins such as ORC2 (origin of complex 2). USP7 has been shown to act as a SUMO DUB, deubiquitinating SUMOylated factors localized at the replication fork [107]. The authors found that the inhibition of USP7 resulted in a displacement of SUMOylated proteins from the replisome. This displacement restricted the progression of the replication fork and firing of new origins, in turn inhibiting DNA replication. Interestingly, SUMO2-conjugated ORC2 has been demonstrated to recruit RBP2 to demethylate H3K4me3 [266]. ORC2 is a subunit of pre-replication complex and is a critical factor for DNA replication in mammalian cells. The recruitment of SUMO2-ORC2 mediated recruitment of RBP2 and promoted the H3K4me3 conversion to H3K4me2. As described previously, H3K4me2 is associated with transcription. The H3K4me2 mark permits the transcription of α-satellite transcripts that play an important role in preventing DNA re-replication, imperative for maintaining genomic stability. Interestingly, ORC2 possesses several putative USP7 interaction

motifs and it would be of interest to explore whether ORC2 is a USP7 substrate. Considering this, the effect of RBP2 downstream function may vary depending on the cell cycle. Thus, it would be interesting to investigate the RBP2-USP7 relationship in cells in the S-phase, undergoing DNA replication.

Another protein that may be involved in the RBP2-USP7 regulatory axis is Retinoblastoma (Rb). Rb has been characterized to interact with and inhibit RBP2, thereby preventing RBP2-dependent repression of genes involved in differentiation [237]. Moreover, USP7 has been shown to stabilize Rb, which is destabilized by the E3 ligase MDM2, another USP7 target [108]. The stability of Rb in the cell has been shown to be proteasomal-dependent. It would be interesting to repeat the USP7 reconstitution and knock-down experiments while probing for Rb and MDM2 to investigate their role in the regulation of RBP2 and the demethylation of H3K4me3.

CHAPTER 4 : CONCLUSIONS

4.1 EZH2 and USP7

The data in chapter 2 demonstrated the stability of EZH2 is dependent on the UPS system and involves USP7. The direct endogenous interaction of USP7 and EZH2 was observed in U2OS cells. We characterized the key residues involved in the interaction using *in vitro* pull-downs and co-immunoprecipitations in U2OS cells. Our data suggested that EZH2 interacts with the ^{761}MDGD^{764} interaction site located in Ubl2 of USP7 via the ^{489}PRKKKRK^{495} sequence. EZH2 was defined as not only an interactor, but a substrate of USP7; demonstrated by the deubiquitination of EZH2 by USP7. The EZH2-USP7 regulatory relationship was further elucidated by exploring the effect of USP7 on H3K27me3 levels. The absence of USP7 coincided with decreased levels of both EZH2 and H3K27me3, suggesting USP7 affects the downstream function of EZH2.

Recent reports by four independent groups similarly described the USP7-EZH2 interaction in neuronal progenitor cells, melanoma, LSCC, and prostate cancer [216–219]. The discovery of the EZH2-USP7 interaction by four other groups and the replication of similar experiments in various cell lines, speaks to the significance and the legitimacy of the interaction. Additionally, the clinical findings and experiments in animal models underscore the biological relevance of the interaction.

However, several questions remain unanswered such as the mechanism by which USP7 and EZH2 contribute to poor prognosis of certain cancers. While two mechanisms have been proposed, one was demonstrated in melanoma and the other was proposed to be a generalized mechanism present in cancer cells. One may thus speculate whether the mechanisms by which the USP7-EZH2 regulatory axis contributes to carcinogenesis varies amongst different forms of neoplasms. Thus, expanding our understanding of the mechanisms underlying the regulation of EZH2 and USP7 may aid in the development of precision therapeutics to benefit clinical outcomes of affected patients.

4.2 RBP2 and USP7

As shown in Chapter 3, our findings showed that RBP2-USP7 participate in an intricate regulatory axis. We were able to demonstrate that USP7 interacts with and stabilizes RBP2, as well as regulates RBP2's H3K4 demethylating ability. RBP2 seems to interact with both the ^{164}DWGF^{167} and ^{761}MDGD^{764} motifs of USP7. Mutating the ^{761}MDGD^{764} domain indeed results in loss of interaction, but some interaction is retained. In contrast, mutation of ^{164}DWGF^{167} and ^{761}MDGD^{764} results in complete abrogation of RBP2 interaction. This suggested that RBP2 interacts with both the NTD and the CTD of USP7. Indeed, RBP2 appears to harbour several interaction sites that may be involved in mediating these interactions. Further studies need to be conducted *in vitro* to determine the nature of the interaction.

In conclusion, the findings in this chapter are critical to understanding the regulation of RBP2 as it currently remains poorly defined. USP7 provides an extensive repertoire of interactors, involved in many cellular processes including epigenetic regulation and genomic stability. Both USP7 and RBP2 have been extensively implicated in human pathologies and are both considered to be attractive drug targets. Developing a better understanding of their regulatory mechanisms may aid in developing more targeted therapeutic interventions.

4.3 USP7 in Epigenetics

Numerous reports have solidified USP7 as a key player in epigenetics, demonstrating both direct and indirect mechanisms of regulation. USP7's targets appear to be associated with both transcriptional activation as well as repression, and many of the targets appear to be H3 modifying enzymes. Thus, it is interesting to speculate possible interplay between USP7 targeted proteins in epigenetics, and the effects on gene expression. For instance, a functional relationship between the PRC2 complex and RBP2 has been described in mouse embryonic stem cells [267]. The use of genome-wide location analysis has revealed that RBP2 and PRC2 share several target genes including HOX, WNT, SOX, and NOTCH. During embryonic stem cell differentiation, the PRC2 complex was found to recruit RBP2 to coordinate repression of developmental genes. The regulatory effect of USP7 on this regulatory axis is a fascinating avenue of investigation that may reveal novel roles of USP7 in development.

REFERENCES

1. Swatek, K. N. & Komander, D. Ubiquitin modifications. *Cell Research* **26**, 399–422 (2016).
2. Mansour, M. A. Ubiquitination: Friend and foe in cancer. *International Journal of Biochemistry and Cell Biology* **101**, 80–93 (2018).
3. Rape, M. Ubiquitylation at the crossroads of development and disease. *Nat. Rev. Mol. Cell Biol.* **19**, 59–70 (2018).
4. Lecker, S. H., Goldberg, A. L. & Mitch, W. E. Protein Degradation by the Ubiquitin-Proteasome Pathway in Normal and Disease States. *J Am Soc Nephrol* **17**, 1807–1819 (2006).
5. Vijay-kumar, S., Bugg, C. E. & Cook, W. J. Structure of ubiquitin refined at 1.8 Å resolution. *J. Mol. Biol.* **194**, 531–544 (1987).
6. Baker, R. T. & Board, P. G. The human ubiquitin-52 amino acid fusion protein gene shares several structural features with mammalian ribosomal protein genes. *Nucleic Acids Res.* **19**, 1035–1040 (1991).
7. Finley, D., Bartel, B. & Varshavsky, A. The tails of ubiquitin precursors are ribosomal proteins whose fusion to ubiquitin facilitates ribosome biogenesis. *Nature* **338**, 394–401 (1989).
8. Wiborg, O. *et al.* The human ubiquitin multigene family: some genes contain multiple directly repeated ubiquitin coding sequences. *EMBO J.* **4**, 755–759 (1985).
9. Bianchi, M. *et al.* Dynamic transcription of ubiquitin genes under basal and stressful conditions and new insights into the multiple UBC transcript variants. *Gene* **573**, 100–109 (2015).
10. Finley, D., Özkaynak, E. & Varshavsky, A. The yeast polyubiquitin gene is essential for resistance to high temperatures, starvation, and other stresses. *Cell* **48**, 1035–1046 (1987).
11. Arif, S. *et al.* MINDY-1 Is a Member of an Evolutionarily Conserved and Structurally Distinct New Family of Deubiquitinating Enzymes. *Mol. Cell* **63**, 146–155 (2016).
12. McClellan, A. J., Ellgaard, L., Laugesen, S. H. & Ellgaard, L. Cellular functions and molecular mechanisms of non-lysine ubiquitination. *Open Biol.* **9**, 190147 (2019).
13. Grice, G. L. & Nathan, J. A. The recognition of ubiquitinated proteins by the proteasome. *Cell. Mol. Life Sci.* **73**, 3497–506 (2016).
14. Rieser, E., Cordier, S. M. & Walczak, H. Linear ubiquitination: a newly discovered regulator of cell signalling. *Trends Biochem. Sci.* **38**, 94–102 (2013).
15. Komander, D. & Rape, M. The Ubiquitin Code. *Annu. Rev. Biochem.* **81**, 203–229 (2012).

16. Thrower, J. S., Hoffman, L., Rechsteiner, M. & Pickart, C. M. Recognition of the polyubiquitin proteolytic signal. *EMBO J.* **19**, 94–102 (2000).

17. Chau, V. *et al.* A multiubiquitin chain is confined to specific lysine in a targeted short-lived protein. *Science (80-.).* **243**, 1576–1583 (1989).

18. Meyer, H. J. & Rape, M. Enhanced protein degradation by branched ubiquitin chains. *Cell* **157**, 910–921 (2014).

19. Jin, L., Williamson, A., Banerjee, S., Philipp, I. & Rape, M. Mechanism of Ubiquitin-Chain Formation by the Human Anaphase-Promoting Complex. *Cell* **133**, 653–665 (2008).

20. Hao, Y. H. *et al.* Regulation of WASH-dependent actin polymerization and protein trafficking by ubiquitination. *Cell* **152**, 1051–1064 (2013).

21. Liu, P. *et al.* K63-linked polyubiquitin chains bind to DNA to facilitate DNA damage repair. *Sci. Signal.* **11**, eaar8133 (2018).

22. Adhikari, A., Xu, M. & Chen, Z. J. Ubiquitin-mediated activation of TAK1 and IKK. *Oncogene* **26**, 3214–3226 (2007).

23. Tokunaga, F. *et al.* Involvement of linear polyubiquitylation of NEMO in NF-κB activation. *Nat. Cell Biol.* **11**, 123–132 (2009).

24. Gatti, M. *et al.* RNF168 promotes noncanonical K27ubiquitination to signal DNA damage. *Cell Rep.* **10**, 226–238 (2015).

25. Durcan, T. M. *et al.* USP8 regulates mitophagy by removing K6-linked ubiquitin conjugates from parkin. *EMBO J.* **33**, 2473–2491 (2014).

26. Manzanillo, P. S. *et al.* The ubiquitin ligase parkin mediates resistance to intracellular pathogens. *Nature* **501**, 512–516 (2013).

27. Hershko, A. & Ciechanover, A. The Ubiquitin System. *Annu. Rev. Biochem* **67**, 425–79 (1998).

28. Deshaies, R. J. & Joazeiro, C. A. P. RING Domain E3 Ubiquitin Ligases. *Annu. Rev. Biochem.* **78**, 399–434 (2009).

29. Miki, Y. *et al.* A strong candidate for the breast and ovarian cancer susceptibility gene BRCA1. *Science (80-.).* **266**, 66–71 (1994).

30. Wu, L. C. *et al.* Identification of a RING protein that can interact in vivo with the BRCA1 gene product. *Nat. Genet.* **14**, 430–440 (1996).

31. Everett, R. D., Earnshaw, W. C., Findlay, J. & Lomonte, P. Specific destruction of kinetochore protein CENP-C and disruption of cell division by herpes simplex virus immediate-early protein Vmw110. *EMBO J.* **18**, 1526–1538 (1999).

32. Duprez, E. *et al.* SUMO-1 modification of the acute promyelocytic leukaemia protein PML: Implications for nuclear localisation. *J. Cell Sci.* **112**, 381–393 (1999).

33. Honda, R. & Yasuda, H. Association of p19(ARF) with Mdm2 inhibits ubiquitin ligase

activity of Mdm2 for tumor suppressor p53. *EMBO J.* **18**, 22–27 (1999).

34. Scheffner, M., Huibregtse, J. M., Vierstra, R. D. & Howley, P. M. The HPV-16 E6 and E6-AP complex functions as a ubiquitin-protein ligase in the ubiquitination of p53. *Cell* **75**, 495–505 (1993).

35. Wenzel, D. M., Lissounov, A., Brzovic, P. S. & Klevit, R. E. UBCH7 reactivity profile reveals parkin and HHARI to be RING/HECT hybrids. *Nature* **474**, 105–108 (2011).

36. Aguirre, J. D., Dunkerley, K. M., Lam, R., Rusal, M. & Shaw, G. S. Impact of altered phosphorylation on loss of function of juvenile Parkinsonism–associated genetic variants of the E3 ligase parkin. *J. Biol. Chem.* **293**, 6337–6348 (2018).

37. Komander, D., Clague, M. J. & Urbé, S. Breaking the chains: Structure and function of the deubiquitinases. *Nature Reviews Molecular Cell Biology* **10**, 550–563 (2009).

38. Nijman, S. M. B. *et al.* A genomic and functional inventory of deubiquitinating enzymes. *Cell* **123**, 773–786 (2005).

39. Amerik, A. Y. & Hochstrasser, M. Mechanism and function of deubiquitinating enzymes. *Biochimica et Biophysica Acta - Molecular Cell Research* **1695**, 189–207 (2004).

40. Hu, M. *et al.* Crystal structure of a UBP-family deubiquitinating enzyme in isolation and in complex with ubiquitin aldehyde. *Cell* **111**, 1041–1054 (2002).

41. Pozhidaeva, A. & Bezsonova, I. USP7: Structure, substrate specificity, and inhibition. *DNA Repair (Amst).* **76**, 30–39 (2019).

42. Daviet, L. & Colland, F. Targeting ubiquitin specific proteases for drug discovery. *Biochimie* **90**, 270–283 (2008).

43. Everett, R. D. *et al.* A novel ubiquitin-specific protease is dynamically associated with the PML nuclear domain and binds to a herpesvirus regulatory protein. *EMBO J.* **16**, 566–577 (1997).

44. Lee, H. J., Kim, M. S., Kim, Y. K., Oh, Y. K. & Baek, K. H. HAUSP, a deubiquitinating enzyme for p53, is polyubiquitinated, polyneddylated, and dimerized. *FEBS Lett.* **579**, 4867–4872 (2005).

45. Bhattacharya, S., Chakraborty, D., Basu, M. & Ghosh, M. K. Emerging insights into HAUSP (USP7) in physiology, cancer and other diseases. *Signal Transduct. Target. Ther.* **3**, 1–12 (2018).

46. Kon, N. *et al.* Inactivation of HAUSP in vivo modulates p53 function. *Oncogene* **29**, 1270–1279 (2010).

47. Fountain, M. D. *et al.* Pathogenic variants in USP7 cause a neurodevelopmental disorder with speech delays, altered behavior, and neurologic anomalies. *Genet. Med.* **21**, 1797–1807 (2019).

48. Song, M. S. *et al.* The deubiquitinylation and localization of PTEN are regulated by a HAUSP-PML network. *Nature* **455**, 813–817 (2008).

49. Wang, Q. *et al.* Stabilization of histone demethylase PHF8 by USP7 promotes breast carcinogenesis. *J. Clin. Invest.* **126**, 2205–2220 (2016).

50. Becker, K., Marchenko, N. D., Palacios, G. & Moll, U. M. A role of HAUSP in tumor suppression in a human colon carcinoma xenograft model. *Cell Cycle* **7**, 1205–1213 (2008).

51. Zhao, G. Y. *et al.* USP7 overexpression predicts a poor prognosis in lung squamous cell carcinoma and large cell carcinoma. *Tumor Biol.* **36**, 1721–1729 (2015).

52. Carrà, G. *et al.* Therapeutic inhibition of USP7-PTEN network in chronic lymphocytic leukemia: A strategy to overcome TP53 mutated/ deleted clones. *Oncotarget* **8**, 35508–35522 (2017).

53. Li, P. & Liu, H. M. Recent advances in the development of ubiquitin-specific-processing protease 7 (USP7) inhibitors. *Eur. J. Med. Chem.* **191**, 112107 (2020).

54. Wang, Z. *et al.* USP7: Novel drug target in cancer therapy. *Front. Pharmacol.* **10**, 427 (2019).

55. Saridakis, V. *et al.* Structure of the p53 binding domain of HAUSP/USP7 bound to epstein-barr nuclear antigen 1: Implications for EBV-mediated immortalization. *Mol. Cell* **18**, 25–36 (2005).

56. Faesen, A. C. *et al.* Mechanism of USP7/HAUSP activation by its C-Terminal ubiquitin-like domain and allosteric regulation by GMP-synthetase. *Mol. Cell* **44**, 147–159 (2011).

57. Gagarina, V. *et al.* Structural Basis of the Interaction Between Ubiquitin Specific Protease 7 and Enhancer of Zeste Homolog 2. *J. Mol. Biol.* **432**, 897–912 (2020).

58. Rougé, L. *et al.* Molecular Understanding of USP7 Substrate Recognition and C-Terminal Activation. *Structure* **24**, 1335–1345 (2016).

59. Pfoh, R. *et al.* Crystal Structure of USP7 Ubiquitin-like Domains with an ICP0 Peptide Reveals a Novel Mechanism Used by Viral and Cellular Proteins to Target USP7. *PLoS Pathog.* **11**, e1004950 (2015).

60. Kim, R. Q., van Dijk, W. J. & Sixma, T. K. Structure of USP7 catalytic domain and three Ubl-domains reveals a connector α-helix with regulatory role. *J. Struct. Biol.* **195**, 11–18 (2016).

61. Lee, H. R. *et al.* Bilateral inhibition of HAUSP deubiquitinase by a viral interferon regulatory factor protein. *Nat. Struct. Mol. Biol.* **18**, 1336–1344 (2011).

62. Chavoshi, S. *et al.* Identification of kaposi sarcoma herpesvirus (KSHV) vIRF1 protein as a novel interaction partner of human deubiquitinase USP7. *J. Biol. Chem.* **291**, 6281–6291 (2016).

63. Sarkari, F. *et al.* Ubiquitin-specific protease 7 is a regulator of ubiquitin-conjugating enzyme UbE2E1. *J. Biol. Chem.* **288**, 16975–16985 (2013).

64. Sheng, Y. *et al.* Molecular recognition of p53 and MDM2 by USP7/HAUSP. *Nat. Struct. Mol. Biol.* **13**, 285–291 (2006).

65. Sarkari, F. *et al.* Further Insight into Substrate Recognition by USP7: Structural and Biochemical Analysis of the HdmX and Hdm2 Interactions with USP7. *J. Mol. Biol.* **402**, 825–837 (2010).

66. Hu, M. *et al.* Structural Basis of Competitive Recognition of p53 and MDM2 by HAUSP/USP7: Implications for the Regulation of the p53–MDM2 Pathway. *PLoS Biol.* **4**, e27 (2006).

67. Jagannathan, M. *et al.* A Role for USP7 in DNA Replication. *Mol. Cell. Biol.* **34**, 132–145 (2014).

68. Cheng, J. *et al.* Molecular mechanism for USP7-mediated DNMT1 stabilization by acetylation. *Nat. Commun.* **6**, 1–11 (2015).

69. Zhang, Z. M. *et al.* An Allosteric Interaction Links USP7 to Deubiquitination and Chromatin Targeting of UHRF1. *Cell Rep.* **12**, 1400–1406 (2015).

70. An, L. *et al.* Dual-utility NLS drives RNF169-dependent DNA damage responses. *Proc. Natl. Acad. Sci.* **144**, E2872–E2881 (2017).

71. Ma, J. *et al.* C-terminal region of USP7/HAUSP is critical for deubiquitination activity and contains a second mdm2/p53 binding site. *Arch. Biochem. Biophys.* **503**, 207–212 (2010).

72. van der Horst, A. *et al.* FOXO4 transcriptional activity is regulated by monoubiquitination and USP7/HAUSP. *Nat. Cell Biol.* **8**, 1064–1073 (2006).

73. Kim, R. Q. & Sixma, T. K. Regulation of USP7: A High Incidence of E3 Complexes. *J. Mol. Biol.* **429**, 3395–3408 (2017).

74. Nathan, J. A. *et al.* The ubiquitin E3 ligase MARCH7 is differentially regulated by the deubiquitylating enzymes USP7 and USP9X. *Traffic* **9**, 1130–1145 (2008).

75. Ma, P. *et al.* The Ubiquitin Ligase RNF220 Enhances Canonical Wnt Signaling through USP7-Mediated Deubiquitination of -Catenin. *Mol. Cell. Biol.* **34**, 4355–4366 (2014).

76. de Bie, P., Zaaroor-Regev, D. & Ciechanover, A. Regulation of the Polycomb protein RING1B ubiquitination by USP7. *Biochem. Biophys. Res. Commun.* **400**, 389–395 (2010).

77. Zlatanou, A. *et al.* USP7 is essential for maintaining Rad18 stability and DNA damage tolerance. *Oncogene* **35**, 965–976 (2016).

78. Zaman, M. M.-U. *et al.* Ubiquitination-Deubiquitination by the TRIM27-USP7 Complex Regulates Tumor Necrosis Factor Alpha-Induced Apoptosis. *Mol. Cell. Biol.* **33**, 4971–4984 (2013).

79. Nicklas, S. *et al.* A complex of the ubiquitin ligase TRIM32 and the deubiquitinase USP7 balances the level of c-Myc ubiquitination and thereby determines neural stem cell fate specification. *Cell Death Differ.* **26**, 728–740 (2019).

80. Qing, P., Han, L., Bin, L., Yan, L. & Ping, W. X. USP7 regulates the stability and function of HLTF through deubiquitination. *J. Cell. Biochem.* **112**, 3856–3862 (2011).

81. Oh, Y. M., Yoo, S. J. & Seol, J. H. Deubiquitination of Chfr, a checkpoint protein, by USP7/HAUSP regulates its stability and activity. *Biochem. Biophys. Res. Commun.* **357**, 615–619 (2007).

82. Khoronenkova, V. S., Dianov, G. L., Khoronenkova, S. V. & Dianov, G. L. USP7S-dependent inactivation of Mule regulates DNA damage signalling and repair. *Nucleic Acids Res.* **41**, 1750–1756 (2013).

83. Zhu, Q., Sharma, N., He, J., Wani, G. & Wani, A. A. USP7 deubiquitinase promotes ubiquitin-dependent DNA damage signaling by stabilizing RNF168. *Cell Cycle* **14**, 1413–1425 (2015).

84. Aguilera, A. & García-Muse, T. Causes of Genome Instability. *Annu. Rev. Genet.* **47**, 1–32 (2013).

85. Smith, J., Tho, L. M., Xu, N. & Gillespie, D. A. The ATM-Chk2 and ATR-Chk1 Pathways in DNA Damage Signaling and Cancer. **108**, 73–112 (2010).

86. Cui, H. *et al.* The stress-responsive gene ATF3 regulates the histone acetyltransferase Tip60. *Nat. Commun.* **6**, 6752 (2015).

87. Dar, A., Shibata, E. & Dutta, A. Deubiquitination of Tip60 by USP7 Determines the Activity of the p53-Dependent Apoptotic Pathway. *Mol. Cell. Biol.* **33**, 3309–3320 (2013).

88. Alonso-de Vega, I. *et al.* Usp7 controls chk1 protein stability by direct deubiquitination. *Cell Cycle* **13**, 3921–3926 (2014).

89. Faustrup, H., Bekker-Jensen, S., Bartek, J., Lukas, J. & Mailand, N. USP7 counteracts SCFβTrCP- but not APCCdh1 -mediated proteolysis of Claspin. *J. Cell Biol.* **184**, 13–19 (2009).

90. Meulmeester, E. *et al.* Loss of HAUSP-mediated deubiquitination contributes to DNA damage-induced destabilization of Hdmx and Hdm2. *Mol. Cell* **18**, 565–576 (2005).

91. Li, M. *et al.* Deubiquitination of p53 by HAUSP is an important pathway for p53 stabilization. *Nature* **416**, 648–653 (2002).

92. Cummins, J. M. *et al.* Tumour suppression: disruption of HAUSP gene stabilizes p53. *Nature* **428**, 486 (2004).

93. Khoronenkova, S. V. *et al.* ATM-Dependent Downregulation of USP7/HAUSP by PPM1G Activates p53 Response to DNA Damage. *Mol. Cell* **45**, 801–813 (2012).

94. Georges, A., Marcon, E., Greenblatt, J. & Frappier, L. Identification and Characterization of USP7 Targets in Cancer Cells. *Sci. Rep.* **8**, 1–12 (2018).

95. Tang, J. *et al.* Critical role for Daxx in regulating Mdm2. *Nat. Cell Biol.* **8**, 855–862 (2006).

96. Tang, J., Qu, L., Pang, M. & Yang, X. Daxx is reciprocally regulated by Mdm2 and Hausp. *Biochem. Biophys. Res. Commun.* **393**, 542–545 (2010).

97. Song, M. S., Song, S. J., Kim, S. Y., Oh, H. J. & Lim, D. S. The tumour suppressor

RASSF1A promotes MDM2 self-ubiquitination by disrupting the MDM2-DAXX-HAUSP complex. *EMBO J.* **27**, 1863–1874 (2008).

98. Zhang, J. *et al.* ABRO1 suppresses tumourigenesis and regulates the DNA damage response by stabilizing p53. *Nat. Commun.* **5**, 5059 (2014).

99. Epping, M. T. *et al.* TSPYL5 suppresses p53 levels and function by physical interaction with USP7. *Nat. Cell Biol.* **13**, 102–108 (2011).

100. He, J. *et al.* Ubiquitin-specific Protease 7 Regulates Nucleotide Excision Repair through Deubiquitinating XPC Protein and Preventing XPC Protein from Undergoing Ultraviolet Light-induced and VCP/p97 Protein-regulated Proteolysis. *J. Biol. Chem.* **289**, 27278–27289 (2014).

101. Schwertman, P. *et al.* UV-sensitive syndrome protein UVSSA recruits USP7 to regulate transcription-coupled repair. *Nat. Genet.* **44**, 598–602 (2012).

102. Higa, M., Zhang, X., Tanaka, K. & Saijo, M. Stabilization of Ultraviolet (UV)-stimulated Scaffold Protein A by Interaction with Ubiquitin-specific Peptidase 7 Is Essential for Transcription-coupled Nucleotide Excision Repair. *J. Biol. Chem.* **291**, 13771–13779 (2016).

103. Kashiwaba, S. ichiro *et al.* USP7 Is a Suppressor of PCNA Ubiquitination and Oxidative-Stress-Induced Mutagenesis in Human Cells. *Cell Rep.* **13**, 2072–2080 (2015).

104. Qian, J. *et al.* USP7 modulates UV-induced PCNA monoubiquitination by regulating DNA polymerase eta stability. *Oncogene* **34**, 4791–4796 (2015).

105. Giovinazzi, S., Morozov, V. M., Summers, M. K., Reinhold, W. C. & Ishov, A. M. USP7 and Daxx regulate mitosis progression and taxane sensitivity by affecting stability of Aurora-A kinase. *Cell Death Differ.* **20**, 721–731 (2013).

106. Papp, S. J. *et al.* DNA damage shifts circadian clock time via hausp-dependent cry1 stabilization. *Elife* **4**, e04883 (2015).

107. Lecona, E. *et al.* USP7 is a SUMO deubiquitinase essential for DNA replication. *Nat. Struct. Mol. Biol.* **23**, 270–277 (2016).

108. Bhattacharya, S. & Ghosh, M. K. HAUSP, a novel deubiquitinase for Rb - MDM2 the critical regulator. *FEBS J.* **281**, 3061–3078 (2014).

109. Giovinazzi, S. *et al.* Usp7 protects genomic stability by regulating Bub3. *Oncotarget* **5**, 3728–3742 (2014).

110. Georges, A. *et al.* USP7 Regulates Cytokinesis through FBXO38 and KIF20B. *Sci. Rep.* **9**, 1–16 (2019).

111. Lallemand-Breitenbach, V. & de Thé, H. PML nuclear bodies: from architecture to function. *Curr. Opin. Cell Biol.* **52**, 154–161 (2018).

112. Bernardi, R. & Pandolfi, P. P. Structure, dynamics and functions of promyelocytic leukaemia nuclear bodies. *Nat. Rev. Mol. Cell Biol.* **8**, 1006–1016 (2007).

113. Sarkari, F., Wang, X., Nguyen, T. & Frappier, L. The herpesvirus associated ubiquitin specific protease, USP7, is a negative regulator of PML proteins and PML nuclear bodies. *PLoS One* **6**, e16598 (2011).

114. Episkopou, H., Diman, A., Claude, E., Viceconte, N. & Decottignies, A. TSPYL5 Depletion Induces Specific Death of ALT Cells through USP7-Dependent Proteasomal Degradation of POT1. *Mol. Cell* **75**, 469-482.e6 (2019).

115. Bhattacharya, S. & Ghosh, M. K. HAUSP regulates c-MYC expression via de-ubiquitination of TRRAP. *Cell. Oncol.* **38**, 265–277 (2015).

116. McMahon, S. B., Van Buskirk, H. A., Dugan, K. A., Copeland, T. D. & Cole, M. D. The novel ATM-related protein TRRAP is an essential cofactor for the c- Myc and E2F oncoproteins. *Cell* **94**, 363–374 (1998).

117. Biswas, K. *et al.* BRE/BRCC45 regulates CDC25A stability by recruiting USP7 in response to DNA damage. *Nat. Commun.* **9**, 1–15 (2018).

118. Clevers, H. & Nusse, R. Wnt/β-catenin signaling and disease. *Cell* **149**, 1192–1205 (2012).

119. Novellasdemunt, L. *et al.* USP7 Is a Tumor-Specific WNT Activator for APC-Mutated Colorectal Cancer by Mediating β-Catenin Deubiquitination. *Cell Rep.* **21**, 612–627 (2017).

120. Ji, L. *et al.* USP7 inhibits Wnt/β-catenin signaling through promoting stabilization of Axin. *Nat. Commun.* **10**, 1–14 (2019).

121. Liu, T., Zhang, L., Joo, D. & Sun, S. C. NF-κB signaling in inflammation. *Signal Transduct. Target. Ther.* **2**, 17023 (2017).

122. Colleran, A. *et al.* Deubiquitination of NF-κB by ubiquitin-specific protease-7 promotes transcription. *Proc. Natl. Acad. Sci. U. S. A.* **110**, 618–623 (2013).

123. Li, T., Guan, J., Li, S., Zhang, X. & Zheng, X. HSCARG downregulates NF-jβ signaling by interacting with USP7 and inhibiting NEMO ubiquitination. *Cell Death Dis.* **5**, 1–9 (2014).

124. Koch, S. *et al.* Kaposi's sarcoma-associated herpesvirus vIRF2 protein utilizes an IFN-dependent pathway to regulate viral early gene expression. *PLoS Pathog.* **15**, e1007743 (2019).

125. Xiang, Q., Ju, H. & Nicholas, J. USP7-Dependent Regulation of TRAF Activation and Signaling by a Viral Interferon Regulatory Factor Homologue. *J. Virol.* **94**, e01553-19 (2020).

126. Isaacson, M. K. & Ploegh, H. L. Ubiquitination, Ubiquitin-like Modifiers, and Deubiquitination in Viral Infection. *Cell Host Microbe* **5**, 559–570 (2009).

127. Rice, A. P. & Mathews, M. B. Transcriptional but not translational regulation of HIV-1 by the tat gene product. *Nature* **332**, 551–3 (1988).

128. Vidal, S. *et al.* Regulation of the Ebola Virus VP24 Protein by SUMO. *J. Virol.* **94**,

e01687-19 (2019).

129. Czech-Sioli, M. *et al.* The Ubiquitin-Specific Protease Usp7, a Novel Merkel Cell Polyomavirus Large T-Antigen Interaction Partner, Modulates Viral DNA Replication. *J. Virol.* **94**, e01638-19 (2019).

130. Ching, W. *et al.* A Ubiquitin-specific Protease Possesses a Decisive Role for Adenovirus Replication and Oncogene-mediated Transformation. *PLoS Pathog.* **9**, e1003273 (2013).

131. Mesri, E. A., Feitelson, M. A. & Munger, K. Human viral oncogenesis: A cancer hallmarks analysis. *Cell Host and Microbe* **15**, 266–282 (2014).

132. Daubeuf, S. *et al.* HSV ICP0 recruits USP7 to modulate TLR-mediated innate response. *Blood* **113**, 3264–3275 (2009).

133. Holowaty, M. N. *et al.* Protein profiling with Epstein-Barr nuclear antigen-1 reveals an interaction with the herpesvirus-associated ubiquitin-specific protease HAUSP/USP7. *J. Biol. Chem.* **278**, 29987–94 (2003).

134. Sarkari, F. *et al.* EBNA1-mediated recruitment of a histone H2B deubiquitylating complex to the Epstein-Barr virus latent origin of DNA replication. *PLoS Pathog.* **5**, e1000624 (2009).

135. Sivachandran, N., Sarkari, F. & Frappier, L. Epstein-Barr nuclear antigen 1 contributes to nasopharyngeal carcinoma through disruption of PML nuclear bodies. *PLoS Pathog.* **4**, e1000170 (2008).

136. Jones, P. A., Issa, J. P. J. & Baylin, S. Targeting the cancer epigenome for therapy. *Nat. Rev. Genet.* **17**, 630–641 (2016).

137. Greer, E. L. & Shi, Y. Histone methylation: A dynamic mark in health, disease and inheritance. *Nature Reviews Genetics* **13**, 343–357 (2012).

138. Kornberg, R. D. & Lorch, Y. Twenty-five years of the nucleosome, fundamental particle of the eukaryote chromosome. *Cell* **98**, 285–294 (1999).

139. Martin, C. & Zhang, Y. The diverse functions of histone lysine methylation. *Nature Reviews Molecular Cell Biology* **6**, 838–849 (2005).

140. Strahl, B. D. & Allis, C. D. The language of covalent histone modifications. *Nature* **403**, 41–45 (2000).

141. Kouzarides, T. Chromatin Modifications and Their Function. *Cell* **128**, 693–705 (2007).

142. Blair, L. P., Cao, J., Zou, M. R., Sayegh, J. & Yan, Q. Epigenetic regulation by lysine demethylase 5 (KDM5) enzymes in cancer. *Cancers (Basel).* **3**, 1383–1404 (2011).

143. Felle, M. *et al.* The USP7/Dnmt1 complex stimulates the DNA methylation activity of Dnmt1 and regulates the stability of UHRF1. *Nucleic Acids Res.* **39**, 8355–8365 (2011).

144. Ma, H. *et al.* M phase phosphorylation of the epigenetic regulator UHRF1 regulates its physical association with the deubiquitylase USP7 and stability. *Proc. Natl. Acad. Sci. U. S. A.* **109**, 4828–4833 (2012).

145. Van Der Knaap, J. A. *et al.* GMP synthetase stimulates histone H2B deubiquitylation by the epigenetic silencer USP7. *Mol. Cell* **17**, 695–707 (2005).

146. Song, N., Cao, C., Tian, S., Long, M. & Liu, L. USP7 Deubiquitinates and Stabilizes SIRT1. *Anat. Rec.* **303**, 1337–1345 (2019).

147. Entrevan, M., Schuettengruber, B. & Cavalli, G. Regulation of Genome Architecture and Function by Polycomb Proteins. *Trends Cell Biol.* **26**, 511–525 (2016).

148. Lecona, E., Narendra, V. & Reinberg, D. USP7 cooperates with SCML2 to regulate the activity of PRC1. *Mol. Cell. Biol.* **35**, 1157–1168 (2015).

149. Maertens, G. N., El Messaoudi-Aubert, S., Elderkin, S., Hiom, K. & Peters, G. Ubiquitin-specific proteases 7 and 11 modulate Polycomb regulation of the INK4a tumour suppressor. *EMBO J.* **29**, 2553–2565 (2010).

150. Wheaton, K. *et al.* UbE2E1/UBCH6 Is a Critical in Vivo E2 for the PRC1-catalyzed Ubiquitination of H2A at Lys-119. *J. Biol. Chem.* **292**, 2893–2902 (2017).

151. Byvoet, P., Shepherd, G. R., Hardin, J. M. & Noland, B. J. The distribution and turnover of labeled methyl groups in histone fractions of cultured mammalian cells. *Arch. Biochem. Biophys.* **148**, 558–67 (1972).

152. Murray, K. The Occurrence of ϵ-N-Methyl Lysine in Histones. *Biochemistry* **3**, 10–15 (1964).

153. Fischle, W., Franz, H., Jacobs, S. A., Allis, C. D. & Khorasanizadeh, S. Specificity of the chromodomain Y chromosome family of chromodomains for lysine-methylated ARK(S/T) motifs. *J. Biol. Chem.* **283**, 19626–35 (2008).

154. Shi, X. *et al.* ING2 PHD domain links histone H3 lysine 4 methylation to active gene repression. *Nature* **442**, 96–99 (2006).

155. Bernstein, B. E. *et al.* A Bivalent Chromatin Structure Marks Key Developmental Genes in Embryonic Stem Cells. *Cell* **125**, 315–26 (2006).

156. Min, G. L. *et al.* Demethylation of H3K27 regulates polycomb recruitment and H2A ubiquitination. *Science (80-.).* **318**, 447–450 (2007).

157. Chandrasekharan, M. B., Huang, F. & Sun, Z. W. Histone H2B ubiquitination and beyond: Regulation of nucleosome stability, chromatin dynamics and the trans-histone H3 methylation. *Epigenetics* **5**, 460–468 (2010).

158. Guccione, E. *et al.* Methylation of histone H3R2 by PRMT6 and H3K4 by an MLL complex are mutually exclusive. *Nature* **449**, 933–7 (2007).

159. Yi, L., Cui, Y., Xu, Q. & Jiang, Y. Stabilization of LSD1 by deubiquitinating enzyme USP7 promotes glioblastoma cell tumorigenesis and metastasis through suppression of the p53 signaling pathway. *Oncol. Rep.* **36**, 2935–2945 (2016).

160. Ding, X. *et al.* Mixed lineage leukemia 5 (MLL5) protein stability is cooperatively regulated by OGlcNac transferase (OGT) and ubiquitin specific protease 7 (USP7). *PLoS One* **10**, e0145023 (2015).

161. Rea, S. *et al.* Regulation of chromatin structure by site-specific histone H3 methyltransferases. *Nature* **406**, 593–9 (2000).

162. Huang, J. & Berger, S. L. The emerging field of dynamic lysine methylation of non-histone proteins. *Curr. Opin. Genet. Dev.* **18**, 152–8 (2008).

163. Klose, R. J. & Zhang, Y. Regulation of histone methylation by demethylimination and demethylation. *Nature Reviews Molecular Cell Biology* **8**, 307–318 (2007).

164. Simon, J. A. & Lange, C. A. Roles of the EZH2 histone methyltransferase in cancer epigenetics. *Mutat. Res. - Fundam. Mol. Mech. Mutagen.* **647**, 21–29 (2008).

165. Shen, X. *et al.* EZH1 Mediates Methylation on Histone H3 Lysine 27 and Complements EZH2 in Maintaining Stem Cell Identity and Executing Pluripotency. *Mol. Cell* **32**, 491–502 (2008).

166. Conway, E., Healy, E. & Bracken, A. P. PRC2 mediated H3K27 methylations in cellular identity and cancer. *Curr. Opin. Cell Biol.* **37**, 42–8 (2015).

167. Lee, T. I. *et al.* Control of Developmental Regulators by Polycomb in Human Embryonic Stem Cells. *Cell* **125**, 301–13 (2006).

168. O'Meara, M. M. & Simon, J. A. Inner workings and regulatory inputs that control Polycomb repressive complex 2. *Chromosoma* **121**, 221–34 (2012).

169. Han, Z. *et al.* Structural Basis of EZH2 Recognition by EED. *Structure* **15**, 1306–1315 (2007).

170. Weaver, T. M. *et al.* The EZH2 SANT1 domain is a histone reader providing sensitivity to the modification state of the H4 tail. *Sci. Rep.* **9**, 987 (2019).

171. Moritz, L. E. & Trievel, R. C. Structure, mechanism, and regulation of polycomb-repressive complex 2. *Journal of Biological Chemistry* **293**, 13805–13814 (2018).

172. Copeland, R. A., Solomon, M. E. & Richon, V. M. Protein methyltransferases as a target class for drug discovery. *Nature Reviews Drug Discovery* **8**, 724–732 (2009).

173. Margueron, R. *et al.* Role of the polycomb protein EED in the propagation of repressive histone marks. *Nature* **461**, 762–767 (2009).

174. Hansen, K. H. *et al.* A model for transmission of the H3K27me3 epigenetic mark. *Nat. Cell Biol.* **10**, 1291–1300 (2008).

175. Højfeldt, J. W. *et al.* Accurate H3K27 methylation can be established de novo by SUZ12-directed PRC2. *Nat. Struct. Mol. Biol.* **25**, 225–232 (2018).

176. Hauri, S. *et al.* A High-Density Map for Navigating the Human Polycomb Complexome. *Cell Rep.* **17**, 583–595 (2016).

177. Laugesen, A., Højfeldt, J. W. & Helin, K. Molecular Mechanisms Directing PRC2 Recruitment and H3K27 Methylation. *Molecular Cell* **74**, 8–18 (2019).

178. Chen, S. *et al.* Unique Structural Platforms of Suz12 Dictate Distinct Classes of PRC2 for Chromatin Binding Graphical abstract. *Mol Cell* **69**, 840–852 (2018).

179. Vaswani, R. G. *et al.* Identification of (R)-N-((4-Methoxy-6-methyl-2-oxo-1,2-dihydropyridin-3-yl)methyl)-2-methyl-1-(1-(1-(2,2,2-trifluoroethyl)piperidin-4-yl)ethyl)-1H-indole-3-carboxamide (CPI-1205), a Potent and Selective Inhibitor of Histone Methyltransferase EZH2, Suitable for Phase i Clinical Trials for B-Cell Lymphomas. *J. Med. Chem.* **59**, 9928–9941 (2016).

180. Kasinath, V. *et al.* Structures of human PRC2 with its cofactors AEBP2 and JARID2. *Science (80-.).* **359**, 940–944 (2018).

181. Ku, M. *et al.* Genomewide Analysis of PRC1 and PRC2 Occupancy Identifies Two Classes of Bivalent Domains. *PLoS Genet.* **4**, e1000242 (2008).

182. Jermann, P., Hoerner, L., Burger, L. & Schübeler, D. Short sequences can efficiently recruit histone H3 lysine 27 trimethylation in the absence of enhancer activity and DNA methylation. *Proc. Natl. Acad. Sci. U. S. A.* **111**, E3415–E3421 (2014).

183. Ferrari, K. J. *et al.* Polycomb-Dependent H3K27me1 and H3K27me2 Regulate Active Transcription and Enhancer Fidelity. *Mol. Cell* **53**, 49–62 (2014).

184. McCabe, M. T. *et al.* Mutation of A677 in histone methyltransferase EZH2 in human B-cell lymphoma promotes hypertrimethylation of histone H3 on lysine 27 (H3K27). *Proc. Natl. Acad. Sci. U. S. A.* **109**, 2989–2994 (2012).

185. Viré, E. *et al.* The Polycomb group protein EZH2 directly controls DNA methylation. *Nature* **439**, 871–874 (2006).

186. Cao, R., Tsukada, Y. I. & Zhang, Y. Role of Bmi-1 and Ring1A in H2A ubiquitylation and hox gene silencing. *Mol. Cell* **20**, 845–54 (2005).

187. Shao, Z. *et al.* Stabilization of chromatin structure by PRC1, a polycomb complex. *Cell* **98**, 37–46 (1999).

188. Dellino, G. I. *et al.* Polycomb silencing blocks transcription initiation. *Mol. Cell* **13**, 887–893 (2004).

189. Wang, L. *et al.* Hierarchical recruitment of polycomb group silencing complexes. *Mol. Cell* **14**, 637–646 (2004).

190. Cao, R. & Zhang, Y. The functions of E(Z)/EZH2-mediated methylation of lysine 27 in histone H3. *Current Opinion in Genetics and Development* **14**, 155–164 (2004).

191. Sparmann, A. & Van Lohuizen, M. Polycomb silencers control cell fate, development and cancer. *Nat. Rev. Cancer* **6**, 846–56 (2006).

192. Ding, L., Erdmann, C., Chinnaiyan, A. M., Merajver, S. D. & Kleer, C. G. Identification of EZH2 as a Molecular Marker for a Precancerous State in Morphologically Normal Breast Tissues. *Cancer Res.* **66**, 4095–4099 (2006).

193. Raman, J. D. *et al.* Increased expression of the polycomb group gene, EZH2, in transitional cell carcinoma of the bladder. *Clin. Cancer Res.* **11**, 8570–6 (2005).

194. Varambally, S. *et al.* The polycomb group protein EZH2 is involved in progression of prostate cancer. *Nature* **419**, 624–9 (2002).

195. Kleer, C. G. *et al.* EZH2 is a marker of aggressive breast cancer and promotes neoplastic transformation of breast epithelial cells. *Proc. Natl. Acad. Sci. U. S. A.* **100**, 11606–11611 (2003).

196. Visser, H. P. J. *et al.* The Polycomb group protein EZH2 is upregulated in proliferating, cultured human mantle cell lymphoma. *Br. J. Haematol.* **112**, 950–8 (2001).

197. Mimori, K. *et al.* Clinical significance of enhancer of zeste homolog 2 expression in colorectal cancer cases. *Eur. J. Surg. Oncol.* **31**, 376–80 (2005).

198. Sudo, T. *et al.* Clinicopathological significance of EZH2 mRNA expression in patients with hepatocellular carcinoma. *Br. J. Cancer* **92**, 1754–58 (2005).

199. Bachmann, I. M. *et al.* EZH2 expression is associated with high proliferation rate and aggressive tumor subgroups in cutaneous melanoma and cancers of the endometrium, prostate, and breast. *J. Clin. Oncol.* **24**, 268–73 (2006).

200. Bracken, A. P. *et al.* The Polycomb group proteins bind throughout the INK4A-ARF locus and are disassociated in senescent cells. *Genes Dev.* **21**, 525–530 (2007).

201. Agherbi, H. *et al.* Polycomb Mediated Epigenetic Silencing and Replication Timing at the INK4a/ARF Locus during Senescence. *PLoS One* **4**, e5622 (2009).

202. Ernst, T. *et al.* Inactivating mutations of the histone methyltransferase gene EZH2 in myeloid disorders. *Nat. Genet.* **42**, 722–6 (2010).

203. Tan, J. Z., Yan, Y., Wang, X. X., Jiang, Y. & Xu, H. E. EZH2: Biology, disease, and structure-based drug discovery. *Acta Pharmacol. Sin.* **35**, 161–174 (2014).

204. Yao, Y. *et al.* Downregulation of enhancer of zeste homolog 2 (EZH2) is essential for the induction of autophagy and apoptosis in colorectal cancer cells. *Genes (Basel).* **7**, 83 (2016).

205. Yomtoubian, S. *et al.* Inhibition of EZH2 Catalytic Activity Selectively Targets a Metastatic Subpopulation in Triple-Negative Breast Cancer. *Cell Rep.* **30**, 755-770.e6 (2020).

206. Shumaker, D. K. *et al.* Mutant nuclear lamin A leads to progressive alterations of epigenetic control in premature aging. *Proc. Natl. Acad. Sci. U. S. A.* **103**, 8703–8 (2006).

207. Yu, Y. L. *et al.* Smurf2-mediated degradation of EZH2 enhances neuron differentiation and improves functional recovery after ischaemic stroke. *EMBO Mol. Med.* **5**, 531–547 (2013).

208. Sahasrabuddhe, A. A. *et al.* Oncogenic Y641 mutations in EZH2 prevent Jak2/β-TrCP-mediated degradation. *Oncogene* **34**, 445–454 (2015).

209. Jin, X. *et al.* CDK5/FBW7-dependent ubiquitination and degradation of EZH2 inhibits pancreatic cancer cell migration and invasion. *J. Biol. Chem.* **292**, 6269–6280 (2017).

210. Consalvi, S., Brancaccio, A., Dall'agnese, A., Puri, P. L. & Palacios, D. Praja1 E3 ubiquitin ligase promotes skeletal myogenesis through degradation of EZH2 upon p38α activation. *Nat. Commun.* **8**, (2017).

211. Shen, Z. *et al.* Downregulation of Ezh2 methyltransferase by FOXP3: New insight of FOXP3 into chromatin remodeling? *Biochim. Biophys. Acta - Mol. Cell Res.* **1833**, 2190–2200 (2013).

212. Wang, X. *et al.* A covalently bound inhibitor triggers EZH 2 degradation through CHIP -mediated ubiquitination . *EMBO J.* **36**, 1243–1260 (2017).

213. Kuser-Abali, G. *et al.* An EZH2-mediated epigenetic mechanism behind p53-dependent tissue sensitivity to DNA damage. *Proc. Natl. Acad. Sci. U. S. A.* **115**, 3452–3457 (2018).

214. Oliviero, G. *et al.* Dynamic protein interactions of the polycomb repressive complex 2 during differentiation of pluripotent cells. *Mol. Cell. Proteomics* **15**, 3450–3460 (2016).

215. Gagarina, V. Identification of Interactions Between Ubiquitin Specific Protease 7 (USP7) and Enhancer of Zeste 2 (EZH2). (York University, 2017).

216. Su, D. *et al.* Bimodal Regulation of the PRC2 Complex by USP7 Underlies Melanomagenesis. *bioRxiv* 641977 (2019). doi:10.1101/641977

217. Lei, A. *et al.* EZH2 regulates protein stability via recruiting USP7 to mediate neuronal gene expression in cancer cells. *Front. Genet.* **10**, 1–18 (2019).

218. Zhang, M.-J. *et al.* Clinical significance of USP7 and EZH2 in predicting prognosis of laryngeal squamous cell carcinoma and their possible functional mechanism. *Int J Clin Exp Pathol* **12**, 2184–2194 (2019).

219. Zheng, N., Chu, M., Lin, M., He, Y. & Wang, Z. USP7 stabilizes EZH2 and enhances cancer malignant progression. *Am. J. Cancer Res.* **10**, 299–313 (2020).

220. Wei, Y. *et al.* CDK1-dependent phosphorylation of EZH2 suppresses methylation of H3K27 and promotes osteogenic differentiation of human mesenchymal stem cells. *Nat. Cell Biol.* **13**, 87–94 (2011).

221. Wu, S. C. & Zhang, Y. CDK1-mediated Phosphorylation of EZH2 Regulates its Stability. *J. Biol. Chem.* **286**, 28511–28519 (2011).

222. Hall, J. A., Tabata, M., Rodgers, J. T. & Puigserver, P. USP7 attenuates hepatic gluconeogenesis through modulation of FoxO1 gene promoter occupancy. *Mol. Endocrinol.* **28**, 912–924 (2014).

223. Han, G. H. *et al.* Prognostic implications of forkhead box protein O1 (FOXO1) and paired box 3 (PAX3) in epithelial ovarian cancer. *BMC Cancer* **19**, 1202 (2019).

224. Bergounioux, J. *et al.* Calpain activation by the Shigella flexneri effector VirA regulates key steps in the formation and life of the bacterium's epithelial niche. *Cell Host Microbe* **11**, 240–252 (2012).

225. Torres, I. O. *et al.* Histone demethylase KDM5A is regulated by its reader domain through a positive-feedback mechanism. *Nat. Commun.* **6**, 2–11 (2015).

226. Rotili, D. & Mai, A. Targeting histone demethylases: A new avenue for the fight against cancer. *Genes and Cancer* **2**, 663–79 (2011).

227. Kooistra, S. M. & Helin, K. Post-translational modifications: Molecular mechanisms and potential functions of histone demethylases. *Nat. Rev. Mol. Cell Biol.* **13**, 297–311 (2012).

228. Brier, A. S. B. *et al.* The KDM5 family is required for activation of pro-proliferative cell cycle genes during adipocyte differentiation. *Nucleic Acids Res.* **45**, 1743–1759 (2017).

229. Horton, J. R. *et al.* Characterization of a linked jumonji domain of the KDM5/JARID1 family of histone H3 lysine 4 demethylases. *J. Biol. Chem.* **291**, 2631–2646 (2016).

230. Liu, X. & Secombe, J. The Histone Demethylase KDM5 Activates Gene Expression by Recognizing Chromatin Context through Its PHD Reader Motif. *Cell Rep.* **13**, 2219–2231 (2015).

231. Shilatifard, A. The COMPASS Family of Histone H3K4 Methylases: Mechanisms of Regulation in Development and Disease Pathogenesis. *Annu. Rev. Biochem.* **81**, 65–95 (2012).

232. Heintzman, N. D. *et al.* Distinct and predictive chromatin signatures of transcriptional promoters and enhancers in the human genome. *Nat. Genet.* **39**, 311–318 (2007).

233. Kim, T. S. & Buratowski, S. Dimethylation of H3K4 by Set1 Recruits the Set3 Histone Deacetylase Complex to 5′ Transcribed Regions. *Cell* **137**, 259–272 (2009).

234. Santos-Rosa, H. *et al.* Active genes are tri-methylated at K4 of histone H3. *Nature* **419**, 407–411 (2002).

235. Defeo-Jones, D. *et al.* Cloning of cDNAs for cellular proteins that bind to the retinoblastoma gene product. *Nature* **352**, 251–254 (1991).

236. Sellers, W. R. & Kaelin Jr., W. G. Role of the retinoblastoma protein in the pathogenesis of human cancer. *J Clin Oncol* **15**, 3301–3312 (1997).

237. Benevolenskaya, E. V., Murray, H. L., Branton, P., Young, R. A. & Kaelin, W. G. Binding of pRB to the PHD protein RBP2 promotes cellular differentiation. *Mol. Cell* **18**, 623–635 (2005).

238. Liefke, R. *et al.* Histone demethylase KDM5A is an integral part of the core Notch-RBP-J repressor complex. *Genes Dev.* **24**, 590–601 (2010).

239. Wang, C. *et al.* KDM5A controls bone morphogenic protein 2-induced osteogenic differentiation of bone mesenchymal stem cells during osteoporosis. *Cell Death Dis.* **7**, e2335 (2016).

240. Beshiri, M. L. *et al.* Coordinated repression of cell cycle genes by KDM5A and E2F4 during differentiation. *Proc. Natl. Acad. Sci. U. S. A.* **109**, 18499–18504 (2012).

241. Pasini, D. *et al.* Coordinated regulation of transcriptional repression by the RBP2 H3K4 demethylase and Polycomb-Repressive Complex 2. *Genes Dev.* **22**, 1345–1355 (2008).

242. Stratmann, A. & Haendler, B. The histone demethylase JARID1A regulates progesterone receptor expression. *FEBS J.* **278**, 1458–1469 (2011).

243. Lopez-Bigas, N. *et al.* Genome-wide Analysis of the H3K4 Histone Demethylase RBP2

Reveals a Transcriptional Program Controlling Differentiation. *Mol. Cell* **31**, 520–530 (2008).

244. Ge, Z. *et al.* Chromatin remodeling: recruitment of histone demethylase RBP2 by Mad1 for transcriptional repression of a Myc target gene, telomerase reverse transcriptase. *FASEB J.* **24**, 579–86 (2010).

245. DiTacchio, L. *et al.* Histone lysine demethylase JARID1a activates CLOCK-BMAL1 and influences the circadian clock. *Science (80-.).* **333**, 1881–5 (2011).

246. Tu, S. *et al.* The ARID domain of the H3K4 demethylase RBP2 binds to a DNA CCGCCC motif. *Nat. Struct. Mol. Biol.* **15**, 419–421 (2008).

247. Hidalgo, A. *et al.* Microarray comparative genomic hybridization detection of chromosomal imbalances in uterine cervix carcinoma. *BMC Cancer* **5**, 77 (2005).

248. Teng, Y. C. *et al.* Histone demethylase RBP2 promotes lung tumorigenesis and cancer metastasis. *Cancer Res.* **73**, 4711–21 (2013).

249. Vogt, T. *et al.* Deficiency of a novel retinoblastoma binding protein 2-homolog is a consistent feature of sporadic human melanoma skin cancer. *Lab. Investig.* **79**, 1615–1627 (1999).

250. Cao, J. *et al.* Histone demethylase RBP2 is critical for breast cancer progression and metastasis. *Cell Rep.* **6**, 868–877 (2014).

251. Zhou, D. *et al.* RBP2 induces stem-like cancer cells by promoting EMT and is a prognostic marker for renal cell carcinoma. *Exp. Mol. Med.* **48**, e238 (2016).

252. Maggi, E. C. *et al.* Retinoblastoma-binding protein 2 (RBP2) is frequently expressed in neuroendocrine tumors and promotes the neoplastic phenotype. *Oncogenesis* **5**, e257–e257 (2016).

253. Oser, M. G. *et al.* The KDM5A/RBP2 histone demethylase represses NOTCH signaling to sustain neuroendocrine differentiation and promote small cell lung cancer tumorigenesis. *Genes Dev.* **33**, 1718–1738 (2019).

254. Wang, G. G. *et al.* Haematopoietic malignancies caused by dysregulation of a chromatin-binding PHD finger. *Nature* **459**, 847–851 (2009).

255. Zeng, J. *et al.* The Histone Demethylase RBP2 Is Overexpressed in Gastric Cancer and Its Inhibition Triggers Senescence of Cancer Cells. *Gastroenterology* **138**, 981–992 (2010).

256. Van Zutven, L. J. C. M. *et al.* Identification of NUP98 abnormalities in acute leukemia: JARIDIA (12p13) as a new partner gene. *Genes Chromosom. Cancer* **45**, 437–446 (2006).

257. Liang, X. *et al.* Histone demethylase RBP2 promotes malignant progression of gastric cancer through TGF-β1-(p-Smad3)-RBP2-E-cadherin-Smad3 feedback circuit. *Oncotarget* **6**, 17661–17674 (2015).

258. Li, L. *et al.* Critical role of histone demethylase RBP2 in human gastric cancer angiogenesis. *Mol. Cancer* **13**, 81 (2014).

259. Liang, X. *et al.* Histone demethylase RBP2 induced by Helicobactor Pylori CagA participates in the malignant transformation of gastric epithelial cells. *Oncotarget* **5**, 5798–5807 (2014).

260. Pointon, J. J. *et al.* The histone demethylase JARID1A is associated with susceptibility to ankylosing spondylitis. *Genes Immun.* **12**, 395–398 (2011).

261. Chai, W. *et al.* JARID1A, JMY, and PTGER4 Polymorphisms Are Related to Ankylosing Spondylitis in Chinese Han Patients: A Case-Control Study. *PLoS One* **8**, 1–8 (2013).

262. Bhushan, B. *et al.* Investigations on small molecule inhibitors targeting the histone H3K4 tri-methyllysine binding PHD-finger of JmjC histone demethylases. *Bioorganic Med. Chem.* **26**, 2984–2991 (2018).

263. van der Knaap, J. A., Kozhevnikova, E., Langenberg, K., Moshkin, Y. M. & Verrijzer, C. P. Biosynthetic Enzyme GMP Synthetase Cooperates with Ubiquitin-Specific Protease 7 in Transcriptional Regulation of Ecdysteroid Target Genes. *Mol. Cell. Biol.* **30**, 736–744 (2010).

264. Maat, H. *et al.* Identification of USP7 as an essential component to maintain integrity and function of non-canonical PRC1.1 in leukemia. *bioRxiv* (2017). doi:10.1101/221093

265. Morera, L., Lübbert, M. & Jung, M. Targeting histone methyltransferases and demethylases in clinical trials for cancer therapy. *Clin. Epigenetics* **8**, 16 (2016).

266. Huang, C. *et al.* SUMOylated ORC2 Recruits a Histone Demethylase to Regulate Centromeric Histone Modification and Genomic Stability. *Cell Rep.* **15**, 147–157 (2016).

267. Pasini, D. *et al.* Coordinated regulation of transcriptional repression by the RBP2 H3K4 demethylase and Polycomb-Repressive Complex 2. *Genes Dev.* **22**, 1345–1355 (2008).

268. Bojagora, A. & Saridakis, V. USP7 manipulation by viral proteins. *Virus Res.* **286**, 198076 (2020).

APPENDIX A: Usp7 Manipulation by Viral Proteins Review

Certain parts of this thesis are included in the review [268].

ELSEVIER

Virus Research

Volume 286, September 2020, 198076

Review

USP7 manipulation by viral proteins

Anna Bojagora, Vivian Saridakis

Abstract

Ubiquitin Specific Protease 7 (USP7) is a deubiquitinating enzyme (DUB) that plays critical roles in the regulation of many cellular processes including epigenetics, tumour suppression, oncogenesis, DNA damage response, immunity and viral infection. USP7 was the first DUB associated with viral infection. Since then other DUB:viral protein interactions have been discovered, however, USP7 continues to be the most targeted DUB interacting with many proteins from various viruses. The selective pressures of evolution have allowed viruses to develop mechanisms that subvert host cellular machinery, promoting survival of the viral niche. Numerous viral proteins have been identified to target and usurp the function of USP7 to their advantage. This review explores novel developments in research focusing on the mechanisms underlying the manipulation of USP7 by viruses.

APPENDIX B: RBP2 Isoform 2 Secondary Structure Prediction

The secondary structure and disorder prediction for the RBP2 sequence (isoform 2) was determined using Phyre2. The analysis was used to determine the most optimal candidates interaction sites (highlighted in blue).

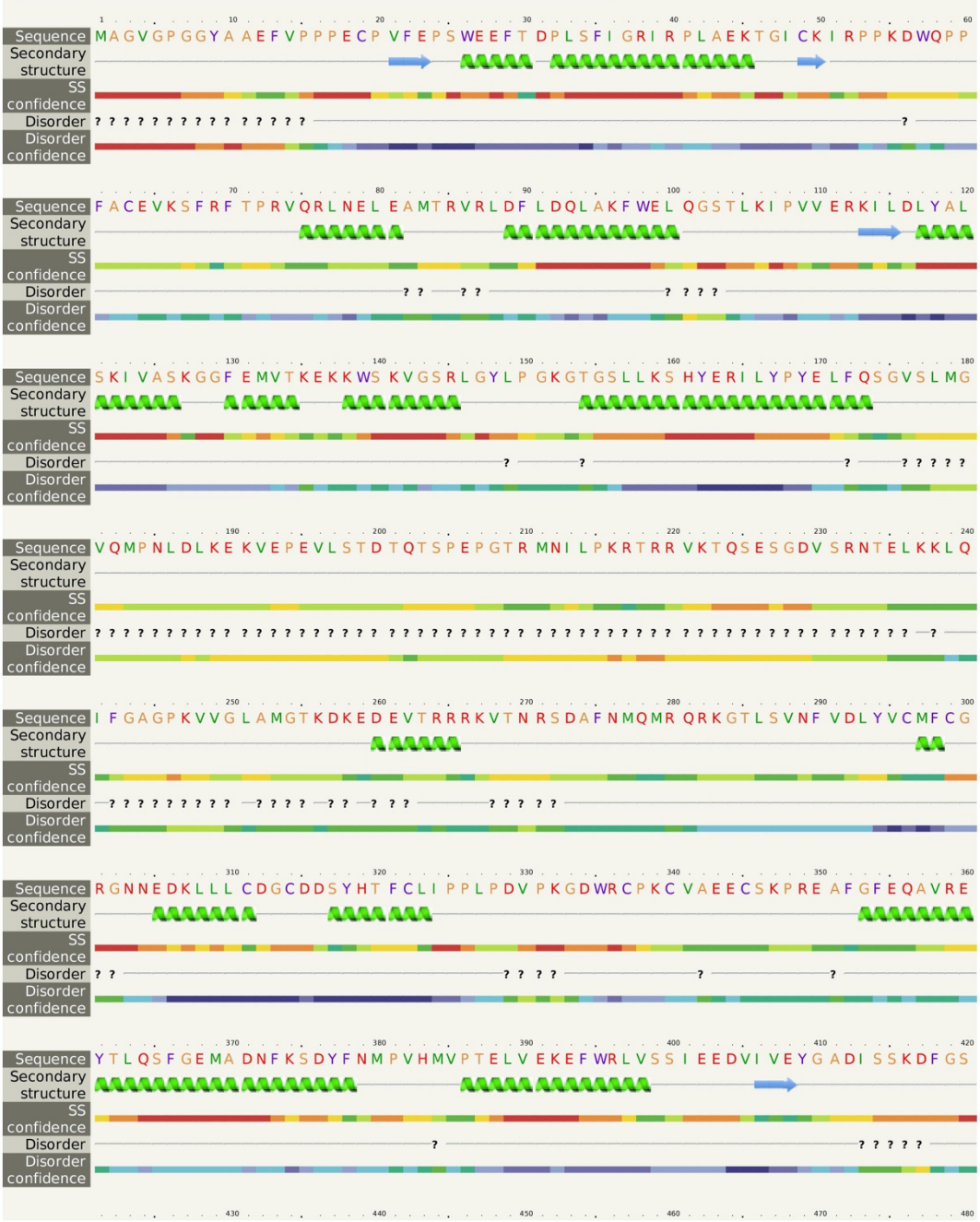

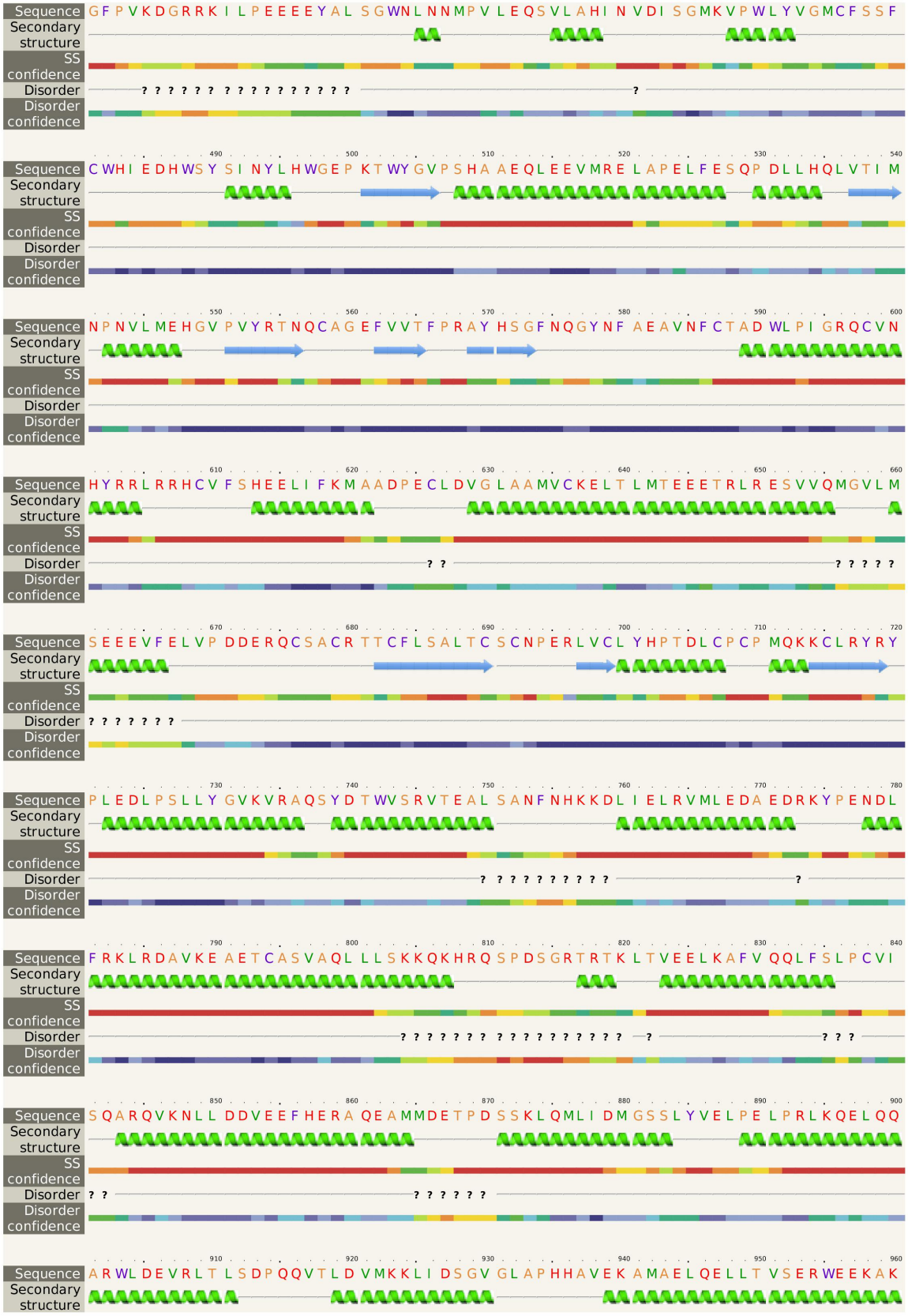
Sequence
Secondary structure
SS confidence
Disorder
Disorder confidence
GFPVKDGRRKILPEEEEEYALSGWNLNNMPVLEQSVLAHINVDISGMKVPWLYVGMCFSSF
CWHIEDHWSYSINYLHWGEPKTWYGVPSHAAEQLEEVMREELAPELFESQPDLLHQLVTIM
NPNVLMEHGVPVYRTNQCAGEFVVTFPRAYHSGFNQGYNFAEAVNFCTADWLPIGRQCVN
HYRRLRRHCVFSHEELIFKMAADPECLDVGLAAMVCKELTLMTEEETRLRESVVQMGVLM
SEEEVFELVPDDERQCSACRTTCFLSALTCSCNPERLVCLYHPTDLCPCPMQKKCLRYRY
PLEDLPSLLYGVKVRAQSYDTWVSRVTEALSANFNHKKDLIELRVMLEDAEDRKYPENDL
FRKLRDAVKEAETCASVAQLLLSKKQKHRQSPDSGRTRTKLTVEELKAFVQQLFSLPCVI
SQARQVKNLLDDVEEFHERAQEAMMDETPDSSKLQMLIDMGSSLYVELPELPRLKQELQQ
ARWLDEVRLTLSDPQQVTLDVMKKLIDSGVGLAPHHAVEKAMAELQELLTVSERWEEKAK

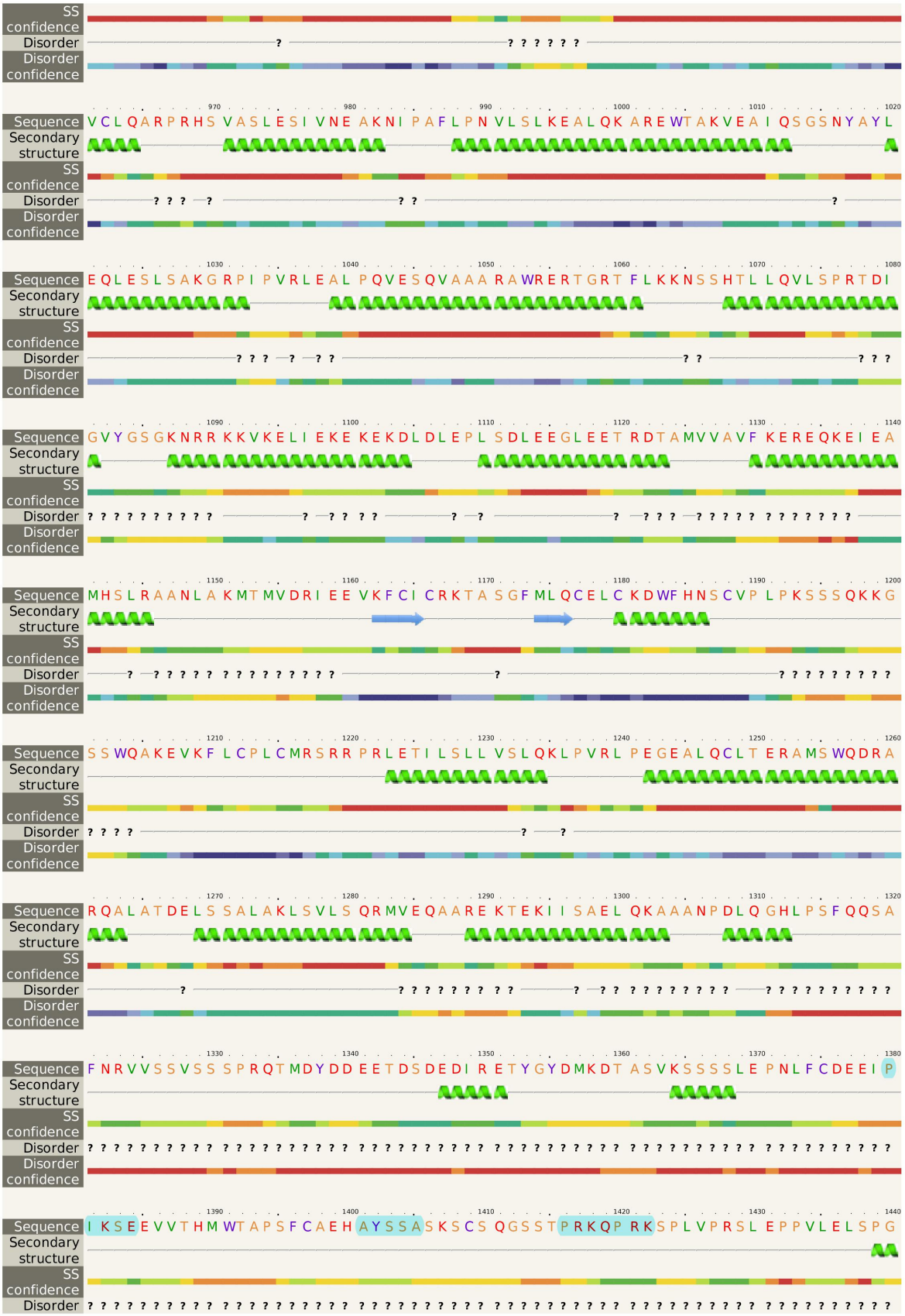
SS confidence
Disorder
Disorder confidence
970 980 990 1000 1010 1020
Sequence V C L Q A R P R H S V A S L E S I V N E A K N I P A F L P N V L S L K E A L Q K A R E W T A K V E A I Q S G S N Y A Y L
Secondary structure
1030 1040 1050 1060 1070 1080
Sequence E Q L E S L S A K G R P I P V R L E A L P Q V E S Q V A A A R A W R E R T G R T F L K K N S S H T L L Q V L S P R T D I
1090 1100 1110 1120 1130 1140
Sequence G V Y G S G K N R R K K V K E L I E K E K E K D L D L E P L S D L E E G L E E T R D T A M V V A V F K E R E Q K E I E A
1150 1160 1170 1180 1190 1200
Sequence M H S L R A A N L A K M T M V D R I E E V K F C I C R K T A S G F M L Q C E L C K D W F H N S C V P L P K S S S Q K K G
1210 1220 1230 1240 1250 1260
Sequence S S W Q A K E V K F L C P L C M R S R R P R L E T I L S L L V S L Q K L P V R L P E G E A L Q C L T E R A M S W Q D R A
1270 1280 1290 1300 1310 1320
Sequence R Q A L A T D E L S S A L A K L S V L S Q R M V E Q A A R E K T E K I I S A E L Q K A A A N P D L Q G H L P S F Q Q S A
1330 1340 1350 1360 1370 1380
Sequence F N R V V S S V S S S P R Q T M D Y D D E E T D S D E D I R E T Y G Y D M K D T A S V K S S S S L E P N L F C D E E I P
1390 1400 1410 1420 1430 1440
Sequence I K S E E V V T H M W T A P S F C A E H A Y S S A S K S C S Q G S S T P R K Q P R K S P L V P R S L E P P V L E L S P G

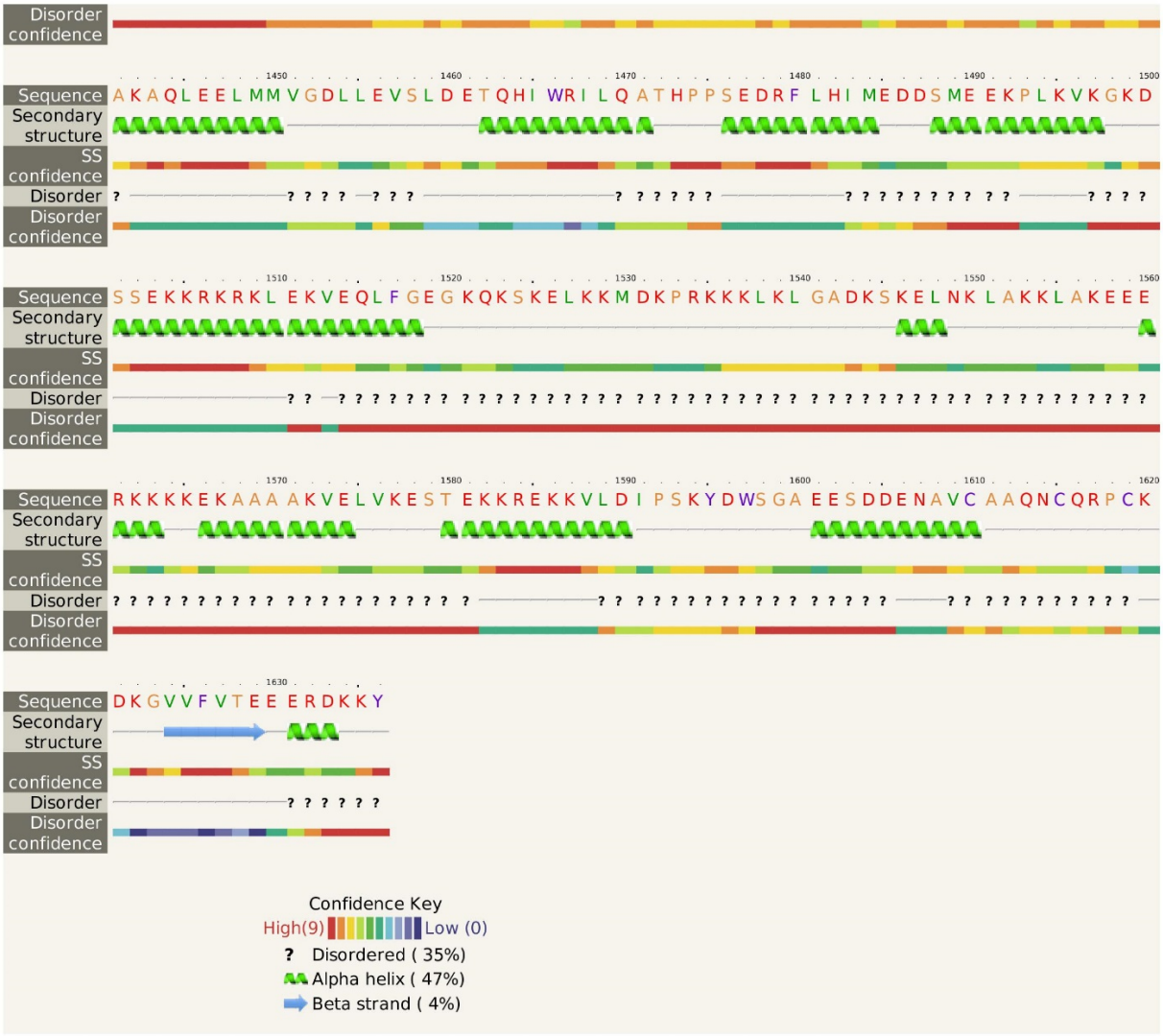
Disorder confidence
Sequence
Secondary structure
SS confidence
Disorder
Disorder confidence
Confidence Key
High(9) Low (0)
? Disordered (35%)
Alpha helix (47%)
Beta strand (4%)